



# ICACCHE

International Conference on Applications  
in Chemistry and Chemical Engineering

## BOOK OF PROCEEDINGS

11 - 15 October 2017 **Sarajevo**

[www.icacche.com](http://www.icacche.com)

## Organized by



## Partners



**INTERNATIONAL CONFERENCE ON APPLICATION IN CHEMISTRY AND  
CHEMICAL ENGINEERING (ICACCHE)**

**ISBN 978-605-67917-0-3**

**BOOK OF FULL TEXTS OF THE  
INTERNATIONAL CONFERENCE ON APPLICATION IN  
CHEMISTRY AND CHEMICAL ENGINEERING (ICACCHE)  
11-15 OCTOBER 2017, SARAJEVO**

**Edited by**  
Prof. Dr. Ömer Şahin

**Published, 2017**

**info@icacche.com**  
**www.icacche.com**

This work is subject to copyright. All rights are reserved, whether the whole or part of the material is concerned. Nothing from this publication may be translated, reproduced, stored in a computerized system or published in any form or in any manner, including, but not limited to electronic, mechanical, reprographic or photographic, without prior written permission from the publisher.

The individual contributions in this publication and any liabilities arising from them remain the responsibility of the authors. The publisher is not responsible for possible damages, which could be a result of content derived from this publication.

## SCIENTIFIC COMMITTEE

1. Prof. Dr. Gülhayat NASÜN SAYGILI - İstanbul Technical University
2. Prof. Dr. Mustafa BÖYÜKATA - Bozok University
3. Prof. Dr. Ferdinand Bego - University of Tirana, Albania
4. Prof. Dr. M. Salih AĞIRTAŞ - Yüzüncü Yıl University
5. Prof. Dr. Spiro Drushku - University of Tirana, Albania
6. Prof. Dr. Mahmut DOĞRU - Fırat University
7. Prof. Dr. Ahmet ÖZER - Fırat University
8. Prof. Dr. Muhtar KOCAKERİM - Çankırı University
9. Prof. Dr. Sinan YAPICI - İnönü University
10. Prof. Dr. Tahir Arbnesi - University of Pristina
11. Prof. Dr. İbrahim DİNÇER - Yıldız Teknik Üniversitesi
12. Prof. Dr. İsmail ÇAKMAK - Kafkas University
13. Prof. Dr. Ahmet KILIÇ - Harran University
14. Prof. Dr. Ahmet Duran ŞAHİN - İstanbul Technical University
15. Prof. Dr. Mustafa DEĞİRMENCİ - Harran University
16. Prof. Dr. Kozeta Vaso - University of Tirana, Albania
17. Prof. Dr. Zübeyde BAYSAL - Dicle University
18. Prof. Dr. Hasan TOĞRUL - Eskişehir Osmangazi University
19. Prof. Dr. Filiz KARAOSMANOĞLU - İstanbul Technical University
20. Prof. Dr. Fikret AKDENİZ - Kafkas University
21. Prof. Dr. Sermet KABASAKAL - Eskişehir Osmangazi University
22. Prof. Dr. Handan KAMIŞ - Selçuk University
23. Prof. Dr. Ülker BEKER - Yıldız Technical University
24. Prof. Dr. Mahmut KUŞ - Selçuk University
25. Prof. Dr. Hafız ALİSOY - Namık Kemal University
26. Prof. Dr. Ömer YAVUZ - Dicle University
27. Prof. Dr. Mesut AKGÜN - Yıldız Technical University
28. Prof. Dr. Birsen Şengul OKSAL - Giresun University
29. Assoc. Prof. Dr. Koray KÖKSAL - Bitlis Eren University
30. Assoc. Prof. Dr. Naser Troni - University of Pristina
31. Assoc. Prof. Dr. Nasrettin GENLİ - Dicle University
32. Assoc. Prof. Dr. M. Zafer KÖYLÜ - Dicle University
33. Assoc. Prof. Dr. Cafer SAKA - Siirt University
34. Assoc. Prof. Dr. Abdurrahman ASAN - Hitit University
35. Assoc. Prof. Dr. Halil DEMİR - Siirt University
36. Assist. Prof. Dr. Yunus ÖNAL - İnönü University
37. Assist. Prof. Dr. A. Abdullah CEYHAN - Selçuk University
38. Assist. Prof. Dr. Vedat ADIGÜZEL - Kafkas University
39. Assist. Prof. Dr. Mustafa ÖZDEMİR - Süleyman Demirel University

## **ORGANIZATION COMMITTEE**

### **Honorary Chairs**

Prof. Dr. Murat Erman – Rector of Siirt University

Prof. Dr. Marjan Dema - Rector of Pristina University

### **Chairman of Conference**

Prof. Dr. Ömer Şahin – Siirt University

### **Members of the Committee**

Assoc. Prof. Dr. Fevzi HANSU - Siirt University

Assist. Prof. Dr. M. Sait İZGİ - Siirt University

Assist. Prof. Dr. Arzu EKİNCİ - Siirt University

Assist. Prof. Dr. Orhan BAYTAR - Siirt University

Assist. Prof. Dr. Arben Haziri - Pristina University

Assist. Prof. Dr. Liridon Berisha - Pristina University

Teaching assistant Amra Banda - University of Sarajevo

Teaching assistant Amina Sivac - University of Sarajevo

Teaching assistant Boris Avdic - University of Sarajevo

Teaching assistant Dilek KILINÇ - Siirt University

Teaching assistant Edin Hrelja - University of Sarajevo

Teaching assistant Sabit HOROZ - Siirt University

Lecturer M. Sena ÇELİK - Siirt University

### **Secretariat of the Committee**

Research assistant Sinan KUTLUAY-Siirt University

Research assistant Yavuz KIRIM-Siirt University

## WELCOME TO ICACCHE 2017

*On behalf of the organizing committee, we are pleased to announce that the International Conference on Application in Chemistry and Chemical Engineering (ICACCHE-2017) is held from October 11 to 15, 2017 in Sarajevo - BOSNIA-HERZEGOVINA. ICACCHE 2017 provides an ideal academic platform to present the latest research findings on design, manufacture and operation of plants and machinery, the development of new materials or substances, developing novel materials and processes, analyzing substances, measuring the physical properties of substances and testing theories. This event gives a chance for all the professionals to gain and share information on Chemistry and Chemical Engineering and other related science branches issues and research.*

*Chemistry and Chemical engineering are multidisciplinary branches of applied engineering and science consisting of the application of physical science (Chemistry & Physics), life sciences including biochemistry with applied mathematics and economics to produce transform and use of chemicals, molecules materials, energy to make the whole production process successful with economic benefits.*

*Over the last 50 years, the discoveries in the basic sciences and the engineering of these inventions have been targeted at the development of applied technology and the prosperity of mankind and the distant and high quality of life away from environmental destructions for a sustainable future. Mathematics, physics, chemistry, and biology, which are accepted as basic sciences, and their engineering applications are now accepted in the scientific circles that have been intertwined and one of which is not worthless. It is foreseen by sectoral and academic stakeholders that these interdisciplinary relationships will continue to increase over the next several years.*

*The ability to identify, model, and solve engineering problems, and the ability to apply engineering knowledge develops with the knowledge of basic sciences. So, in terms of engineering education and the application of the engineering profession, the basic sciences have an important place and the necessary importance should be given.*

*Our goal is to transform this conference into an exchange of views on future vision and scenarios in chemistry, chemical engineering and related sciences, and to make science a tool of peace and justice.*

***Best regards,***

***Prof. Dr. Ömer ŞAHİN***

| <b>CONTENT</b>   | <b>PAGE</b> |
|--|-------------|
| <b>SOLUBILITY BEHAVIOR OF <math>Na^+</math>, <math>Zn^{2+}</math>/ <math>H_2PO_4^-</math>//<math>H_2O</math> TERNARY SYSTEM AT DIFFERENT TEMPERATURES</b>                              | <b>1.</b>   |
| <b>MEP DIAGRAMS AND SOLVATION FREE ENERGIES OF THE C1-SUBSTITUTED 9-METHYL-BC ALKALOIDS</b>  | <b>2.</b>   |
| <b>A COMPUTATIONAL STUDY ON THE NOR-HARMAN DERIVATIVES</b>   | <b>3.</b>   |
| <b>PRODUCTION OF LITHIUM TETRABORATE TETRAHYDRATE BY SPRAY DRIER METHOD AND DETERMINATION OF PRODUCTION CONDITIONS</b>   | <b>4.</b>   |
| <b>EFFECT OF ADDITIVES ON META-STABLE ZONE WIDTH FOR BORIC ACID CRYSTALLIZATION</b>  | <b>5.</b>   |
| <b>REMOVAL OF THE WATER FROM RAW BIODIESEL BY SUNFLOWER HULLS</b>  | <b>6.</b>   |
| <b>A NEW TECHNIQUE FOR THE MEASUREMENT OF MIXING TIME</b>  | <b>7.</b>   |
| <b>OPTIMIZATION OF PRODUCTION OF BORIC ACID FROM COLEMANITE ORE WITH <math>SO_2</math> GAS IN AQUEOUS MEDIUM</b>   | <b>8.</b>   |
| <b>REMOVAL OF SULFATE ANIONS FROM BORAX SOLUTION BY PUROLITE A 400 MB</b>  | <b>9.</b>   |
| <b>REMOVAL OF BORON FROM AQUEOUS SOLUTION USING TANNINS FROM TURKISH ACORNS (VALONIA)</b>  | <b>10.</b>  |
| <b>EVOLUTION OF BORIC ACID CRYSTAL SIZE DISTRIBUTION AND SHAPE IN A CSMMPR CRYSTALLIZER-THE EFFECT OF RESIDENCE TIME, STIRRING SPEED, FEED FLOW RATE AND AMOUNT OF SUPERSATURATION</b> | <b>11.</b>  |
| <b>DETERMINATION OF BORAX PENTAHYDRATE CRYSTAL SIZE DISTRIBUTION AND SHAPE IN A CSMMPR CRYSTALLIZER-THE EFFECT OF SUPERSATURATION, FEED FLOW RATE AND STIRRING SPEED WITH TIME</b>     | <b>12.</b>  |
| <b>EFFECT OF PROCESSING TIME ON HIGH TEMPERATURE CARBONIZATION OF TEA PLANT WASTES</b>   | <b>13.</b>  |
| <b>THE EFFECT OF HIGH FREQUENCY COLD PLASMA OBTAINED IN VARIOUS PARAMETERS, ON THE ELECTROCHEMICAL ACTIVITY OF CO-CR-B BASED CATALYSTS</b>   | <b>14.</b>  |
| <b>A KINETIC STUDY FOR OLIVE OIL RESIDUE PYROLYSIS: MODEL FREE APPROACHES</b>  | <b>15</b>   |



# Solubility Behavior of $\text{Na}^+$ , $\text{Zn}^{2+}$ / $\text{H}_2\text{PO}_2^-$ // $\text{H}_2\text{O}$ Ternary System at Different Temperatures

Sevilay Demirci<sup>1</sup>, Vedat Adıgüzel, Ömer Şahin, M. Sait İzgi

## Abstract

In this work, the (solid-liquid) phase equilibrium of  $\text{NaH}_2\text{PO}_2$ -  $\text{Zn}(\text{H}_2\text{PO}_2)_2$ - $\text{H}_2\text{O}$  ternary system at 313 and 333 K was studied experimentally. The solubility of the ternary systems was measured using isothermal solubility equilibrium method and the corresponding phase diagrams were plotted. In the phase diagrams, there are three solid phase crystalline zones, which correspond to  $\text{Zn}(\text{H}_2\text{PO}_2)_2 \cdot \text{H}_2\text{O}$ ,  $\text{Zn}(\text{H}_2\text{PO}_2)_2$  and  $\text{NaH}_2\text{PO}_2 \cdot \text{H}_2\text{O}$ . The composition of ternary system's invariant points (as a weight) were characterized by as following; 1.62% mass  $\text{Zn}(\text{H}_2\text{PO}_2)_2$ , 56.8% mass  $\text{NaH}_2\text{PO}_2$ , 41.58% mass  $\text{H}_2\text{O}$  at 313K and 7.05% mass  $\text{Zn}(\text{H}_2\text{PO}_2)_2$ , 37.94% mass  $\text{NaH}_2\text{PO}_2$ , 55.01% mass  $\text{H}_2\text{O}$  at 313K . The density and viscosity of invariant point are  $1405 \text{ kg/m}^3$ , 12,2 cP at 313K and  $1271 \text{ kg/m}^3$ , 3.42 cP at 333K , respectively. We concluded that  $\text{NaH}_2\text{PO}_2$  has strong salting-out effect on  $\text{Zn}(\text{H}_2\text{PO}_2)_2$  salt at all temperatures.

**Keywords:** Hypophosphite, phase diagram, physicochemical properties, solid-liquid equilibria

## 1. INTRODUCTION

Hypophosphite salts have a wide range of usage area. In the existence of a catalyst, hypophosphite compounds are used in hydrogen production [1]. Deya et al. have reported the synergism stimulated by zinc hypophosphite in an anticorrosive pigment mixture [2]. In recent years, metal hypophosphite compounds have been noted to be the significant inorganic compounds [3-6]. In the pharmacology and production of nylon carpet fibers and linear condensation polymers, manganese hypophosphite is highly valued [1].

Recycling process of these salts is quite important.

Phase diagrams are widely used for separating salts and production of important chemicals [7].

There are some articles related to the solubility phase systems of the hypophosphite salts at different temperatures.

$\text{Ca}(\text{H}_2\text{PO}_2)_2$ - $\text{NaH}_2\text{PO}_2$ - $\text{H}_2\text{O}$  at 298.15 K [8],

$\text{NaH}_2\text{PO}_2$ - $\text{Mn}(\text{H}_2\text{PO}_2)_2$ -  $\text{H}_2\text{O}$  at 293.15 K [10],

$\text{NaH}_2\text{PO}_2$ - $\text{Ba}(\text{H}_2\text{PO}_2)_2$ -  $\text{H}_2\text{O}$  at 273.15 K [11],

$\text{NaCl}$ - $\text{NaH}_2\text{PO}_2$ - $\text{H}_2\text{O}$  at 273.15 K [11]-[12],

$\text{NaH}_2\text{PO}_2$ - $\text{Zn}(\text{H}_2\text{PO}_2)_2$ -  $\text{H}_2\text{O}$  at 273.15 K [12].

\*Corresponding author: Sevilay Demirci, Kafkas University, Faculty of engineering and architecture, Department of chemical engineering, 36100 Kars Turkey, [incesevilay@gmail.com](mailto:incesevilay@gmail.com).

In this study, the solid-liquid phase equilibrium (SLE) of  $\text{NaH}_2\text{PO}_2$ -  $\text{Zn}(\text{H}_2\text{PO}_2)_2$ - $\text{H}_2\text{O}$  ternary system at 313 and 333 K was studied experimentally.

## 2.1. Materials

NaH<sub>2</sub>PO<sub>2</sub> (≥99%) has been purchased from Sigma-Aldrich without further purification. The solution condition has been provided with the use of pure water whose pH is 6.6 and conductivity is <10<sup>-4</sup> Sm<sup>-1</sup>. Zn(H<sub>2</sub>PO<sub>2</sub>)<sub>2</sub> has been synthesized and purified in our lab [12].

For the analysis of the density, a Mettler Toledo 30PX densitometer (accuracy ± 0.001 g/cm<sup>3</sup>) was utilized and the viscosity was completed with the Brookfield DV2T viscometer (accuracy 1%). For the titration measurements, 50 mL a Hirschmann Solarus titration unit (accuracy 0.2% was used. However, for the stability of the temperature for experimental conditions, polyscience refrigerated circulator water bath (accuracy ± 0.05 K) was used.

## 2.2. Experimental method

In order to establish Zn(H<sub>2</sub>PO<sub>2</sub>)<sub>2</sub> / NaH<sub>2</sub>PO<sub>2</sub> / H<sub>2</sub>O ternary system, 60 mL of the saturated Zn(H<sub>2</sub>PO<sub>2</sub>)<sub>2</sub> solution were prepared in a waterproof and sealed bottle, then the bottle was put into refrigerated circulating bath at 313 K/333 K (until Zn(H<sub>2</sub>PO<sub>2</sub>)<sub>2</sub> crystals appeared in solid phase). Then, a small amount of NaH<sub>2</sub>PO<sub>2</sub> crystals was added into the prepared saturated Zn(H<sub>2</sub>PO<sub>2</sub>)<sub>2</sub> solution which was stirred for one day and stabilized during the day. Then by obtaining samples from the solid and liquid phases the viscosity, density and the composition of liquid phases were measured by using classical analytical methods [13]. This operation was repeated until finding the invariant point. Same procedure was repeated adding Zn(H<sub>2</sub>PO<sub>2</sub>)<sub>2</sub> into saturated NaH<sub>2</sub>PO<sub>2</sub> solution up to invariant point [12].

## 3. RESULTS AND DISCUSSION

Solubility of binary systems were determined as 57.03% mass NaH<sub>2</sub>PO<sub>2</sub> and 22.22% mass Zn(H<sub>2</sub>PO<sub>2</sub>)<sub>2</sub> at 313 K and 61.13% mass NaH<sub>2</sub>PO<sub>2</sub> and 27.23% mass Zn(H<sub>2</sub>PO<sub>2</sub>)<sub>2</sub> at 333 K. Values related to invariant points of the density, viscosity and, per cent compositions of ternary system were shown below (Table 1-2).

Totally, 8, 10 test points were studied at 313 K and 333K, respectively.

The invariant point of Zn(H<sub>2</sub>PO<sub>2</sub>)<sub>2</sub> / NaH<sub>2</sub>PO<sub>2</sub> / H<sub>2</sub>O ternary system is analyzed as 1.62% mass Zn(H<sub>2</sub>PO<sub>2</sub>)<sub>2</sub>, 56.8% mass NaH<sub>2</sub>PO<sub>2</sub>, 41.58% mass H<sub>2</sub>O at 313 K. It is determined that Zn(H<sub>2</sub>PO<sub>2</sub>)<sub>2</sub>.H<sub>2</sub>O and NaH<sub>2</sub>PO<sub>2</sub>.H<sub>2</sub>O crystal hydrates are in equilibrium with liquid phase. The density and viscosity of invariant point are 1405 kg/m<sup>3</sup>, 12,2 cP, respectively (Table 1).

The invariant point of Zn(H<sub>2</sub>PO<sub>2</sub>)<sub>2</sub> / NaH<sub>2</sub>PO<sub>2</sub> / H<sub>2</sub>O ternary system is analyzed as 7.05% mass Zn(H<sub>2</sub>PO<sub>2</sub>)<sub>2</sub>, 37.94% mass NaH<sub>2</sub>PO<sub>2</sub>, 55.01% mass H<sub>2</sub>O at 333 K. It is determined that Zn(H<sub>2</sub>PO<sub>2</sub>)<sub>2</sub> and NaH<sub>2</sub>PO<sub>2</sub>.H<sub>2</sub>O crystals are in equilibrium with liquid phase. The density and viscosity of invariant point are 1271 kg/m<sup>3</sup>, 3.42 cP, respectively (Table 2).

Table and graphics were created using experimental data. (Table 1-2 and Figure 1-4)

The experimental phase diagrams and physicochemical properties vs. composition diagrams of the systems were drawn for the first time in the literature.

In the ternary system of Zn(H<sub>2</sub>PO<sub>2</sub>)<sub>2</sub>-NaH<sub>2</sub>PO<sub>2</sub>-H<sub>2</sub>O, we concluded that NaH<sub>2</sub>PO<sub>2</sub> has strong salting-out effect on Zn(H<sub>2</sub>PO<sub>2</sub>)<sub>2</sub> salt.

Experimental results and figures can be used both in the salt industry and recycling units. These Zn(H<sub>2</sub>PO<sub>2</sub>)<sub>2</sub> and NaH<sub>2</sub>PO<sub>2</sub> salts, which may contain industrial waste and natural salt composition, are suggested to supply an efficient method for separation.

## ACKNOWLEDGMENT

This work was supported by The Scientific and Technological Research Council of Turkey (TÜBİTAK), under Project no. 114Z651.

## REFERENCES

- [1] P. Noisong, C. Danvirutai, T. Srihanratana, B. Boonchom, "Synthesis, characterization and non-isothermal decomposition kinetics of manganese hypophosphite monohydrate," *Solid State Sci.*, 10, 1598-1604, 2008.
- [2] M.C. Deya, G. Blustein, R. Romagnoli, B. del Amo, "Zinc hypophosphite: a suitable additive for anticorrosive paints to promote pigments synergism," *J. Coat. Technol. Res.*, 6, 369-376, 2009.
- [3] S. Marincean, R. Custelcean, R.S. Stein, J.E. Jackson, "Structural reinvestigation of ammonium hypophosphite: Was dihydrogen bonding observed long ago?," *Inorg. Chem.*, 44, 45-48, 2005.
- [4] J.R. Van Vazer, *Phosphorus and its compounds*, Interscience Publishers, New York, 1958.
- [5] P.A.Tanner, Y.L. Liu, T.C.W. Mak, "Synthesis, crystal structures and vibrational spectra of zinc hypophosphites," *Polyhedron*, 16, 495, 1997.

- [6] P.A. Tanner, M.D. Faucher, T.C.W. Mak, "Synthesis, structure, and spectroscopy of rare earth hypophosphites. I. anhydrous and monohydrated lanthanide hypophosphites," *Inorg. Chem.*, 38, 6008-6023, 1999.
- [7] Z. Li, X. Yu, Q. Yin, Y. Zeng, "Thermodynamics metastable phase equilibria of aqueous quaternary system  $\text{LiCl}+\text{KCl}+\text{RbCl}+\text{H}_2\text{O}$  at 323.15 K," *Fluid Phase Equilib.*, 358, 131-136, 2013.
- [8] L. Tan, J. Wang, H. Zhou, L. Wang, P. Wang, X. Bai, "Solid-liquid phase equilibria of  $\text{Ca}(\text{H}_2\text{PO}_2)_2-\text{CaCl}_2-\text{H}_2\text{O}$  and  $\text{Ca}(\text{H}_2\text{PO}_2)_2-\text{NaH}_2\text{PO}_2-\text{H}_2\text{O}$  ternary systems at 298.15 K," *Fluid Phase Equilib.*, 388, 66-70, 2015.
- [9] H. Cao, H. Zhou, X. Bai, R. Ma, L. Tan, "(Solid+liquid) phase equilibria of  $\text{Ca}(\text{H}_2\text{PO}_2)_2+\text{CaCl}_2+\text{H}_2\text{O}$  and  $(\text{Ca}(\text{H}_2\text{PO}_2)_2+\text{NaH}_2\text{PO}_2+\text{H}_2\text{O})$  ternary systems at  $T=323.15\text{ K}$ ," *J. Chem. Thermodynamics*, 93, 255-263, 2016.
- [10] R.M. Dolinina, V.A. Aliev, I.N. Lepeschkov, *Zh. Neorg. Khim.* 34, 1324-1327, 1990.
- [11] H. Erge, V. Adıgüzel, V. Alısoglu, "Study of the solubility in  $\text{Na}-\text{Ba}-\text{Cl}-\text{H}_2\text{O}$ ,  $\text{Na}-\text{Ba}-\text{H}_2\text{PO}_2-\text{H}_2\text{O}$ ,  $\text{Na}-\text{Cl}-\text{H}_2\text{PO}_2-\text{H}_2\text{O}$ , and  $\text{Ba}-\text{Cl}-\text{H}_2\text{PO}_2-\text{H}_2\text{O}$  ternaries, and in  $\text{Na}^+$ ,  $\text{Ba}^{2+}/\text{Cl}^-$ ,  $(\text{H}_2\text{PO}_2^-)/\text{H}_2\text{O}$  reciprocal quaternary system at 0 °C," *Fluid Phase Equilib.*, 344, 13-18, 2013.
- [12] V. Adıgüzel, H. Erge, V. Alısoglu, H. Necefoglu, "Study of the solubility, viscosity and density in  $\text{Na}^+$ ,  $\text{Zn}^{2+}/\text{Cl}^- - \text{H}_2\text{O}$ ,  $\text{Na}^+ - \text{Zn}^{2+} - (\text{H}_2\text{PO}_2^-) - \text{H}_2\text{O}$ ,  $\text{Na}^+$ ,  $\text{Cl}^-/(\text{H}_2\text{PO}_2^-) - \text{H}_2\text{O}$ , and  $\text{Zn}^{2+}$ ,  $\text{Cl}^-/(\text{H}_2\text{PO}_2^-) - \text{H}_2\text{O}$  ternary systems, and in  $\text{Na}^+$ ,  $\text{Zn}^{2+}/\text{Cl}^-$ ,  $(\text{H}_2\text{PO}_2^-)/\text{H}_2\text{O}$  reciprocal quaternary system at 273.15 K," *J. Chem. Thermodyn.*, 75, 35-44, 2014.
- [13] T. Gündüz, *Kantitatif Analiz Laboratuvar Kitabı*, Gazi Kitabevi, Ankara-Turkey, 1999.

## BIOGRAPHY

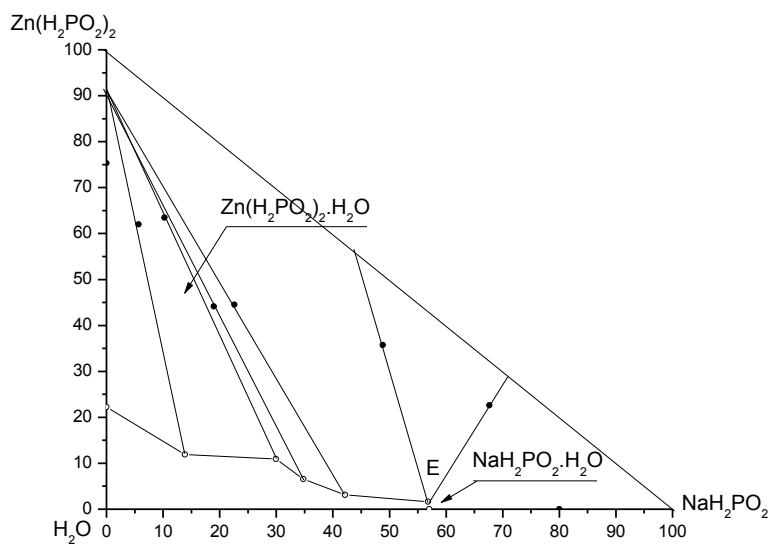
Dr. Sevilay Demirci has been working as an assistant professor at Department of Chemical Engineering, Faculty of Engineering and Architecture, Kafkas University. Her working area includes phase equilibria and renewable energy. She has various publications related to these areas.

Table 1. Solubility, Viscosity, and Density for the Ternary ( $\text{NaCl}-\text{Zn}(\text{H}_2\text{PO}_2)_2-\text{H}_2\text{O}$ ) system at 313K

| No | Liquid Phase<br>(% mass)  |                                      | Solid Phase<br>(% mass)   |                                      | 100 mole composition of salts |                                      | Density     | Viscosity   | Equilibrium Salt  |
|----|---------------------------|--------------------------------------|---------------------------|--------------------------------------|-------------------------------|--------------------------------------|-------------|-------------|---|
|    | $\text{NaH}_2\text{PO}_2$ | $\text{Zn}(\text{H}_2\text{PO}_2)_2$ | $\text{NaH}_2\text{PO}_2$ | $\text{Zn}(\text{H}_2\text{PO}_2)_2$ | $\text{NaH}_2\text{PO}_2$     | $\text{Zn}(\text{H}_2\text{PO}_2)_2$ |             |             |   |
| 1  | 0                         | 22.22                                | 0                         | 75.31                                | 0                             | 100                                  | 1165        | 1.66        | $\text{Zn}(\text{H}_2\text{PO}_2)_2 \cdot \text{H}_2\text{O}$   |
| 2  | 13.86                     | 11.9                                 | 5.69                      | 62                                   | 72.02                         | 27.98                                | 1193        | 1.81        | $\text{Zn}(\text{H}_2\text{PO}_2)_2 \cdot \text{H}_2\text{O}$   |
| 3  | 29.96                     | 10.95                                | 10.25                     | 63.46                                | 85.89                         | 14.11                                | 1236        | 2.49        | $\text{Zn}(\text{H}_2\text{PO}_2)_2 \cdot \text{H}_2\text{O}$   |
| 4  | 34.8                      | 6.53                                 | 18.95                     | 44.14                                | 92.28                         | 7.72                                 | 1265        | 3.35        | $\text{Zn}(\text{H}_2\text{PO}_2)_2 \cdot \text{H}_2\text{O}$   |
| 5  | 42.17                     | 3.09                                 | 22.59                     | 44.52                                | 96.76                         | 3.24                                 | 1295        | 4.56        | $\text{Zn}(\text{H}_2\text{PO}_2)_2 \cdot \text{H}_2\text{O}$   |
| 6E | <b>56.8</b>               | <b>1.62</b>                          | <b>48.84</b>              | <b>35.73</b>                         | <b>98.77</b>                  | <b>1.23</b>                          | <b>1405</b> | <b>12.2</b> | $\text{Zn}(\text{H}_2\text{PO}_2)_2 \cdot \text{H}_2\text{O} +$<br>$\text{NaH}_2\text{PO}_2 \cdot \text{H}_2\text{O}$ |
| 7E | <b>56.8</b>               | <b>1.62</b>                          | <b>67.66</b>              | <b>22.6</b>                          | <b>98.77</b>                  | <b>1.23</b>                          | <b>1405</b> | <b>12.2</b> | $\text{Zn}(\text{H}_2\text{PO}_2)_2 \cdot \text{H}_2\text{O} +$<br>$\text{NaH}_2\text{PO}_2 \cdot \text{H}_2\text{O}$ |
| 8  | 57.03                     | 0                                    | 80.02                     | 0                                    | 100                           | 0                                    | 1393        | 11.7        | $\text{NaH}_2\text{PO}_2 \cdot \text{H}_2\text{O}$  |

Table 2. Solubility, Viscosity, and Density for the Ternary ( $\text{NaH}_2\text{PO}_2$ - $\text{Zn}(\text{H}_2\text{PO}_2)_2$ - $\text{H}_2\text{O}$ ) system at 333 K

| No        | Liquid Phase              |                                      | Solid Phase               |                                      | 100 mole composition of salts |                                      | Density     | Viscosity   | Equilibrium Salt  |
|-----------|---------------------------|--------------------------------------|---------------------------|--------------------------------------|-------------------------------|--------------------------------------|-------------|-------------|---|
|           | (% mass)                  |                                      | (% mass)                  |                                      |                               |                                      |             |             |   |
|           | $\text{NaH}_2\text{PO}_2$ | $\text{Zn}(\text{H}_2\text{PO}_2)_2$ | $\text{NaH}_2\text{PO}_2$ | $\text{Zn}(\text{H}_2\text{PO}_2)_2$ | $\text{NaH}_2\text{PO}_2$     | $\text{Zn}(\text{H}_2\text{PO}_2)_2$ |             |             |   |
| 1         | 0                         | 27.23                                | 0                         | 82.18                                | 0                             | 100                                  | 1194        | 2.91        | $\text{Zn}(\text{H}_2\text{PO}_2)_2$  |
| 2         | 8.48                      | 18.98                                | 2.59                      | 76.51                                | 49.69                         | 50.31                                | 1200        | 2.53        | $\text{Zn}(\text{H}_2\text{PO}_2)_2$  |
| 3         | 18.08                     | 16.52                                | 5.84                      | 73.78                                | 70.98                         | 29.02                                | 1216        | 2.86        | $\text{Zn}(\text{H}_2\text{PO}_2)_2$  |
| 4         | 25.28                     | 15.95                                | 7.96                      | 73.74                                | 77.88                         | 22.12                                | 1232        | 3.11        | $\text{Zn}(\text{H}_2\text{PO}_2)_2$  |
| 5         | 29.17                     | 13.70                                | 17.14                     | 50.97                                | 82.55                         | 17.45                                | 1240        | 3.11        | $\text{Zn}(\text{H}_2\text{PO}_2)_2$  |
| <b>6E</b> | <b>37.94</b>              | <b>7.05</b>                          | <b>34.08</b>              | <b>50.26</b>                         | <b>92.29</b>                  | <b>7.71</b>                          | <b>1271</b> | <b>3.42</b> | <b><math>\text{Zn}(\text{H}_2\text{PO}_2)_2</math>+<br/><math>\text{NaH}_2\text{PO}_2 \cdot \text{H}_2\text{O}</math></b> |
| <b>7E</b> | <b>37.94</b>              | <b>7.05</b>                          | <b>55.54</b>              | <b>22.12</b>                         | <b>92.29</b>                  | <b>7.71</b>                          | <b>1271</b> | <b>3.42</b> | <b><math>\text{Zn}(\text{H}_2\text{PO}_2)_2</math>+<br/><math>\text{NaH}_2\text{PO}_2 \cdot \text{H}_2\text{O}</math></b> |
| 8         | 40.78                     | 4.2                                  | 69.95                     | 1.65                                 | 95.56                         | 4.44                                 | 1310        | 9.33        | $\text{NaH}_2\text{PO}_2 \cdot \text{H}_2\text{O}$  |
| 9         | 50.12                     | 1.4                                  | 63.87                     | 1.13                                 | 98.77                         | 1.23                                 | 1396        | 13.66       | $\text{NaH}_2\text{PO}_2 \cdot \text{H}_2\text{O}$  |
| 10        | 61.13                     | 0                                    | 76.19                     | 0                                    | 100                           | 0                                    | 1415        | 15.58       | $\text{NaH}_2\text{PO}_2 \cdot \text{H}_2\text{O}$  |

Figure 1. Solubility diagram for the ternary  $\text{NaH}_2\text{PO}_2$ + $\text{Zn}(\text{H}_2\text{PO}_2)_2$ + $\text{H}_2\text{O}$  system at  $T=313\text{K}$

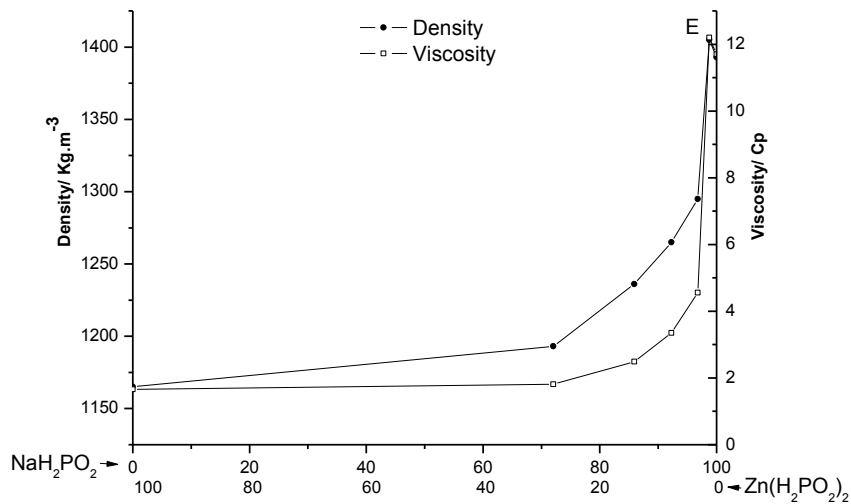


Figure 2. Viscosity and density diagram for for the ternary  $\text{NaH}_2\text{PO}_2+\text{Zn}(\text{H}_2\text{PO}_2)_2+\text{H}_2\text{O}$  system at  $T=313\text{K}$

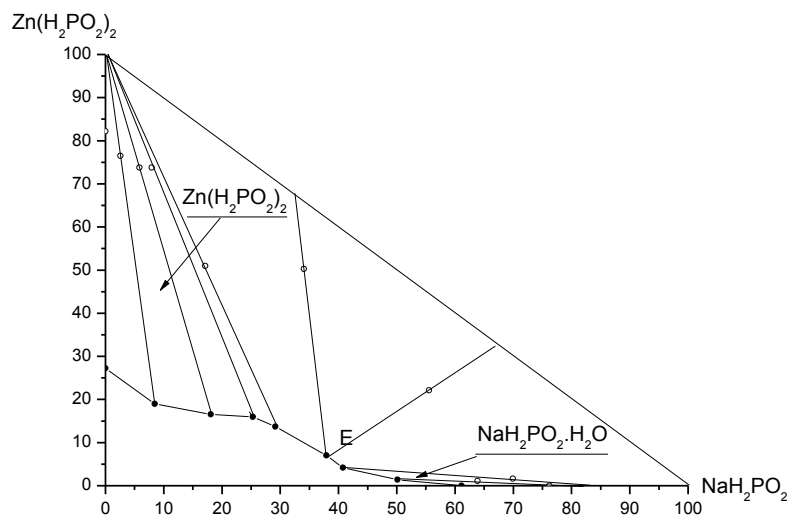


Figure 3. Solubility diagram for the ternary  $\text{NaH}_2\text{PO}_2+\text{Zn}(\text{H}_2\text{PO}_2)_2+\text{H}_2\text{O}$  system at  $T=333\text{K}$

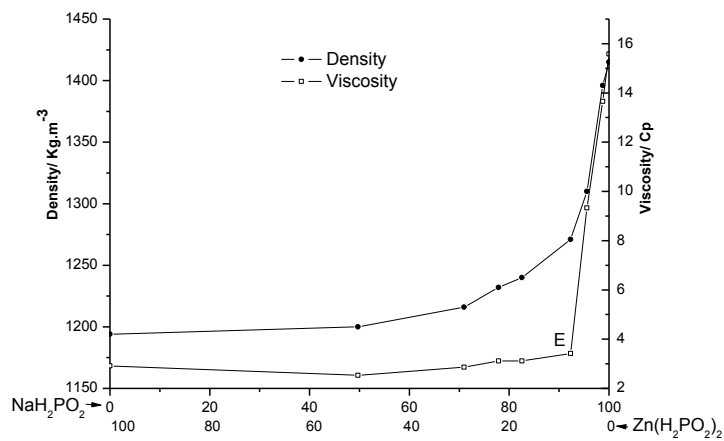


Figure 4. Viscosity and density diagram for for the ternary  $\text{NaH}_2\text{PO}_2+\text{Zn}(\text{H}_2\text{PO}_2)_2+\text{H}_2\text{O}$  system at  $T=333\text{K}$

**Figure and Table Captions**

**Table 1.** Solubility, Viscosity, and Density for the Ternary ( $\text{NaCl}-\text{Zn}(\text{H}_2\text{PO}_2)_2-\text{H}_2\text{O}$ ) system at 313K

**Table 2.** Solubility, Viscosity, and Density for the Ternary ( $\text{NaH}_2\text{PO}_2-\text{Zn}(\text{H}_2\text{PO}_2)_2-\text{H}_2\text{O}$ ) system at 333 K

**Figure 1.** Solubility diagram for the ternary  $\text{NaH}_2\text{PO}_2+\text{Zn}(\text{H}_2\text{PO}_2)_2+\text{H}_2\text{O}$  system at  $T=313\text{K}$

**Figure 2.** Viscosity and density diagram for for the ternary  $\text{NaH}_2\text{PO}_2+\text{Zn}(\text{H}_2\text{PO}_2)_2+\text{H}_2\text{O}$  system at  $T=313\text{K}$

**Figure 3.** Solubility diagram for the ternary  $\text{NaH}_2\text{PO}_2+\text{Zn}(\text{H}_2\text{PO}_2)_2+\text{H}_2\text{O}$  system at  $T=333\text{K}$

**Figure 4.** Viscosity and density diagram for for the ternary  $\text{NaH}_2\text{PO}_2+\text{Zn}(\text{H}_2\text{PO}_2)_2+\text{H}_2\text{O}$  system at  $T=333\text{K}$



# MEP Diagrams and Solvation Free Energies of the C1- substituted 9-methyl- $\beta$ C alkaloids

Goncagül Serdaroğlu<sup>1</sup>

---

## Abstract

*In order to calculate the quantum chemical parameters and stabilization energies of the  $\beta$ C alkaloids given in Figure 1, the geometry optimization and frequency calculations have been performed using DFT with 3 basis sets in both the gas phase and the aqueous phase. It has been determined that as the solvent dielectric constant increases and as the basis set rises, each structure becomes increasingly more stable. In water phase, the solvation free energy changing is calculated as following order: **D** (10.513) > **A** (9.374) > **C** (9.214) > **E** (9.098) > **B** (8.564) in kcalmol<sup>-1</sup> unit at B3LYP/6-311++G\*\* basis set. It can be said that the stabilization energy ordering agrees with the aromaticity of the substituent group to attach to the C1 position. In accord with the calculated electrophilicity index, the most electrophilic structure was the structure **B** which is quite compatible with the MEP diagrams. Hopefully, the calculated parameters will help to explain the process of action of existing drugs and are expected to provide useful information prior to the synthesis of future new ligands.*

**Keywords:** Descriptors, FMO analysis, global reactivity, substituent effect, solvent effect,

---

## 1. INTRODUCTION

9-hydro-pyrido (3,4-*b*) indole compounds ( $\beta$ C alkaloids) are natural-occurring in many medicinal plants, also they are produced from the marine organism and human tissues as secondary metabolism [1-3]. In the many of scientific fields such as biochemistry, medicinal chemistry, pharmacology, neurological chemistry and so on, scientists have studied on  $\beta$ C compounds because these compounds act on different receptor sites in central nervous system (CNS) such as Benzodiazepine Receptor (BzR), imidazoline and serotonin receptors. [4-6] Because of their actions on the different receptor sites, they have very important pharmacological properties such as cytotoxic effect [7-12], oxidative stress [2], photochemical metabolism [13], antitumor activity [14] and anti-HIV activity [14]. In literature, there are numerous experimental studies have been carried out to synthesizing the novel  $\beta$ C drug/agent and their activities on several receptors, also their basic biochemical properties have been clarified, but there are still controversial matters about it. The cytotoxicity of the  $\beta$ Cs have mainly been investigated by scientists [7-12] and it is suggested that  $\beta$ Cs actions are related to their interaction with DNA base pairs with high affinity [11] because of their polycyclic aromatic structures, but the exact explanation of the relationship between  $\beta$ Cs and DNA base pairs are still not clear. And, the cytotoxicity in vivo and in vitro can be affected by light [13]. Because of this, scientists have commonly studied on photochemical properties of  $\beta$ Cs [13, 15-16]. Cao and et. al have suggested that the position 1- and 9- are very important to increase the cytotoxic potency [9] because the substituent group type and its location on  $\beta$ Cs main structure have a great role to explain the photochemical/ photo physical and corresponding properties of  $\beta$ Cs. As well known, the molecular structure of these group derivatives are very important to be able to get a good antitumor drug. [14]

As it is stated before, there is much research about both the  $\beta$ C and their derivatives because of their pharmaceutical importance, but still, the fundamental biochemical phenomena underlying some key properties have been speculative. For this purpose, I have selected the full aromatic  $\beta$ C alkaloids and its aromatic substituent groups to determine the physicochemical properties underlying key biochemical phenomena that play an important role in developing or in improving the more potent  $\beta$ C agents with the lower toxicity and with lower side effect. And, I aim to get the global reactivity descriptors such as electronic chemical potential ( $\mu$ ), global hardness ( $\eta$ ), electrophilicity ( $\omega$ ), Energy Gap ( $\Delta E$ ), the maximum charge transfer index ( $\Delta N$ ) to evaluate the substituent effect on the physicochemical behavior of these compounds. Hope, the results will provide useful information about the molecular structure and chemical reactivity behavior of the investigated compounds being here.

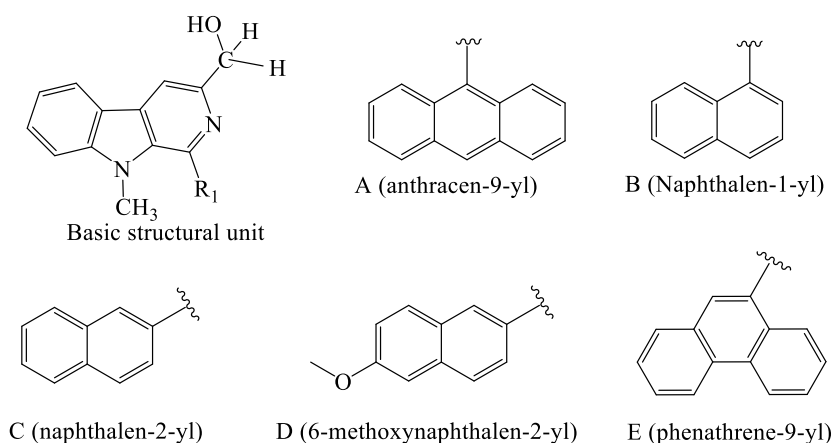


Figure 1. The βC alkaloid as the basic chemical structure and its substituent groups: A, anthracen-9-yl); B, naphthalene-1-yl, C, naphthalene-2-yl; D, 6-methoxynaphthalene-2-yl; E phenanthrene-9-yl

## 2. COMPUTATIONAL METHOD

The geometry optimizations and frequency calculations of the basic structural unit and its aromatic substituted derivatives given in Figure 1 were employed with 6-31G(d,p) basis set in the gas phase. Then, the optimized structures have been used for the solvent media calculations as the starting structure. All calculations to look for the basis set effect on the chemical reactivity behavior were repeated at the 6-31+G(d,p) and 6-311++G(d,p) basis sets in the B3LYP level of the theory. [17-18] by using the Gaussian 09W [19] software package. The Polarized Continuum Model (PCM) [20-21] have been used to obtain the stabilization energy to look for the solvent effect on chemical stability behavior of 1, 3 di-substituted βC alkaloids. The optimized structures were verified by the absence of any imaginary frequency. The Ionization energy (I) and electron affinity (A) were obtained from Koopmans Theorem ( $I = -E_{\text{HOMO}}$  and  $A = -E_{\text{LUMO}}$ ). [22-23] The electronic chemical potential ( $\mu$ ), global hardness ( $\eta$ ), electrophilicity ( $\omega$ ) and the maximum charge transfer index ( $\Delta N_{\text{max}}$ ) defined by Parr and co-workers [24] are given below as:

$$\mu = -\frac{I+A}{2} \quad (1)$$

$$\eta = \frac{I-A}{2} \quad (2)$$

$$\omega = \frac{\mu^2}{2\eta} \quad (3)$$

$$\Delta N = \frac{I+A}{(I-A)} \quad (4)$$

### 3. RESULTS AND DISCUSSION

Figure 2 has shown the solvation free energy on going from the gas phase to the water phase for 1,3 di- substituted  $\beta$ C alkaloids. First, when the basis set is enlarged from the 6-31G(d,p) to 6-31+g(d,p) and then from 6-31+g(d,p) to 6-311++g(d,p) basis set, it can be seen from Figure 2a that the solvation free energy increased. In Figure 2a, the solvation free energy for the 6-31+g(d,p) basis set is indicated by red line, is indicated by blue line for the 6-311++g(d,p) basis set and is shown by green line for 6-31G(d,p) basis set. On the other hand, Figure 2b, c, and d have shown the solvation free energy of the di-substituted compounds for the 6-31G(d,p), 6-31+g(d,p), 6-311++g(d,p) basis sets. The structure **B** is the less stabilized structure with solvent media while the structure **D** is the most stabilized one, at all basis sets and in the all solvent media because the structure **D** has the more polarizable group as 6-methoxynaphthalene-2-yl substitution at C1 position. But the structure **B** has the naphthalene-1-yl substitution, which is the less aromatic group than the other substituent groups [25]. In fact, it should be mentioned that the solvation free energy ordering for these structures strongly depend on the solvent media as well as the basis set: for the 6-31g(d,p) basis set in the toluene, the stabilization free energy has changed in the following order: **B**< **A**< **E**< **C**< **D** while it has changed in these ordering: **B**< **C**< **A**< **C**< **D**. It is clear that the structure **A** and the structure **C** are replaced with each other in the other solvents at the same basis set.

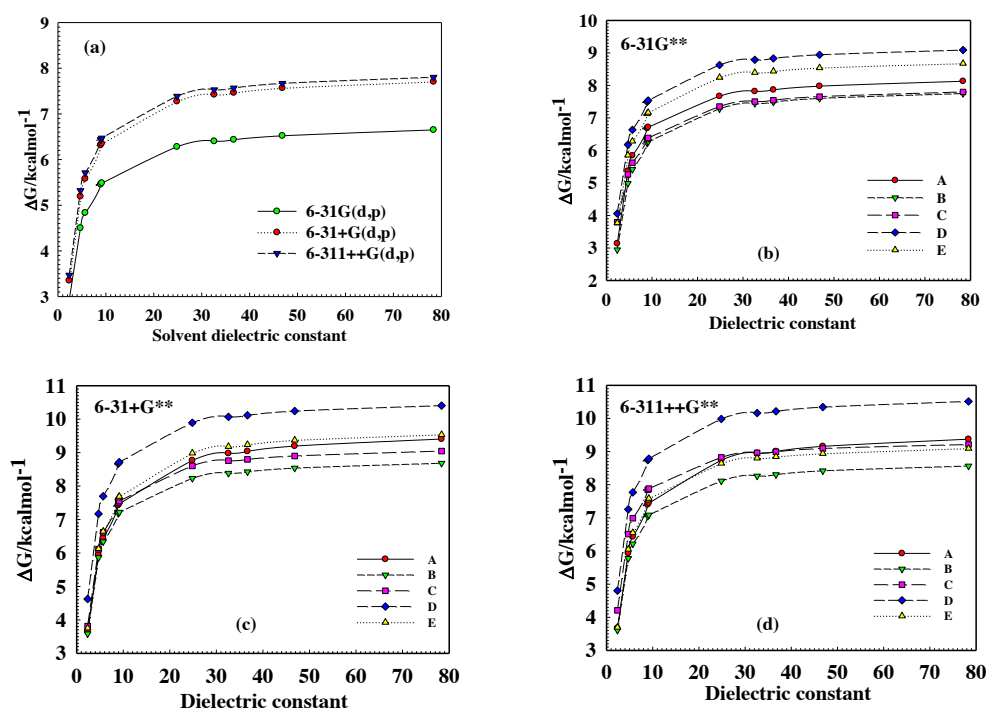


Figure 2. Solvation Free Energies as a function of solvent dielectric constant (a) the basic structure; (b) B3LYP/6-31G\*\*, (c) B3LYP/6-31+G\*\*, (d) B3LYP/6-311++G\*\* level of the theory of the aromatic substituted derivatives of the basic structure

Table 1. Solvation Free Energies as a function of solvent dielectric constant for the basic structure

| Solvent         | Dielectric constants | 6-31G(dP) | 6-31+G(dP) | 6-311++G(dP) |
|-----------------|----------------------|-----------|------------|--------------|
| Toluene         | $\epsilon=2.37$      | 2.935489  | 3.350901   | 3.470128     |
| Chloroform      | $\epsilon=4.71$      | 4.501126  | 5.192641   | 5.319398     |
| Chlorobenzene   | $\epsilon=5.70$      | 4.833078  | 5.578559   | 5.710964     |
| Dichloromethane | $\epsilon=8.93$      | 5.454313  | 6.315883   | 6.437620     |
| quinoline       | $\epsilon=9.16$      | 5.484433  | 6.351024   | 6.471505     |
| Ethanol         | $\epsilon=24.85$     | 6.280115  | 7.274090   | 7.386414     |
| Methanol        | $\epsilon=32.61$     | 6.401224  | 7.422182   | 7.527604     |
| Acetonitrile    | $\epsilon=36.69$     | 6.434482  | 7.462343   | 7.567137     |
| DMSO            | $\epsilon=46.83$     | 6.519824  | 7.565882   | 7.668166     |
| Water           | $\epsilon=78.36$     | 6.649091  | 7.705817   | 7.802453     |

Table 2. Solvation Free Energies as a function of solvent dielectric constant for the basic structure at B3LYP/6-31G(d,p) level of the theory in the ten solvent environments

| Solvent         | A     | B     | C     | D     | E     |
|-----------------|-------|-------|-------|-------|-------|
| Toluene         | 3.137 | 2.946 | 3.795 | 4.059 | 3.774 |
| Chloroform      | 5.366 | 4.986 | 5.263 | 6.179 | 5.855 |
| Chlorobenzene   | 5.843 | 5.415 | 5.622 | 6.635 | 6.285 |
| Dichloromethane | 6.680 | 6.226 | 6.349 | 7.494 | 7.128 |
| quinoline       | 6.716 | 6.265 | 6.385 | 7.537 | 7.169 |
| Ethanol         | 7.669 | 7.281 | 7.353 | 8.629 | 8.247 |
| Methanol        | 7.818 | 7.445 | 7.504 | 8.788 | 8.397 |
| Acetonitrile    | 7.865 | 7.489 | 7.547 | 8.832 | 8.438 |
| DMSO            | 7.978 | 7.602 | 7.656 | 8.943 | 8.542 |

|       |       |       |       |       |       |
|-------|-------|-------|-------|-------|-------|
| Water | 8.129 | 7.751 | 7.800 | 9.088 | 8.677 |
|-------|-------|-------|-------|-------|-------|

Table 3. Solvation Free Energies as a function of solvent dielectric constant for the basic structure at B3LYP/6-31+G(d,p) level of the theory in the ten solvent environments

| Solvent         | A     | B     | C     | D      | E     |
|-----------------|-------|-------|-------|--------|-------|
| Toluene         | 3.643 | 3.587 | 3.814 | 4.624  | 3.758 |
| Chloroform      | 5.949 | 5.863 | 6.109 | 7.169  | 6.131 |
| Chlorobenzene   | 6.446 | 6.338 | 6.618 | 7.696  | 6.647 |
| Dichloromethane | 7.427 | 7.182 | 7.513 | 8.671  | 7.646 |
| quinoline       | 7.471 | 7.219 | 7.555 | 8.714  | 7.692 |
| Ethanol         | 8.766 | 8.230 | 8.604 | 9.893  | 8.986 |
| Methanol        | 8.978 | 8.384 | 8.759 | 10.069 | 9.184 |
| Acetonitrile    | 9.038 | 8.427 | 8.798 | 10.116 | 9.240 |
| DMSO            | 9.196 | 8.537 | 8.900 | 10.242 | 9.373 |
| Water           | 9.406 | 8.682 | 9.046 | 10.405 | 9.539 |

Table 4. Solvation Free Energies as a function of solvent dielectric constant for the basic structure at B3LYP/6-311++G(d,p) level of the theory in the ten solvent environments

| Solvent         | A     | B     | C     | D      | E     |
|-----------------|-------|-------|-------|--------|-------|
| Toluene         | 3.671 | 3.608 | 4.209 | 4.803  | 3.697 |
| Chloroform      | 5.932 | 5.773 | 6.510 | 7.257  | 6.051 |
| Chlorobenzene   | 6.431 | 6.215 | 6.988 | 7.770  | 6.554 |
| Dichloromethane | 7.399 | 7.048 | 7.846 | 8.742  | 7.539 |
| quinoline       | 7.445 | 7.086 | 7.883 | 8.787  | 7.588 |
| Ethanol         | 8.739 | 8.114 | 8.825 | 9.984  | 8.648 |
| Methanol        | 8.950 | 8.263 | 8.963 | 10.163 | 8.803 |
| Acetonitrile    | 9.006 | 8.306 | 8.993 | 10.215 | 8.846 |
| DMSO            | 9.158 | 8.420 | 9.095 | 10.343 | 8.941 |
| Water           | 9.374 | 8.564 | 9.214 | 10.513 | 9.098 |

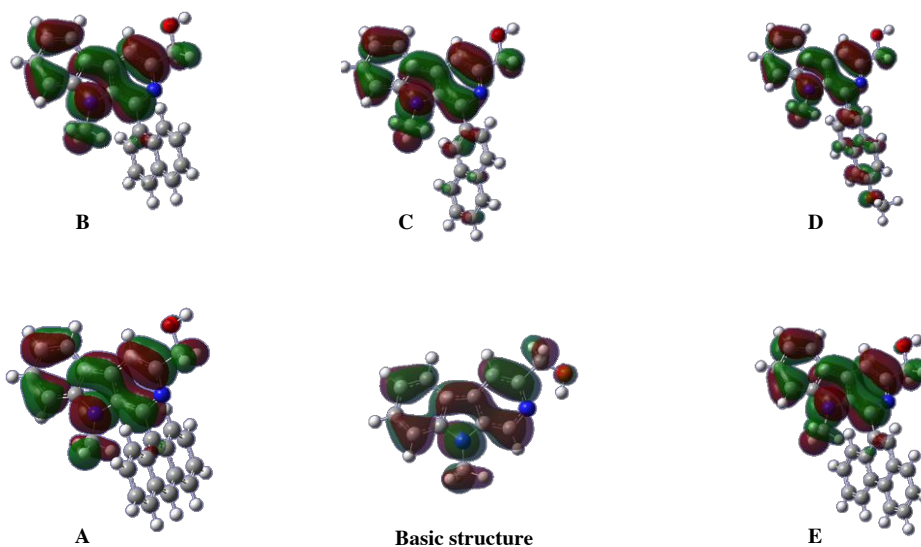


Figure 3. HOMO amplitudes of the basic structure and its aromatic substituted derivatives at B3LYP/6-311++G(d,p) level of the theory in the water phase

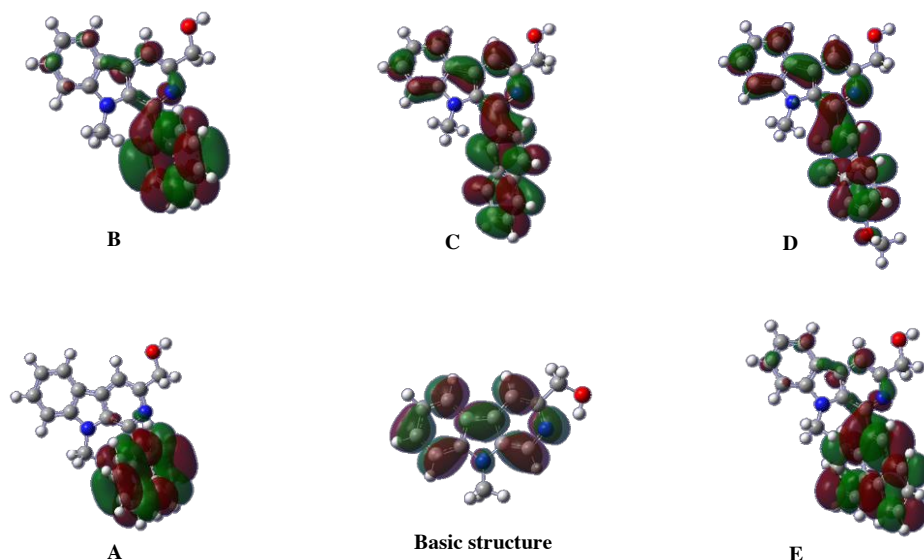


Figure 4. LUMO amplitudes of the basic structure and its aromatic substituted derivatives at B3LYP/6-311++G(d,p) level of the theory in the water phase

Figure 3 shows the HOMO amplitudes of the basic structure and its aromatic substituted derivatives at B3LYP/6-311++G(d, p) level of the theory in the water phase. The HOMO is localized on the whole molecular surface of the basic structure. On the other hand, the HOMO amplitudes of C1 aromatic substituted  $\beta$ C derivatives are very similar to that of the basic structural unit, except for the compound **D**. Although the HOMO is localized on the substituent part of each compound, just a little, it is enormously localized on the substituent part of the structure **D**. It can be concluded that the largest electron delocalization is calculated for the compound **D** more than the other substituted compounds. Also, it can be seen from Figure 3 that there is no HOMO localization on the aromatic substituent part of the compounds **A** and **B**. The LUMO amplitudes of the studied compounds are given in Figure 4, at B3LYP/6-311++G(d, p) level of the theory in the water phase. The LUMO is only localized on the aromatic part of the basic structure. For the substituted compounds, the LUMO presents very different localization from the basic structure. At first, it should be noticed that the methoxy group at C3 position and  $-\text{CH}_3$  group at N9 position are not very effective for electrophilic attack reactions of di-substituted compounds because there is no LUMO localization on these groups for all compounds including the basic structure and the substituted compounds. Second, the largest LUMO localization is calculated for the structure **D**. Finally, the LUMO of the structure **A** is only localized on the substituent group which is anthracene 9-yl substitution at C1 position of the basic structure.

Table 5. The calculated quantum chemical parameters at the B3LYP/6311++G\*\* level of the theory

| Molecule | Solvent                                    | $\Delta E$ | $\mu$  | $\eta$ | $\omega$ | $\Delta N$ |
|----------|--|------------|--------|--------|----------|------------|
| Basic    |  | 4.232      | -3.834 | 2.116  | 3.473    | 1.812      |
| A        | Toluene<br>( $\epsilon=2.37$ )             | 3.484      | -3.866 | 1.742  | 4.290    | 2.219      |
| B        |  | 4.210      | -3.653 | 2.105  | 3.170    | 1.736      |
| C        |  | 4.001      | -3.706 | 2.001  | 3.432    | 1.852      |
| D        |  | 3.985      | -3.584 | 1.993  | 3.224    | 1.799      |
| E        |  | 4.164      | -3.664 | 2.082  | 3.224    | 1.760      |
| Basic    |  | 4.221      | -3.827 | 2.111  | 3.470    | 1.813      |
| A        | Chloroform<br>( $\epsilon=4.71$ )          | 3.487      | -3.908 | 1.743  | 4.381    | 2.242      |
| B        |  | 4.205      | -3.699 | 2.102  | 3.254    | 1.759      |
| C        |  | 4.002      | -3.748 | 2.001  | 3.511    | 1.873      |
| D        |  | 3.995      | -3.636 | 1.998  | 3.309    | 1.820      |
| E        |  | 4.175      | -3.708 | 2.087  | 3.294    | 1.776      |
| Basic    |  | 4.219      | -3.827 | 2.110  | 3.471    | 1.814      |
| A        | Chloro<br>benzene<br>( $\epsilon=5.70$ )   | 3.487      | -3.918 | 1.744  | 4.403    | 2.247      |
| B        |  | 4.203      | -3.709 | 2.101  | 3.274    | 1.765      |
| C        |  | 4.002      | -3.758 | 2.001  | 3.528    | 1.878      |
| D        |  | 3.997      | -3.648 | 1.998  | 3.329    | 1.825      |
| E        |  | 4.176      | -3.718 | 2.088  | 3.310    | 1.781      |
| Basic    |  | 4.215      | -3.827 | 2.107  | 3.475    | 1.816      |
| A        | Dichloro<br>methane<br>( $\epsilon=8.93$ ) | 3.489      | -3.938 | 1.744  | 4.445    | 2.258      |
| B        |  | 4.198      | -3.729 | 2.099  | 3.313    | 1.777      |
| C        |  | 4.003      | -3.776 | 2.002  | 3.562    | 1.887      |
| D        |  | 3.999      | -3.671 | 1.999  | 3.369    | 1.836      |
| E        |  | 4.179      | -3.738 | 2.089  | 3.343    | 1.789      |
| Basic    |  | 4.215      | -3.827 | 2.107  | 3.475    | 1.816      |
| A        | Quin<br>oline<br>( $\epsilon=9.16$ )       | 3.489      | -3.939 | 1.744  | 4.447    | 2.258      |
| B        |  | 4.198      | -3.730 | 2.099  | 3.315    | 1.777      |

|       |                                      |       |        |       |       |       |
|-------|--------------------------------------|-------|--------|-------|-------|-------|
| C     |                                      | 4.003 | -3.777 | 2.002 | 3.564 | 1.887 |
| D     |                                      | 3.999 | -3.672 | 1.999 | 3.371 | 1.836 |
| E     |                                      | 4.179 | -3.739 | 2.089 | 3.345 | 1.790 |
| Basic |                                      | 4.209 | -3.828 | 2.105 | 3.481 | 1.819 |
| A     | Ethanol<br>( $\epsilon=24.85$ )      | 3.490 | -3.965 | 1.745 | 4.504 | 2.272 |
| B     |                                      | 4.190 | -3.756 | 2.095 | 3.368 | 1.793 |
| C     |                                      | 4.003 | -3.801 | 2.002 | 3.609 | 1.899 |
| D     |                                      | 3.999 | -3.701 | 1.999 | 3.425 | 1.851 |
| E     |                                      | 4.179 | -3.764 | 2.090 | 3.390 | 1.801 |
| Basic |                                      | 4.209 | -3.828 | 2.104 | 3.483 | 1.819 |
| A     | Methanol<br>( $\epsilon=32.61$ )     | 3.490 | -3.969 | 1.745 | 4.512 | 2.274 |
| B     |                                      | 4.188 | -3.760 | 2.094 | 3.376 | 1.796 |
| C     |                                      | 4.003 | -3.805 | 2.002 | 3.616 | 1.901 |
| D     |                                      | 3.999 | -3.705 | 1.999 | 3.433 | 1.853 |
| E     |                                      | 4.180 | -3.768 | 2.090 | 3.397 | 1.803 |
| Basic |                                      | 4.209 | -3.828 | 2.104 | 3.483 | 1.819 |
| A     | Acetonitrile<br>( $\epsilon=36.69$ ) | 3.490 | -3.970 | 1.745 | 4.515 | 2.275 |
| B     |                                      | 4.188 | -3.762 | 2.094 | 3.378 | 1.796 |
| C     |                                      | 4.003 | -3.806 | 2.002 | 3.618 | 1.901 |
| D     |                                      | 3.999 | -3.706 | 1.999 | 3.435 | 1.854 |
| E     |                                      | 4.180 | -3.769 | 2.090 | 3.399 | 1.804 |
| Basic |                                      | 4.208 | -3.829 | 2.104 | 3.484 | 1.820 |
| A     | DMSO<br>( $\epsilon=46.83$ )         | 3.490 | -3.973 | 1.745 | 4.522 | 2.276 |
| B     |                                      | 4.187 | -3.764 | 2.094 | 3.384 | 1.798 |
| C     |                                      | 4.003 | -3.808 | 2.002 | 3.623 | 1.903 |
| D     |                                      | 3.998 | -3.710 | 1.999 | 3.442 | 1.856 |
| E     |                                      | 4.179 | -3.772 | 2.090 | 3.405 | 1.805 |
| Basic |                                      | 4.207 | -3.829 | 2.103 | 3.485 | 1.820 |
| A     | Water<br>( $\epsilon=78.36$ )        | 3.491 | -3.976 | 1.745 | 4.530 | 2.278 |
| B     |                                      | 4.186 | -3.768 | 2.093 | 3.392 | 1.800 |
| C     |                                      | 4.003 | -3.812 | 2.002 | 3.629 | 1.904 |
| D     |                                      | 3.998 | -3.714 | 1.999 | 3.450 | 1.858 |
| E     |                                      | 4.179 | -3.776 | 2.090 | 3.411 | 1.807 |

\*  $\Delta E$ (Energy Gap),  $\mu$ ,  $\eta$ ,  $\omega$  and  $\Delta N_{max}$  are in eV.

Until now, I tried to give the picture of the regions in where the molecules work to be effective for electrophilic or nucleophilic attack reactions. It is worth to mention of the global reactivity descriptors to estimate the chemical reactivity behavior also with numerical data. Table 5 summarizes the quantum chemical parameters at the B3LYP/6-311++G(d,p) level of the theory. Recently, the DFT based quantum chemical descriptors provide a very useful information related to the pharmaceutical important molecules to explain their chemical activity behavior. The  $\Delta E$  (energy gap) order of the di-substituted structures has been computed as **A < D < C < E < B < Basic** for most of the solvents at 6-31g(d,p) and 6-31+g(d,p) basis sets just like the 6-311++g(d,p) basis set. The structure **A** has the lowest energy gap which means that it is the most reactive structure in according to these results. The electronic chemical potential of the investigated molecules has changed in the following order: **Basic < A < C < E < B < D** for more than half calculations. Here, it is estimated that the structure **A** has the lowest electronic chemical potential while the structure **D** has the highest electrochemical potential, just like the stabilization energies. The global hardness of the studied structures has varied as follow: **A < D < C < E < B < Basic** for most of the solvents at all basis sets. As it is predicted in the discussion of the energy gap, the structure **B** and basic structure seem to be the hardest molecules in all studied derivatives because they have the highest global hardness value. On the other hand, the structure **A** is the soft molecule, therefore it is the most reactive structure among the being studied structures. The electrophilicity index changes in the following order as **B < E < D < Basic < C < A** for most of the solvents at all basis sets. In accord with these results, the structure **A** seems to be the best electrophile among in all studied structures. The  $\Delta N$  changes **Basic < E < B < D < C < A** for more than half of the solvents at all basis sets, and the structure **A** has the highest  $\Delta N$ . Finally, the structure **A** is the soft, least stable and therefore more reactive structure in addition to having the best electron transfer capability and it can be suggested that the anthracene-9-yl substitution at C1 position has increased the chemical activity more than the other substituent groups.

#### 4. CONCLUSIONS

This work dealt with the chemical reactivity behavior of the 9-hydro-pyrido (3,4-*b*) indole compounds by using the computational tools to obtain the solvation free energy and global reactivity descriptors, at three basis sets and in ten solvent environments. One of the most important results is that the solvation free energy depends on the solvent media as well as the basis set. In accordance with the quantum chemical descriptor results, the compound **A** is predicted as the most reactive compound in all studied compounds with the lowest energy gap, lowest electronic chemical potential and, lowest hardness value. Also, the structure **A** was determined as the best electrophile as well as having the highest maximum charge transfer capability. In conclusion, it can be suggested that the anthracene-9-yl substitution at C1 position has increased the chemical activity more than the other substituent groups.

## ACKNOWLEDGMENT

The author thanks to acknowledge the financial support of the scientific research projects of Cumhuriyet University (Project No: EĞT-066). The all calculations have been conducted at TUBITAK ULAKBIM, High Performance and Grid Computing Center (TR-Grid e- Infrastructure).

## REFERENCES

- [1] L. Martin, A. Leon, M. A. Martin, B. Castillo and J.C. Menendez, "Detection and characterization of cyclodextrin complexes with  $\beta$ -carboline derivatives by spectroscopic techniques", *Journal of Pharmaceutical and Biomedical Analysis*, 32, 991-1001, 2003.
- [2] K. Pari, C.S. Sundari, S. Chandani and D. Balasubramanian, " $\beta$ -Carbolines That Accumulate in Human Tissues May Serve a Protective Role against Oxidative Stress. *THE JOURNAL OF BIOLOGICAL CHEMISTRY*", 275(4), 2455-2462, 2000.
- [3] M. R. Prinsep, J. W. Blunt and M. H. G. Munro, "New Cytotoxic  $\beta$ -Carboline Alkaloids from the Marine Bryozoan, *Cribricellina Cribraria*", *Journal of Natural Products*, 54(4), 1068-1076, 1991.
- [4] K. P. Lippke, W. G. Schunack, W. Wenning and W. E.Müller WE, " $\beta$ -Carbolines as Benzodiazepine Receptor Ligands. 1. Synthesis and Benzodiazepine Receptor Interaction of Esters of  $\beta$ -Carboline-3-carboxylic Acid", *J. Med. Chem.*, 26, 499-503, 1983.
- [5] T. J. Hagen, P. Skolnick and J.M. Cook JM, "Synthesis of 6-Substituted  $\beta$ -Carbolines That Behave as Benzodiazepine Receptor Antagonists or Inverse Agonists" *J. Med. Chem.*, 30: 750-753, 1983.
- [6] G. Dorey, G. Poissonnet, M.C. Potier, L.P. Carvalho, P. Venault, G. Chapouthier, J. Rossier, P. Potier and R. H. Dodd, "Synthesis and Benzodiazepine Receptor Affinities of Rigid Analogs of 3-Carboxy- $\beta$ -carbolines: Demonstration That the Benzodiazepine Receptor Recognizes Preferentially the *s*-Cis Conformation of the 3-Carboxy Group" *J. Med. Chem.*, 32, 1799-1804, 1989.
- [7] J. Jimenez, L. Riveron-Negrete, F. Abdullaev, J. Espinosa-Aguirre and R. Rodriguez-Arnaiz, "Cytotoxicity of the  $\beta$ -carboline alkaloids harmine and harmaline in human cell assays in vitro", *Experimental and Toxicologic Pathology*, 60, 381-389, 2008.
- [8] M. A. Rashid, K. R. Gustafson, R. Michael and M. R. Boyd "New Cytotoxic *N*-Methylated  $\beta$ -Carboline Alkaloids from the Marine Ascidian *Eudistoma gilboverde*", *J. Nat. Prod.*, 64, 1454-1456, 2001.
- [9] R. Cao, W. Peng, H. Chen, X. Hou, H. Guan, Q. Chen, Y. Ma and A. Xu, "Synthesis and in vitro cytotoxic evaluation of 1,3-bisubstituted and 1,3,9-trisubstituted  $\beta$ -carboline derivatives", *European Journal of Medicinal Chemistry*, 40, 249-257, 2005.
- [10] B. Bai, X. Y. Li, L. Liu, Y. Li and H. J. Zhu, "Design, synthesis and cytotoxic activities of novel  $\beta$ -amino alcohol derivatives" *Bioorganic & Medicinal Chemistry Letters*, 21, 2302-2304, 2011.
- [11] Z. Chen, R. Cao, B. Shi, L. Guo, J. Sun, Q. Ma, W. Fan and H. Song, "Synthesis and biological evaluation of 1,9-disubstituted  $\beta$ -carbolines as potent DNA intercalating and cytotoxic agents", *European Journal of Medicinal Chemistry*, 46, 5127-5137, 2011.
- [12] P. Salehi, K. Babanezhad-Harikandei, M. Bararjanian, A. Al-Harrasi, M. A. Esmaeili and A. Aliahmadi, "Synthesis of novel 1,2,3-triazole tethered 1,3-disubstituted  $\beta$ -carboline derivatives and their cytotoxic and antibacterial activities", *Med. Chem. Res.*, 25, 1895-1907, 2016.
- [13] O. I. Tarzi and R. Erra-Balsells, "Effect of chlorine as substituent on the photochemistry and acid-base properties of  $\beta$ -carboline alkaloids", *Journal of Photochemistry and Photobiology B: Biology*, 82, 79-93, 2006.
- [14] R. S. Kusrkar and S. K. Goswami, "Efficient one-pot synthesis of anti-HIV and anti-tumour  $\beta$ -carbolines", *Tetrahedron*, 60, 5315-5318, 2004.
- [15] O. I. Tarzi and R. Erra-Balsells, "Effect of chlorine as substituent on the photochemistry and acid-base properties of  $\beta$ -carboline alkaloids", *Journal of Photochemistry and Photobiology B: Biology*, 82, 79-93, 2006.
- [16] D. Reyman, M. J. Tapia, C. Carcedob and M. H. Vinas, "Photophysical properties of methyl  $\beta$ -carboline-3-carboxylate mediated by hydrogen-bonded complexes—a comparative study in different solvents", *Biophysical Chemistry*, 104, 683-696, 2003.
- [17] A. D. Becke, "A new mixing of Hartree-Fock and local density-functional theories", *J. Chem. Phys.*, 98, 1372- 1377, 1993.
- [18] P. Lee, W. Yang and R. G. Parr, "Development of the Colle-Salvetti correlation-energy formula into a functional of the electron density", *Phys Rev.*, B37, 785- 789, 1988.
- [19] Gaussian 09 D.01. (2013) Gaussian, Inc, Wallingford CT.
- [20] J. B. Foresman, T. A. Keith, K. B. Wiberg, J. Snoonian, M. J. Frisch M.J, "Solvent Effects. 5. Influence of Cavity Shape, Truncation of Electrostatics, and Electron Correlation on *ab Initio* Reaction Field Calculations", *J. Phys. Chem.* 100, 16098-16104, 1996.
- [21] J. Tomasi, B. Mennuci and R. Cammi, "Quantum Mechanical Continuum Solvation Models", *Chem. Rev.*, 105, 2999- 3093, 2005.
- [22] Fukui K., "Role of frontier orbitals in chemical reactions", *Science*, 218(4574), 747- 754, 1982.
- [23] F. Jensen, *Introduction to Computational Chemistry*, John Wiley and Sons Ltd., West Sussex, Chapter 6, p. 257, 2007.
- [24] R. G. Parr, L. V. Szentpaly and S. Liu, "Electrophilicity Index", *J. Am. Chem. Soc.*, 121, 1922-1924, 1999.
- [25] K. B. Wiberg, "Properties of Some Condensed Aromatic Systems", *J. Org. Chem.*, 62, 5720-5727, 1997.

## BIOGRAPHY

Goncagül Serdaroglu has completed her PhD from Cumhuriyet University (2008) and postdoctoral studies from Auburn University (2013). Her major research interests are in electronic structure methods and their applications to pharmaceutical important molecules by using the computational tool. Recently, she has focused on the spectral analysis of organic molecules.

# A Computational Study on the Nor-Harman derivatives

*Goncagül Serdaroğlu<sup>1</sup>, Mustafa Elik*

## Abstract

*DFT calculations have been conducted to predict of their stabilization energies in the gas phase and water phase performed with the three basis sets. Table 1 clearly shows that, as the basis set grows, the calculate solvation free energy of each structure increases. Also, each structure exhibits a more stable structure in water phase than that of the gas phase. The Solvation free energy decreases as 1> 2> 3 for all basis sets in both the gas phase and water phase from Table 1 because the substituted groups on N9 position is different with each other. As the hydrophobic character of the substituted group on position N9 increases, then solvation free energy decreases. Some quantum chemical parameters such as electrophilic properties and chemical potentials have been determined as well as solvation energies and these parameters have been used to predict how these compounds will have chemical behavior on electrophilic/ nucleophilic reactions.*

**Keywords:** Global reactivity descriptors, MEP diagrams, nor-harman derivatives, solvent effect

## 1. INTRODUCTION

Nor-Harman (9H-pyrido[3,4-b]indole) as a member of the  $\beta$ C alkaloids [1]. has been studied commonly because of its biochemical and pharmaceutical importance. These group compounds are an important role in pharmaceutical chemistry, medicinal chemistry, biological science, etc. [2] because of their tricyclic hetero-aromatic structures make them potential donor-acceptor hydrogen-bonding sites, as well as the strong electron donor centers. [3] In the past, many of the studies focused on the effect of these compounds acting on central nervous system (CNS). [4-8] Cao and co-worker [4] concluded that a short alkyl or benzyl substituent at position -9 is very important the more antitumor activities and lower toxicities than the other compounds. Moreover, they [9] searched the novel compounds by synthesizing the -2, 7 and 9 substituted  $\beta$ Cs and confirmed that the substituent group in the position -2 and -9 were a very important role in modulation of their antitumor activities. In another work, the cytotoxicity of the  $\beta$ - carboline alkaloids [10] was investigated and it was concluded that harmine was defined as a useful inhibitor of the tumor development. Etienne and co-workers [11] investigated the absorption behaviors of the Harmane by using the QM/MM; they found out the two stable non-covalent interaction between harmane and DNA. Photophysical properties of the nor- harmane were investigated by Mallick and co-worker in different aqueous micellar media because of the fluorescent molecules susceptible to proton transfer reactions. [12]

As we have searched in literature, there is much research of the nor-Harman and its derivatives because of their pharmaceutical importance, but still, the fundamental biochemical phenomena underlying these properties is not clear. For this reason, we have decided to search the physicochemical and quantum chemical parameters to explain the chemical reactivity behavior of these compounds.

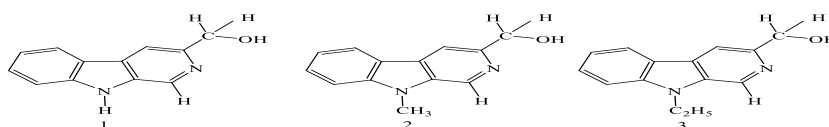


Figure 1. The chemical structures of the nor-harman derivatives.

## 2. COMPUTATIONAL METHOD

All studied nor-Harman derivatives depicted in Figure 1 were optimized at 6-31G(d,p) basis set in the gas phase. Accordingly, the stable structures optimized in the gas phase were used as starting structure in the 10 solvents media to look for the solvent effect on the physicochemical and quantum chemical parameters at the 6-31G(d,p). Also, the optimized structures at the 6-31G(d,p) basis set in the gas phase were used as the starting structure for the upper basis set. The same calculation routes were repeated for the 6-31+G(d,p) the 6-311++G(d,p) basis sets to look for the basis set effect on the chemical reactivity behavior of these compounds. Gaussian 09W [13] software package was used for all DFT calculations at B3LYP level of theory [14-15] at three basis sets. The IPCM (Polarized Continuum Model (PCM) with Isodensity version) was used to investigate the solvent effect on the chemical reactivity behavior of the studied compounds. The solvent media calculations [16-17] in the 10 solvent environments with  $\epsilon=2.37, 4.71, 5.70, 8.93, 9.16, 24.85, 32.61, 36.69, 46.83, 78.36$  were performed to simulate Toluene (T),  $\text{CHCl}_3$  (Chloroform, C),  $\text{C}_6\text{H}_5\text{Cl}$  (Chlorobenzene, CB),  $\text{CH}_2\text{Cl}_2$  (Dichloromethane, DCM), Quinoline (Q),  $\text{C}_2\text{H}_5\text{OH}$  (ethanol, E),  $\text{CH}_3\text{OH}$  (Methanol, M), Acetonitrile (A), DMSO (dimethylsulfoxide, DMSO),  $\text{H}_2\text{O}$  (water), respectively. All optimized structures in both the gas and water phases were verified by absence of any imaginary frequency by performing the frequency calculations. The Ionization energy (I) and electron affinity (A) in according to the Koopmans Theorem [18] as follow: can be expressed through HOMO and LUMO orbital energies [19] as follow:

$$I = -E_{\text{HOMO}} \quad (1)$$

$$A = -E_{\text{LUMO}} \quad (2)$$

Parr R.G. and co-workers [20] have defined the DFT based global descriptors which are electronic chemical potential ( $\mu$ ), global hardness ( $\eta$ ), electrophilicity ( $\omega$ ) and the maximum charge transfer index ( $\Delta N_{\text{max}}$ ) as follow:

$$\mu = -\frac{I+A}{2} \quad (3)$$

$$\eta = \frac{I-A}{2} \quad (4)$$

$$\omega = \frac{\mu^2}{2\eta} \quad (5)$$

$$\Delta N_{\text{max}} = \frac{I+A}{2(I-A)} \quad (6)$$

## 3. RESULTS AND DISCUSSION

Figure 1 shows the solvation free energy ongoing from the gas phase to the water phase for nor-Harmane derivatives. As it is seen, the solvation free energy increases as the solvent dielectric constant increases, in systematically, because of the more dielectric constant causing the more polarization resulting the more stabilization in the molecule. But, this systematic changing in the solvation free energy changing for each structure was not calculated for the basis sets used in this work; the solvation free energy for the 631+g\*\* basis set is bigger than the 6311++g\*\* basis set which is the largest basis set than those of the other basis sets used in this work. Also, the selected numerical data for the toluene and water phases were given in Table 1. In according to these results, the structure **1** is predicted as the most stabilized structure also there is a systematic increase in solvation free energy with the solvent dielectric constant at all basis sets.

Table 1. The Solvation Free Energies both in the toluene phase and in the aqueous phase

| Molecule | Toluene |          |            | Water   |          |            |
|----------|---------|----------|------------|---------|----------|------------|
|          | 6-31G** | 6-31+G** | 6-311++G** | 6-31G** | 6-31+G** | 6-311++G** |
| <b>1</b> | 3.2951  | 3.7764   | 3.7211     | 7.36696 | 8.47138  | 8.36972    |
| <b>2</b> | 2.9355  | 3.3509   | 3.4701     | 6.64909 | 7.70582  | 7.80245    |
| <b>3</b> | 2.5527  | 2.8439   | 2.9267     | 6.44703 | 7.55270  | 7.45858    |

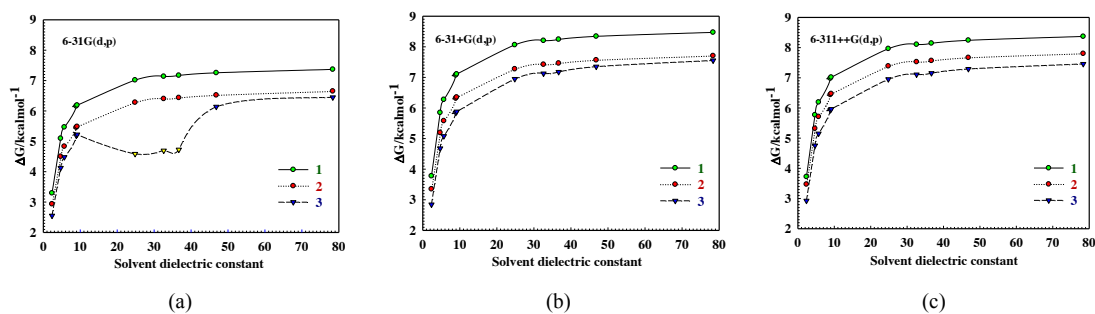


Figure 2. Solvation Free Energies as a function of the solvent dielectric constant for the Nor harman derivatives. (a) B3LYP/ 6-31g(d,p), (b) B3LYP/ 6-31+g(d,p), (c) B3LYP/ 6-311++g(d,p)

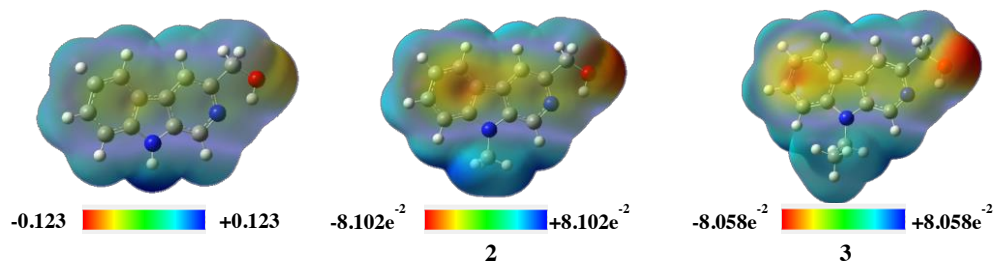


Figure 3. ESP (electrostatic potential) mapped on the electron density surface calculated by B3LYP/6-311++G\*\* level of theory for the nor-harmane derivatives in the aqueous phase

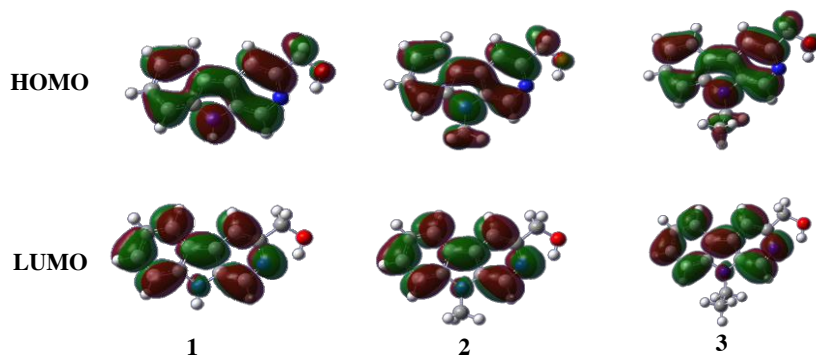


Figure 4. HOMO and LUMO amplitudes of nor-Harman derivatives with B3LYP/6311++G\*\* basis set in water

Figure 3 shows the ESP (electrostatic potential) mapped on the electron density surface calculated by B3LYP/6-311++G\*\* level of theory for the nor-harmane derivatives in the aqueous phase (Iso value:0.0004). It is determined that the lone pair electrons of the oxygen atom on each compound are the electron-rich region with the red color which shows the nucleophilic attack center of each molecule. Moreover, it can be seen that the indole ring for the compounds **2** and **3** is the red color. The electron density value on the total density surface has changed in the following order of **1** < **2** < **3**. It is clear that the structure **1** most stabilized with solvent dielectric constant has the lowest electrostatic potential value on the total density surface of itself. Figure 4 has visualized the HOMO and LUMO amplitudes of nor-Harman derivatives with B3LYP/6-311++G\*\* basis set in water. The HOMO is localized on the whole molecular surface of each compound. On the other hand, LUMO is localized on the aromatic part of each compound. Here, it is important to see that the substituent groups on position -9 and methoxy group on the position -3 are not effective for the electrophilic attack reactions because there is no LUMO localization for each compound.

Table 2. The calculated quantum chemical parameters with the B3LYP/6-311++G\*\* basis set

| Molecule | Solvent               | $\Delta E$ | $\mu$   | $\eta$ | $\omega$ | $\Delta N_{max}$ |
|----------|-----------------------|------------|---------|--------|----------|------------------|
| 1        | Toluen                | 4.3571     | -3.9141 | 2.1785 | 3.5161   | 1.7967           |
| 2        | ( $\epsilon= 2.37$ )  | 4.2325     | -3.8341 | 2.1162 | 3.4732   | 1.8118           |
| 3        |                       | 4.2199     | -3.8191 | 2.1100 | 3.4564   | 1.8100           |
| 1        | Chloroform            | 4.3478     | -3.8997 | 2.1739 | 3.4977   | 1.7938           |
| 2        | ( $\epsilon= 4.71$ )  | 4.2213     | -3.8274 | 2.1107 | 3.4703   | 1.8134           |
| 3        |                       | 4.2107     | -3.8161 | 2.1053 | 3.4585   | 1.8126           |
| 1        | Chlorobenzen          | 4.3457     | -3.8978 | 2.1728 | 3.4960   | 1.7939           |
| 2        | e                     | 4.2191     | -3.8269 | 2.1096 | 3.4711   | 1.8141           |
| 3        | ( $\epsilon= 5.70$ )  | 4.2088     | -3.8165 | 2.1044 | 3.4608   | 1.8136           |
| 1        | Dichloromethane       | 4.3416     | -3.8949 | 2.1708 | 3.4942   | 1.7942           |
| 2        |                       | 4.2148     | -3.8269 | 2.1074 | 3.4747   | 1.8159           |
| 3        | ( $\epsilon= 8.93$ )  | 4.2050     | -3.8182 | 2.1025 | 3.4669   | 1.8160           |
| 1        | Quinoline             | 4.3413     | -3.8948 | 2.1707 | 3.4942   | 1.7943           |
| 2        |                       | 4.2145     | -3.8267 | 2.1073 | 3.4747   | 1.8160           |
| 3        | ( $\epsilon= 9.16$ )  | 4.2050     | -3.8182 | 2.1025 | 3.4669   | 1.8160           |
| 1        | Ethanol               | 4.3364     | -3.8929 | 2.1682 | 3.4947   | 1.7954           |
| 2        | ( $\epsilon= 24.85$ ) | 4.2093     | -3.8280 | 2.1047 | 3.4811   | 1.8188           |
| 3        |                       | 4.2006     | -3.8214 | 2.1003 | 3.4765   | 1.8195           |
| 1        | Methanol              | 4.3359     | -3.8926 | 2.1679 | 3.4946   | 1.7955           |
| 2        | ( $\epsilon= 32.61$ ) | 4.2085     | -3.8284 | 2.1043 | 3.4826   | 1.8193           |

|   |                      |        |         |        |        |        |
|---|----------------------|--------|---------|--------|--------|--------|
| 3 |                      | 4.2001 | -3.8220 | 2.1000 | 3.4779 | 1.8200 |
| 1 | Acetonitrile         | 4.3353 | -3.8926 | 2.1677 | 3.4951 | 1.7958 |
| 2 | ( $\epsilon=36.69$ ) | 4.2085 | -3.8284 | 2.1043 | 3.4826 | 1.8193 |
| 3 |                      | 4.1998 | -3.8221 | 2.0999 | 3.4784 | 1.8201 |
| 1 | DMSO                 | 4.3350 | -3.8925 | 2.1675 | 3.4950 | 1.7958 |
| 2 | ( $\epsilon=46.83$ ) | 4.2080 | -3.8286 | 2.1040 | 3.4835 | 1.8197 |
| 3 |                      | 4.1993 | -3.8227 | 2.0996 | 3.4798 | 1.8206 |
| 1 | Water                | 4.3342 | -3.8923 | 2.1671 | 3.4955 | 1.7961 |
| 2 | ( $\epsilon=78.36$ ) | 4.2069 | -3.8289 | 2.1034 | 3.4849 | 1.8203 |
| 3 |                      | 4.1990 | -3.8233 | 2.0995 | 3.4813 | 1.8211 |

\*  $\Delta E$ (Energy Gap),  $\mu$ ,  $\eta$ ,  $\omega$  and  $\Delta N_{max}$  are in eV.

Table 2 presents the calculated quantum chemical parameters of the studied compounds, at the B3LYP/6-311++G\*\* basis set. The energy gap ( $\Delta E$ ) of nor-Harman derivatives increased in the following order: **3** < **2** < **1** at B3LYP/6-311++G\*\* basis set in solvent environments. The electronic chemical potential ( $\mu$ ) changed as follows: **1** < **2** < **3** in all solvents. The global hardness ( $\eta$ ) calculated in the order of **3** < **2** < **1** in all solvent media. On the other hand, the electrophilicity ( $\omega$ ) changed in the order of **3** < **2** < **1**, and the maximum charge transfer capability ( $\Delta N$ ) has changed as **1** < **2** < **3**, at B3LYP/6-311++G\*\* level of the theory in all solvent media. As known-well, the lowest energy gap and lowest global hardness mean the highest chemical reactivity. In according to the energy gap, global hardness, and electronic chemical potential value, it can be suggested that the structure **3** is more reactive than the other compounds while the structure **1** is the less reactive than the other compounds in all solvents. Finally, we can suggest that the structure **1** is the best electrophile more than the other compounds and the structure **3** has the biggest charge transfer capability more than the other compound.

#### 4. CONCLUSIONS

In this work, the three nor-Harman compounds were investigated by computational tools to explain the chemical stability and reactivity behavior of them. It is estimated that the solvation free energy strongly depends on the basis set and on the solvent media. The electron density value on the total density surface has changed in the following order of **1** < **2** < **3**. In according to the global reactivity descriptors, the structure **1** is most reactive whereas the structure **3** is the less reactive.

#### ACKNOWLEDGMENT

The author thanks to acknowledge the financial support of the scientific research projects department of Cumhuriyet University (Project No: EĞT-053). The all calculations have been conducted at TUBITAK ULAKBIM, High Performance and Grid Computing Center (TR-Grid e- Infrastructure).

#### REFERENCES

- [1] T. Herraiz, H. Guillen and V. J. Aran, "Oxidative Metabolism of the Bioactive and Naturally Occurring  $\beta$ -Carboline Alkaloids, Norharman and Harman, by Human Cytochrome P450 Enzymes", *Chem. Res. Toxicol.*, 21, 2172–2180, 2008.
- [2] M. C. Biondic M. C and R. Erra-Balsells, "Photochemical behaviour of  $\beta$ -carbolines. Part 4.1 Acid–base equilibria in the ground and excited states in organic media", *J. Chem. Soc., Perkin Trans.*, 2, 1323-1327, 1997.
- [3] M. A. Munoz, O. Sama, M. Galan, P. Guardado, C. Carmona and M. Balon, "Interactions between Betacarboline and Benzenoid  $\pi$  Bases: FTIR Evidence for the Formation of NH- $\pi$  Hydrogen Bonds", *J. Phys. Chem. B.*, 103, 8794-8798, 1999.
- [4] R. Cao, Q. Chen, X. Hou, H. Chen, H. Guan, Y. Ma, W. Peng and A. Xu. "Synthesis, acute toxicities, and antitumor effects of novel 9-substituted  $\beta$ -carboline derivatives", *Bioorganic & Medicinal Chemistry* 12, 4613–4623, 2004.
- [5] R. S. Kusrkar and S. K. Goswami, "Efficient one-pot synthesis of anti-HIV and anti-tumour  $\beta$ -carbolines", *Tetrahedron*, 60, 5315–5318, 2004.
- [6] A. Mallick and N. Chattopadhyay, "Photophysics of norharmane in micellar environments: a fluorometric study", *Biophysical Chemistry* 109, 261–270, 2004.

- [7] Q. Chen<sup>1</sup>, R. Chao, H. Chen, X. Hou, H. Yan, S. Zhou, W. Peng and A. Xu, "Antitumor and neurotoxic effects of novel harmine derivatives and structure-activity relationship analysis", *Int. J. Cancer*: 114, 675–682, 2004.
- [8] O. I. Tarzi and R. Erra-Balsells, "Effect of chlorine as substituent on the photochemistry and acid–base properties of  $\beta$ -carboline alkaloids", *Journal of Photochemistry and Photobiology B: Biology*, 82, 79–93, 2006.
- [9] R. Cao, W. Fan, L. Guo, Q. Ma, G. Zhang, J. Li and X. Chen, "Synthesis and structure eactivity relationships of harmine derivatives as potential antitumor agents" *European Journal of Medicinal Chemistry* 60, 135- 143, 2013.
- [10] J. Jimenez, L. Riveron-Negrete, F. Abdullaev, J. Espinosa-Aguirre and R. Rodriguez-Arnaiz, "Cytotoxicity of the  $\beta$ -carboline alkaloids harmine and harmaline in human cell assays in vitro" *Experimental and Toxicologic Pathology*, 60, 381–389, 2008.
- [11] T. Etienne, T. Very, E. A. Perpète, A. Monari and X. Assfeld, "A QM/MM Study of the Absorption Spectrum of Harmane in Water Solution and Interacting with DNA: The Crucial Role of Dynamic Effects", *J. Phys. Chem. B*, 117, 4973–4980, 2013.
- [12] A. Mallick and N. Chattopadhyay, "Photophysics of norharmane in micellar environments: a fluorometric study", *Biophysical Chemistry*, 109, 261–270, 2004.
- [13] Gaussian 09 D.01. (2013) Gaussian, Inc, Wallingford CT.
- [14] A. D. Becke, "A new mixing of Hartree–Fock and local density-functional theories", *J. Chem. Phys.*, 98, 1372- 1377, 1993.
- [15] C. Lee, W. Yang and R. G. Parr, "Development of the Colle-Salvetti correlation-energy formula into a functional of the electron density", *Phys Rev.*, B37, 785- 789, 1988.
- [16] J. B. Foresman, T. A. Keith, K. B. Wiberg, J. Snoonian, M. J. Frisch M.J., "Solvent Effects. 5. Influence of Cavity Shape, Truncation of Electrostatics, and Electron Correlation on *ab Initio* Reaction Field Calculations", *J. Phys. Chem.* 100, 16098-16104, 1996.
- [17] J. Tomasi, B. Mennucci and R. Cammi, "Quantum Mechanical Continuum Solvation Models", *Chem. Rev.*, 105, 2999- 3093, 2005.
- [18] Fukui K., "Role of frontier orbitals in chemical reactions", *Science*, 218(4574), 747- 754, 1982.
- [19] F. Jensen, *Introduction to Computational Chemistry*, John Wiley and Sons Ltd., West Sussex, Chapter 6, p. 257, 2007.
- [20] R. G. Parr, L. V. Szentpaly and S. Liu, "Electrophilicity Index", *J. Am. Chem. Soc.*, 121, 1922-1924, 1999.

## BIOGRAPHY

Goncagül Serdaroğlu has completed her PhD from Cumhuriyet University (2008) and postdoctoral studies from Auburn University (2013). Her major research interests are in electronic structure methods and their applications to pharmaceutical important molecules by using the computational tool. Recently, she has focused on the spectral analysis of organic molecules.



## PRODUCTION OF LITHIUM TETRABORATE TETRAHYDRATE BY SPRAY DRIER METHOD AND DETERMINATION OF PRODUCTION CONDITIONS

Mehmet Sait İZGİ<sup>1</sup>, Halil DEMİR, Orhan BAYTAR,

Vedat ADIGÜZEL, Sevilay DEMİRCİ

---

### Abstract

The crystallization process, which is a surface process, consists of the step of diffusing the substance from the crystal surface in an oversaturated solution and the step of depositing the substance from the surface into the crystal network. Each of these stages is under the influence of different forces and factors. The various impurities present in the solution medium affect the crystal's exterior appearance and particle size distribution as the pH of the medium and the hydrodynamic conditions of the environment in which the crystallization is carried out are affected. It is aimed to determine the industrial production conditions of lithium tetraborate tetrahydrate. Since Lithium Tetraborate Tetrahydrate is prone to oversaturation, the production was carried out using the Spray Dryer system. When the input air temperature of 230 °C was used, the product was found to be in the product trihydrate structure in the TG-DTA and boroxide analysis results. When 170 °C drying air was used, the obtained structure was determined to be between tetra and trihydrate. On the other hand, it has been determined that it is possible to produce 5% -20% of Lithium Tetraborate Trihydrate using Spray Dryer.

**Keywords:** Crystallization, Lithium Tetraborate Tetrahydrate, Spraydrier, TG-Dta

---

## 1. INTRODUCTION

### 1.1. Crystallization

**a-** Crystallization is a process which is carried out in the chemical process industry in order to obtain the reaction product in solution or to obtain it in solid form and in purified form. In order to be able to carry out the crystallization process with very common use as purification and separation technique; the solubilized material must become saturated in the solution. This condition, which is considered to be a condition for the crystallization to take place, may not be sufficient for crystal formation. Some solutions are known to continuously increase oversaturation without crystallization. These;

1. By cooling (solution cooled)
2. Evaporation of the solvent
3. With chemical reaction
4. Use of a second solvent

**b-** Nucleation of the supersaturated solution is required. This creates sufficient conditions for crystallization. Nucleation is the process of forming a new solid surface in clear solution.

- c. The last condition is that the nuclei formed in the supersaturated solution grow due to the concentration driving force [1-3]. In recent years there have been studies of particle size distribution in solution that can capture the crystal image at the same time as FBRM technology controlled in industrial crystallization technology[4].

### 1.2. Boron Element

The boron (B) element is the only nonmetal in the IIIA group of the periodic table. Carbon (C) and Silicon (Si) are much more similar to other elements in the boron element group with atomic weight 10.81 g / mol, atomic number 5. There are two stable boron isotopes in nature, <sup>10</sup>B, which is 19.10-20.31% and <sup>11</sup>B, which is 79.69-80.90%. Boron minerals found mostly in nature are alkali and alkaline earth borates, borax, Na<sub>2</sub>B<sub>4</sub>O<sub>7</sub>·10H<sub>2</sub>O, kernite, Na<sub>2</sub>B<sub>4</sub>O<sub>7</sub>·4H<sub>2</sub>O, colemanite, Ca<sub>2</sub>B<sub>6</sub>O<sub>11</sub>·5H<sub>2</sub>O and ulexite NaCaB<sub>5</sub>O<sub>9</sub>·8H<sub>2</sub>O.

### 1.3. Fields of application

The boron element is used in a wide variety of industrial branches, from metallurgy to electronics. Other fields of application are ceramic, pyrotechnics and nuclear chemistry. Boron is not toxic. Inhaling boron powder in workplaces should be avoided. The pipe is used as a deoxidizing and degassing agent in brass and bronze alloys to increase the conductivity of copper in turbojet engines [5, 6], ] to harden steel mixtures made from other metals. Examples are ferroboron and manganese boron alloys. Another metallurgical application area is the construction of amorphous magnetic alloys containing iron, nickel or cobalt as well as boron.

Boron is used as a raw magnet to pull the voltage from high voltage to low level in power converters. Another material with permanent magnetic properties is neodymium-iron-boron, Nd<sub>2</sub>Fe<sub>14</sub>B. Aimants Ugima, a member of the Pechiney Group, leads the production of rare earth magnets both in the United States and in Europe. Japanese Sunitomo Special Metals produces these rare earth magnets (magnets), which are known under the trade name of Neomax. In 1987, the first world solar challenge race won the electric motor produced using Nd<sub>2</sub>Fe<sub>14</sub>B. It has also patented Nd<sub>2</sub>Fe<sub>14</sub>B -bonded polymer materials that can be easily shaped to make electronic devices such as computer switches and speakers. Polycrystalline silicon carbide was prepared using SiC, ceramic boron and β-silicon carbide [7]. Boron is used as a sintering agent to concentrate the sintered body by 0.3 to 3% by weight. The increased density increases the strength.

The boron fibers are formed by a chemical vapor deposition process on boron trichloride over tungsten metal. High performance enhancer boron fibers can be obtained with a diameter of 10-20 μm. These are mainly used in aluminum and titanium in epoxy resins. It is used commercially in golf club shafts, tennis rackets and fishing rods. Besides these, aviation industry is mainly used. Boron is an important material to work on as a solid fuel in jets [8]. On the other hand, fine particles (average size of 0.3μm) are used as solid fuel producing gas in rockets [6]. Boron mixed with an oxide is used pyrotechnically. Thus, it is used in the construction of war equipment such as missiles and bullets in terms of military. However, it is used in the airbag, which is a safety accessory in cars. At this point, sodium azide, which fills the air bag with nitrogen in the event of danger, is started. Other boron compounds can also be used in air cushion and pyrotechnic applications.

### 1.4. Lithium Borates

Two compounds of lithium borate have commercial designation, tetraborate tetrahydrate and metaborate hydrates. Dilithium tetraborate tetrahydrate has a density of 1.188 g/mL, expressed as Li<sub>2</sub>B<sub>4</sub>O<sub>7</sub>·3H<sub>2</sub>O or Li<sub>2</sub>O<sub>2</sub>B<sub>2</sub>O<sub>3</sub>·3H<sub>2</sub>O. Lithium Tetraborate Tetrahydrate is hardly crystallized after boiling for a few hours in oversaturated solutions of boric acid and lithium hydroxide, but converting it to a gelatinous structure. The trihydrate is stable up to 180 °C. After this temperature it turns into anhydrous structure at 320 °C and melts at 800 °C. Lithium Metabolic Octahydrate LiBO<sub>2</sub>·8H<sub>2</sub>O or Li<sub>2</sub>OB<sub>2</sub>O<sub>3</sub>·16H<sub>2</sub>O in crystal structure hexagonal, density 1.825 g/mL. The structural formula is Li[B(OH)<sub>4</sub>·16H<sub>2</sub>O]. When heated up to 70 °C, 6 moles of water is lost and the remaining 2 moles of water is lost between 140 and 280 °C.

## 2. MATERIAL METHOD

### 2.1. Spray Dryer

Spray dryer is a one-step process that turns the system into flowing liquid. The fluid is sprayed with a rotating disk or nozzle and the sprayed droplet is brought into contact with a hot gas and generally air. A rapid evaporation does not affect the product when the resultant temperature causes it to fall. The drying time of falling drops is shorter than many other systems. Low temperature drying and short drying allow spray drying of products sensitive to temperature. Spray dryers are used in sensitive chemicals for food, daily products, blood plasma, various organic and inorganic compounds, plastics, ceramic powders, detergents and so on. The moisture content and temperature of some spray dryer-dried products and the inlet and outlet air used during drying are given as the spray type.

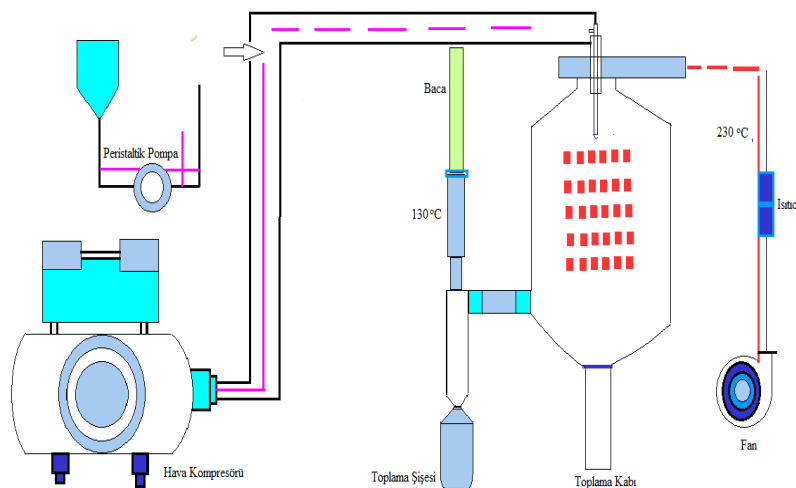


Figure 1. Flow Chart of Spray Dryer.

We can list the advantages of the spray dryer as follows:

- 1- Product characteristics and quality are effectively controlled.
- 2- Heat sensitive foods, biological products and pharmaceuticals can be dried at atmospheric pressure and at low temperatures. In some cases, it may create an inert atmosphere.
- 3- Spray dryer allows continuous and simple production of high quantity products.
- 4- The product comes into dry contact with the surface of the system where it is produced. This eliminates the corrosion problem and simplifies the selection of the material used in the production of the system.
- 5- Spray dryer produces uniform products with homogeneous, spherical and almost identical structure.
- 6- Operation temperature can be changed between 1500C - 600C. Productivity is comparable to direct dryers.

Despite all these advantages, there are disadvantages that Spray Dryer systems have.

- 1- Spray dryer systems fail in the case of high cast density products.
- 2- They are usually not flexible. The production of large particles or vice versa cannot be done in a system with a small spray.
- 3- Despite other dryers, the first investment is more.
- 4- The removal of the product and the collection of the resulting dusting increase the drying rate.
- 5- For a higher evaporation than the given capacity, a desiccant different from the others is usually desired. The feed should be pumpable.

Spray dryer system consists of 3 parts.

- a) Spraying (Atomization)
- b) Spraying air mixture and removal of air
- c) Separation of the dry product from the outlet air

Each step is carried out according to the design and operation of the desiccant and the physical and chemical properties of the nutrient, which determine the quality of the final product.

To produce lithium tetraborate trihydrate, LiOH and H<sub>3</sub>BO<sub>3</sub> were mixed in solution medium according to the stoichiometry of the following reaction.



As already mentioned, Li<sub>2</sub>B<sub>4</sub>O<sub>7</sub> solutes are stable solutions and crystallization of lithium tetraborate production loses industrial economics. For this reason, the production was carried out using a spray dryer system, which would be more economical instead of crystallization. Experimental studies were carried out in the spray drier with 7%, 15%, 20% Li<sub>2</sub>B<sub>4</sub>O<sub>7</sub>·3H<sub>2</sub>O solutions at inlet temperatures of 230 ° C, 40, 50, 60, 80 ml/min. The various experimental studies and the system parameters applied to the spray drier are given in Table 1

Table 1 Experimental Results Related to Spray Dryer

| <b>Li<sub>2</sub>B<sub>4</sub>O<sub>7</sub>·3H<sub>2</sub>O</b> |   |   |  |
|---|---|---|--|
| <b>%5 Li<sub>2</sub>B<sub>4</sub>O<sub>7</sub></b>              |   | <b>%10 Li<sub>2</sub>B<sub>4</sub>O<sub>7</sub></b> |  |
| 1   | Feed rate: 40 ml/min<br>Input air temperature: 230 °C<br>Temperature of output air: 115 °C<br>Air-blower: 80.00<br>De-block piston: 900.0<br>Amount of liquid remaining on the bottom: None<br>Amount of substance taken: 11,99 gr<br>Theoretical% boronoxide = 62.6<br>Experimental% boronoxide = 62.8 | 5   | Feed rate: 40 ml / min<br>Input air temperature: 230 °C<br>Temperature of output air: 130 °C<br>Air-blower: 80.00<br>De-block piston: 900.0<br>Amount of liquid remaining on the bottom: None<br>Amount of substance taken: 31.2 gr<br>Theoretical% boronoxide = 62.6<br>Experimental% boronoxide = 62.8 |
| 2   | Feed rate: 50 ml/min<br>Input air temperature: 230 °C<br>Temperature of output air: 115 °C<br>Air-blower: 80.00<br>De-block piston: 900.0<br>Amount of liquid remaining on the bottom: None<br>Amount of substance taken: 11,99 gr  | 6   | Feed rate: 40 ml / min<br>Input air temperature: 230 oC<br>Temperature of output air: 130 oC<br>Air-blower: 80.00<br>De-block piston: 900.0<br>Amount of liquid remaining on the bottom: None<br>Amount of substance taken: 31.2 gr<br>Theoretical% boronoxide = 62.6<br>Experimental% boronoxide = 62.8 |
| 3   | Feed rate: 60 ml / min<br>Input air temperature: 230 °C<br>Temperature of output air: 115 °C<br>Air-blower: 80.00<br>De-block piston: 900.0<br>Amount of liquid remaining on the bottom: None<br>Amount of substance taken: 11,99 gr  | 7   | Feed rate: 60 ml / min<br>Input air temperature: 230 °C<br>Temperature of output air: 105 °C<br>Air-blower: 80.00<br>De-block piston: 900.0<br>Amount of liquid remaining on the bottom: None<br>Amount of substance taken: 22.5 gr  |
| 4   | Feed rate: 80 ml / min<br>Input air temperature: 230 °C<br>Temperature of output air: 115 °C<br>Air-blower: 80.00<br>De-block piston: 900.0   | 8   | Feed rate: 80 ml / min<br>Input air temperature: 230 °C<br>Temperature of output air: 105 °C<br>Air-blower: 80.00<br>De-block piston: 900.0  |

|  |  |
|--|--|
| Amount of liquid remaining on the bottom: None<br>Amount of substance taken: 11,99 | Amount of liquid remaining on the bottom: 10 ml<br>Amount of the substance taken: 15.78 gr |
|--|--|

| % 15 Li <sub>2</sub> B <sub>4</sub> O <sub>7</sub> |   |    |  |
|--|---|----|--|
| 9  | Feed rate: 40 ml / min<br>Input air temperature: 230 °C<br>Temperature of output air: 115 °C<br>Air-blower: 80.00<br>De-block piston: 900.0<br>Amount of liquid remaining on the bottom: None<br>Amount of the substance taken: 43.4 gr | 13 | Feed rate: 40 ml / min<br>Input air temperature: 175 °C<br>Temperature of output air: 90 °C<br>Air-blower: 80.00<br>De-block piston: 900.0<br>Amount of liquid remaining on the bottom: None<br>Amount of substance taken: 38.8 gr       |
| 10   | Feed rate: 50 ml / min<br>Input air temperature: 230 °C<br>Output air temperature: 110 °C<br>Air-blower: 80.00<br>De-block piston: 900,0<br>Amount of liquid remaining on the bottom: None<br>Amount of substance taken: 32.3 gr        | 14 | Feed rate: 50 ml / min<br>Input air temperature: 175°C<br>Output air temperature: 95 °C<br>Air-blower: 80.00<br>De-block piston: 900,0<br>Amount of liquid remaining on the bottom: None<br>Amount of the substance taken: 31.1 gr       |
| 11   | Feed rate: 60 ml / min<br>Input air temperature: 230 °C<br>Temperature of output air: 120 °C<br>Air-blower: 80.00<br>De-block piston: 900.0<br>Amount of liquid remaining on the bottom: None<br>Amount of the substance taken: 29.8 gr | 15 | Feed rate: 60 ml / min<br>Input air temperature: 175 °C<br>Temperature of output air: 80 °C<br>Air-blower: 80.00<br>De-block piston: 900.0<br>Amount of liquid remaining on the bottom: 16 ml<br>Amount of the substance taken: 21.72 gr |
| 12   | Feed rate: 80 ml / min<br>Input air temperature: 230 °C<br>Temperature of output air: 105 °C<br>Air-blower: 80.00<br>De-block piston: 900.0<br>Amount of liquid remaining on the  | 16 | Feed rate: 80 ml / min<br>Input air temperature: 175 °C<br>Temperature of output air: 80 °C<br>Air-blower: 80.00<br>De-block piston: 900.0<br>Amount of liquid remaining on the  |

|   |   |
|---|---|
| bottom: 15 ml<br>Amount of the substance taken: 25.6 gr | bottom: 106 ml<br>Amount of substance taken: 7.2 gr |
|---|---|

As shown in Table 1. the solutions containing lithium tetraborate at different concentrations were allowed to dry in the system in the case of different feed rates, with initial concentrations of 5-10%  $\text{Li}_2\text{B}_4\text{O}_7$  in the spray drier at 40-60 ml / min feed rates in the system. In solutions containing 15%  $\text{Li}_2\text{B}_4\text{O}_7$ , a slight amount of solution accumulates on the bottom of the system as the drying force of the spray dryer at 60-80 ml/min feed rates is not sufficient to evaporate the water in the solution. There are two possible reasons for this; the increase in concentration of lithium tetraborate in the solution may be due to an increase in the concentration of residual solution in the air in the final drying environment and another reason is the increase in the attraction forces between the two compounds by increasing the concentration of lithium tetraborate in the solution and this may become increasingly difficult to remove the resulting water.

In another part of the study, the temperature of the inlet air is taken as 175 °C and when the product feed rate of the product is 40-50 ml / min, all water can be evaporated in the system, but in higher feed rates some solution accumulates in the system.

Two different methods have been tried to determine whether the product obtained is  $\text{Li}_2\text{B}_4\text{O}_7 \cdot 3\text{H}_2\text{O}$ . The first of these was examined in the thermal degradation TG-DTG device at a temperature of inlet air of 230°C and the other at 175°C to determine the amount of water contained in the products obtained at 700 ° C with a heating rate of 50 °C / min. The results obtained are given in Figures 4.72 and 4.73.

According to our calculations in Figure 4.72, the product obtained at 230 ° C is in  $\text{Li}_2\text{B}_4\text{O}_7 \cdot 3\text{H}_2\text{O}$ , but the product obtained at 175 ° C inlet air temperature was found to be  $\text{Li}_2\text{B}_4\text{O}_7 \cdot 3.5\text{H}_2\text{O}$  as shown in Figure 4.73. Furthermore, boron oxide analysis of the obtained products was confirmed by titrimetric method.

### 3. RESULTS

Lithium Tetraborate Trihydrate is produced in a spray drier system, which is produced by reacting boric acid and lithium hydroxide in a solution environment at stoichiometric ratios instead of crystallization, since Lithium Tetraborate Trihydrate is very stable. When 230 ° C inlet air temperature was used, the product obtained was found to be in trihydrate structure in the results obtained in TG-DTA and boroxide analyzes. When 170 ° C drying air was used, the obtained structure was determined to be between tetra and trihydrate. On the other hand it is possible to produce 5-20% of Lithium Tetraborate Trihydrate using Spray Dryer.

### ACKNOWLEDGMENT

This work was supported by Turkish Scientific and Technological Research Center (TUBITAK) (No: 108M043)

### REFERENCES

- [1]. Mullin, J.W., *Crystallization, 3rd*. 1993, University of London: Butterworth-Heinemann, Reed Educational and Professional Publishing Ltd.
- [2]. Nývlt, J., et al., *The kinetics of industrial crystallization Elsevier*. 1985, Amsterdam.
- [3]. Mullin, J., *Crystallization, third e d*. 1993, Butterworth-Heinemann, Oxford Boston.
- [4]. Kutluay, S., et al., *Design and optimization of production parameters for boric acid crystals with the crystallization process in an MSMR crystallizer using FBRM® and PVM® technologies*. Journal of Crystal Growth, 2017. 467(Supplement C): p. 172-180.
- [5]. Smith, T.D., *Metallised fabric*. 1985, Google Patents.
- [6]. Bell Jr, W.R., *BORON, ELEMENTAL*. Kirk-Othmer Encyclopedia of Chemical Technology, Bearing Materials to Carbon, 1992. 4: p. 360.
- [7]. Prochazka, S., *Polycrystalline silicon carbide with increased conductivity*. 1976, Google Patents.
- [8]. Gany, A. and D. Netzer, *Combustion studies of metallized fuels for solid-fuel ramjets*. Journal of Propulsion and Power, 1986. 2(5): p. 423-427.

### BIOGRAPHY

I completed my Ph.D. education at Kafkas University in the science of chemistry. My work areas; Energy, Crystallization, Hydrogen Energy



# Effect of Additives on Meta-stable Zone Width for Boric Acid Crystallization

Muhammed Bora Akin<sup>1</sup>, Ömer Şahin

---

## Abstract

*In this work, meta-stable zone has been investigated for boric acid crystallization at 20 °C by using different cooling rates and using some additives: calcium nitrate, magnesium chloride and sulfuric acid. Boric acid production is commonly uses precipitation from some boron minerals by crystallization. In these crystallization processes, meta-stable zone width was very important role because of processes often have gone through in the meta-stable zone. Processes have different crystallization temperatures in the present of different ions. These ions also find in the boric acid crystallization processes. In this work, calcium, magnesium and sulfate ions have used between 150-1800 ppm; 2000-12000 ppm and 5000-30000 ppm respectively. Effect of calcium, magnesium and sulfate ions at crystallization temperature has been found between in these limits.*

**Keywords:** Additive, Boric acid, Crystallization, Meta-stable zone

---

## 1. INTRODUCTION

To design and to operate of crystallization process systems is complex matter and requiring extensive data including crystal, solution and slurry characteristics. The meta-stable zone (MSZ) is included in solution characteristics [1]. MSZ emerges as the one of the most important notions in terms of industrial crystallization. Characterizing nucleation and determining the crystallization process operating range is possible with Metastable Zone Width (MSZW) measurements [2]. Although important, the creation of models is still not possible due to some uncertainties on MSZ, and for this reason still practical methods are used for defining metastable zone. The meta-stable zone is explained as the area between the concentration of solubility and the concentration of detection the first nucleus [3]. The MSZW can easily be determined by studying the difference between the saturation temperature of a solution and the temperature at which crystals are first sensed during a constant cooling of a clear solution. [2,4].

Boric acid can be produced from colemanite, ulexite and borax with different acid solutions [5]. For example if it will manufactured Colemanite ore, the Colemanite ore will be reacted with sulfuric acid at 90 °C. Generally, Ca<sup>2+</sup>, Mg<sup>2+</sup> and SO<sub>4</sub><sup>2-</sup> ions are present in the solution as impurities during these reactions. These ions change the nucleation and growth mechanism of the boric acid. In the crystallization, process operates at the same time as both nucleation and crystal growth. Supersaturation affects both mechanisms. So the supersaturation becomes important that where it begins and ends. It is easy to describe for pure solutions but it is difficult to find if them contain foreign ions. There are several works have been studied [6-8].

## 2. MATERIALS AND METHODS

Boric acid was obtained from the Eti Maden R&D and Technology Development Department. The other additives to be used as impurities are provided by Sigma-Aldrich (>99.0%). The additives are calcium nitrate, magnesium chloride and sulfuric

---

<sup>1</sup> Corresponding author: Cankiri Karatekin University, Faculty of Engineering, 18200 Cankiri, Turkey. mbakin@karatekin.edu.tr

acid. The type II water used for doing experiments and cleaning experimental was produced with the Merck Millipore Elix Essential Metastable zone studies were performed with a 250 mL double-jacket reactor. The temperature control of the reactor was carried out with a circulating water bath (cryostat). Cryostat heating / cooling rate was adjustable (Polyscience - AP07R-20-A12E). The cryostat was controlled by a probe that measures the temperature inside the reactor used. Reactor has been mixed using a magnetic stirrer. The experiments were recorded directly to a computer with the external camera and the crystallization temperatures were determined by watching these experiments recorded. The boric acid solution is cooled at a constant rate from saturation temperature down to the temperature of appearance of the first visible nuclei. This method is called polythermal method. MSZW was measured by this method [9]. The difference in these temperatures is described as a maximal supercooling ( $\Delta T_{max}$ ). The maximal supercooling ( $\Delta T_{max}$ ) is related to the cooling rate ( $-T'$ ) by following equation [6, 7]:

$$\log(\Delta T_{max}) = \frac{1-m}{m} \cdot \log\left(\frac{dw_{eq}}{dT}\right) - \frac{1}{m} \cdot \log k - \frac{1}{m} \cdot \log(-T') \quad (1)$$

According to Eq. 1 the dependence of  $\Delta T_{max}$  on ( $-T'$ ) is linear on a logarithmic plot and corresponds to the equation of a straight line

$$Y = a + b \cdot X \quad (2)$$

Where  $X = \log(-T')$  and  $Y = \log(\Delta T_{max})$

The values of nucleation parameters  $m$  and  $k$  are obtained from the fitted constant of the correlation equation.

$$m = \frac{1}{b} \quad (3)$$

$$k = (1 - m) \cdot \log\left(\frac{dw_{eq}}{dT}\right) - a \cdot m \quad (4)$$

Where  $k$  is nucleation rate constant,  $m$  is apparent nucleation order,  $T$  is temperature ( $^{\circ}\text{C}$ ),  $-T$  is cooling rate ( $^{\circ}\text{C}/\text{h}$ ) and  $w_{eq}$  is solubility ( $\text{kg}/\text{kg}$ ).

In the experiments, the saturation value for the boric acid was used for  $20^{\circ}\text{C}$ . The dissolution process was carried out at a temperature of  $10^{\circ}\text{C}$  above the dissolution temperature. The temperatures which the nucleation begins have been noted by experiments with / without addition using four different cooling rates after dissolution. Cooling rates are  $5^{\circ}\text{C}/\text{h}$ ,  $10^{\circ}\text{C}/\text{h}$ ,  $15^{\circ}\text{C}/\text{h}$  and  $20^{\circ}\text{C}/\text{h}$ . If additive is to be used in the experiment, it is added into the reactor after the dissolution of the boric acid. Used amounts of additives are given as ppm in Table 1.

Table 1. Used additives as impurities in experiments

| Additives                                     | Point 1 | Point 2 | Point 3 | Point 4 |
|---|---------|---------|---------|---------|
| Calcium nitrate ( $\text{Ca}^{2+}$ source)    | 150     | 450     | 900     | 1800    |
| Magnesium chloride ( $\text{Mg}^{2+}$ source) | 2000    | 4000    | 8000    | 12000   |
| Sulfuric acid ( $\text{SO}_4^{2-}$ source)    | 5000    | 10000   | 20000   | 30000   |

### 3. RESULTS AND DISCUSSION

Nucleation temperatures are worked with / without additives. Firstly boric acid solution cooled down desired to describe what temperature is crystallization began. The other experiments are done by using additive as impurities.

#### 3.1 Without Additive

After solution solubility was arranged at  $20^{\circ}\text{C}$ , than four different cooling rates have been examined to see nucleation temperatures. The nucleation temperatures were obtain  $16.26^{\circ}\text{C}$ ,  $16.00^{\circ}\text{C}$ ,  $15.86^{\circ}\text{C}$  and  $15.78^{\circ}\text{C}$ , respectively.

As we see that the nucleation temperature decreasing by the high cooling rate. The entire experiments are proved this situation.

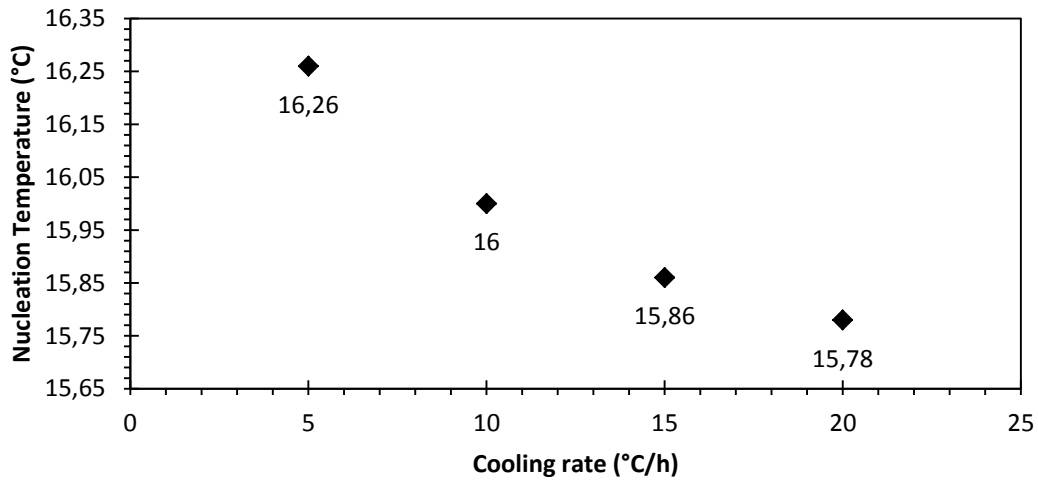


Figure 1. Effect of cooling rate on nucleation temperature without impurities

### 3.2 In the Presence of Calcium Ions

After solution solubility was arranged desired temperature, four different cooling rates have been examined to see nucleation temperatures. Experiments have been done at 20 °C. Calcium ion concentration is used at 150 ppm, 450 ppm, 900 ppm, and 1800 ppm. Figure 2 shows the nucleation temperatures obtained in experiments in the presence of calcium ions.

After solution solubility was arranged at 20 °C, than four different cooling rates have been examined to see nucleation temperatures: 5 °C/h, 10 °C/h, 15 °C/h and 20 °C/h. In the presence of 150 ppm  $\text{Ca}^{2+}$  ions, the nucleation temperatures were obtain 16.54 °C, 16.18 °C, 15.85 °C and 15.65 °C, respectively. In the presence of 450 ppm  $\text{Ca}^{2+}$  ions, the nucleation temperatures were obtain 16.92 °C, 16.47 °C, 16.11 °C and 15.78 °C, respectively. In the presence of 900 ppm  $\text{Ca}^{2+}$  ions, the nucleation temperatures were obtain 17.02 °C, 16.61 °C, 16.27 °C and 15.79 °C, respectively. In the presence of 1800 ppm  $\text{Ca}^{2+}$  ions, the nucleation temperatures were obtain 17.35 °C, 16.82 °C, 16.42 °C and 15.94 °C, respectively.

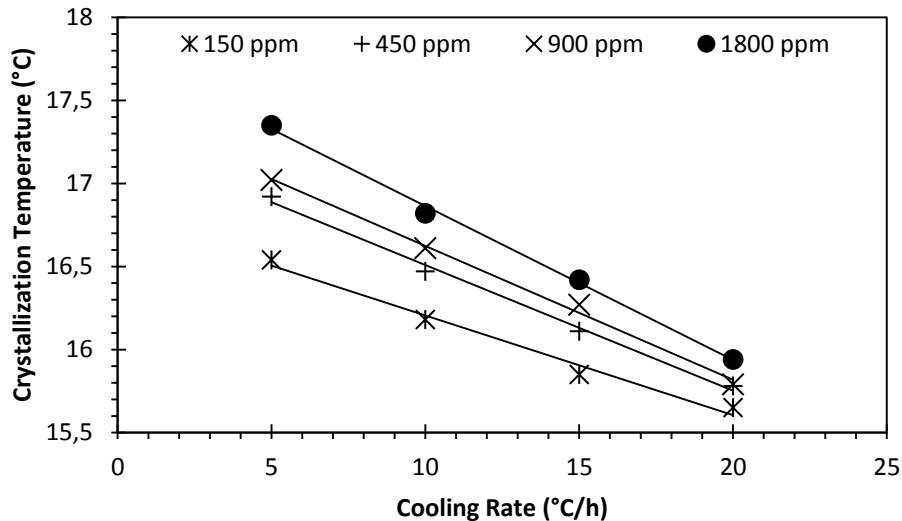


Figure 2. Effect of cooling rate on nucleation temperature in the presence of  $\text{Ca}^{2+}$  ions at 20°C.

### 3.3 In the Presence of Magnesium Ions

After solution solubility was arranged desired temperature, four different cooling rates have been examined to see nucleation temperatures. Experiments have been done at 20 °C. Magnesium ion concentration is used at 2000 ppm, 4000 ppm, 8000 ppm, and 12000 ppm. Figure 3 shows the nucleation temperatures obtained in experiments in the presence of magnesium ions.

After solution solubility was arranged at 20 °C, than four different cooling rates have been examined to see nucleation temperatures: 5 °C/h, 10 °C/h, 15 °C/h and 20 °C/h. In the presence of 2000 ppm  $Mg^{2+}$  ions, the nucleation temperatures were obtain 16.70 °C, 16.31 °C, 16.05 °C and 15.70 °C, respectively. In the presence of 4000 ppm  $Mg^{2+}$  ions, the nucleation temperatures were obtain 17.08 °C, 16.72 °C, 16.43 °C and 16.07 °C, respectively. In the presence of 8000 ppm  $Mg^{2+}$  ions, the nucleation temperatures were obtain 17.38 °C, 17.16 °C, 16.71 °C and 16.44 °C, respectively. In the presence of 12000 ppm  $Mg^{2+}$  ions, the nucleation temperatures were obtain 18.17 °C, 17.71 °C, 17.31 °C and 17.10 °C, respectively.

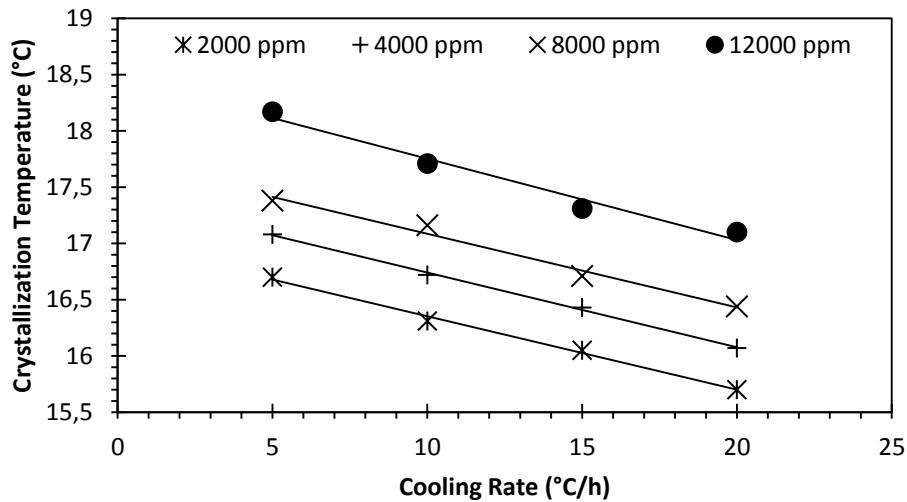


Figure 3. Effect of cooling rate on nucleation temperature in the presence of  $Mg^{2+}$  ions at 20 °C

### 3.4 In the Presence of Sulfate Ions

After solution solubility was arranged desired temperature, four different cooling rates have been examined to see nucleation temperatures. Experiments have been done at 20 °C. Sulfate ion concentration is used at 5000 ppm, 10000 ppm, 20000 ppm, and 30000 ppm. Figure 4 shows the nucleation temperatures obtained in experiments in the presence of sulfate ions.

After solution solubility was arranged at 20 °C, than four different cooling rates have been examined to see nucleation temperatures: 5 °C/h, 10 °C/h, 15 °C/h and 20 °C/h. In the presence of 5000 ppm  $SO_4^{2-}$  ions, the nucleation temperatures were obtain 18.13 °C, 17.82 °C, 17.63 °C and 17.39 °C, respectively. In the presence of 10000 ppm  $SO_4^{2-}$  ions, the nucleation temperatures were obtain 18.30 °C, 18.11 °C, 17.75 °C and 17.48 °C, respectively. In the presence of 20000 ppm  $SO_4^{2-}$  ions, the nucleation temperatures were obtain 18.40 °C, 18.14 °C, 17.90 °C and 17.64 °C, respectively. In the presence of 30000 ppm  $SO_4^{2-}$  ions, the nucleation temperatures were obtain 18.70 °C, 18.57 °C, 18.33 °C and 18.08 °C, respectively.

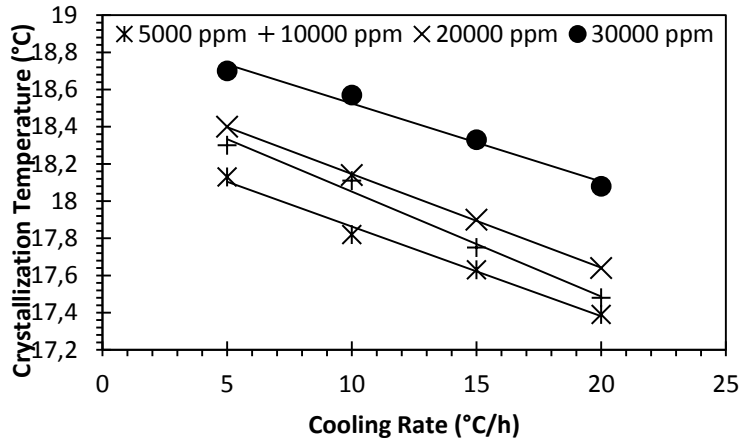


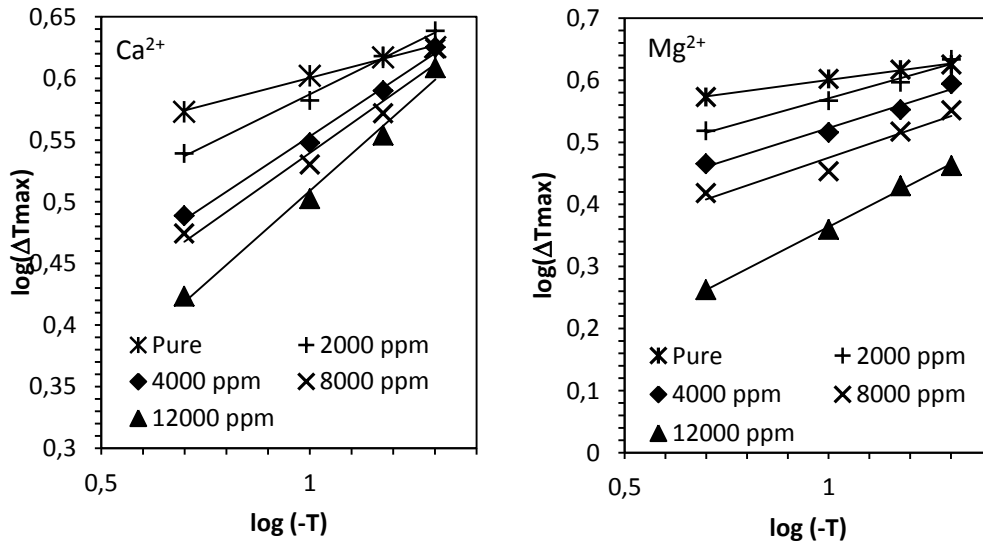
Figure 4. Effect of cooling rate on nucleation temperature in the presence of  $SO_4^{2-}$  ions at 20°C.

The experimental data were calculated using Eq. 1. The result of measurements of the MSZW in the presence of impurities is summarized in the Table 2. The variation of maximum allowable undercooling rate with  $Ca^{2+}$ ,  $Mg^{2+}$ , and  $SO_4^{2-}$  ions at 20 °C presented in Figure 5.

Table 2. Metastable zone width in the presence of various impurities at 20 °C

| Impurity    | Impurity Concentration (ppm) | Maximal Undercooling (K) at different cooling rate |         |         |         | Nucleation Order |
|-------------|------------------------------|--|---------|---------|---------|------------------|
|             |                              | 5 °C/h   | 10 °C/h | 15 °C/h | 20 °C/h |                  |
| Pure        | -                            | 3.74   | 4,00    | 4.14    | 4.22    | 11.35            |
| $Ca^{2+}$   | 150                          | 3.46   | 3.82    | 4.15    | 4.35    | 6.00             |
|             | 450                          | 3.08   | 3.53    | 3.89    | 4.22    | 4.45             |
|             | 900                          | 2.98   | 3.39    | 3.73    | 4.21    | 4.18             |
| $Mg^{2+}$   | 1800                         | 2.65   | 3.18    | 3.58    | 4.06    | 3.33             |
|             | 2000                         | 3.30   | 3.69    | 3.95    | 4.30    | 5.42             |
|             | 4000                         | 2.92   | 3.28    | 3.57    | 3.93    | 4.82             |
|             | 8000                         | 2.62   | 2.84    | 3.29    | 3.56    | 4.47             |
| $SO_4^{2-}$ | 12000                        | 1.83   | 2.29    | 2.69    | 2.90    | 2.96             |
|             | 5000                         | 1.87   | 2.18    | 2.37    | 2.61    | 9.70             |
|             | 10000                        | 1.70   | 1.89    | 2.25    | 2.52    | 9.07             |
|             | 20000                        | 1.60   | 1.86    | 2.1     | 2.36    | 3,06             |
|             | 30000                        | 1.30   | 1.43    | 1.67    | 1.92    | 3.46             |

Figure 5 shows the variation of maximum allowable undercooling with cooling rate in the presence  $Ca^{2+}$ ,  $Mg^{2+}$ , and  $SO_4^{2-}$  ions at 20 °C. Figure 5 is obtained by use equation 1.



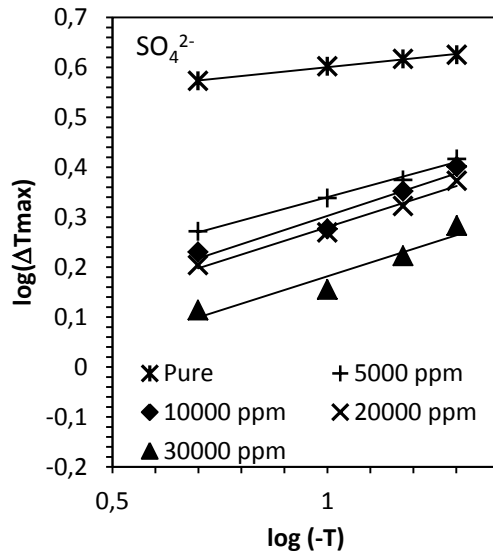
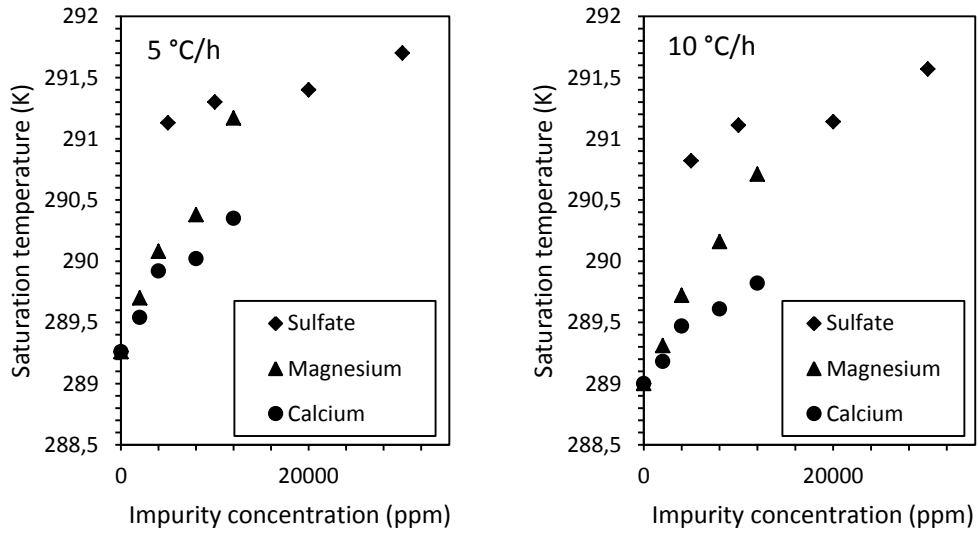


Figure 5. The variation of maximum allowable undercooling with cooling rate in the presence  $Ca^{2+}$ ,  $Mg^{2+}$ , and  $SO_4^{2-}$  ions at 20 °C.

For different cooling rates, as it can be seen from Figure 6, in the presence  $Ca^{2+}$  ions there is significant change in the equilibrium saturation temperature of the solution. Similar results have been reported  $Ca^{2+}$  ions used on boric acid solution by Sayan and Ulrich in 2001. In the presence  $Mg^{2+}$  and  $SO_4^{2-}$  ions is also change in the equilibrium saturation temperature of the solution. Karakaya's and Teodossiev's results indicated that in the presence of  $SO_4^{2-}$  ions there is significant change in the equilibrium saturation temperature of the solution [10, 11].



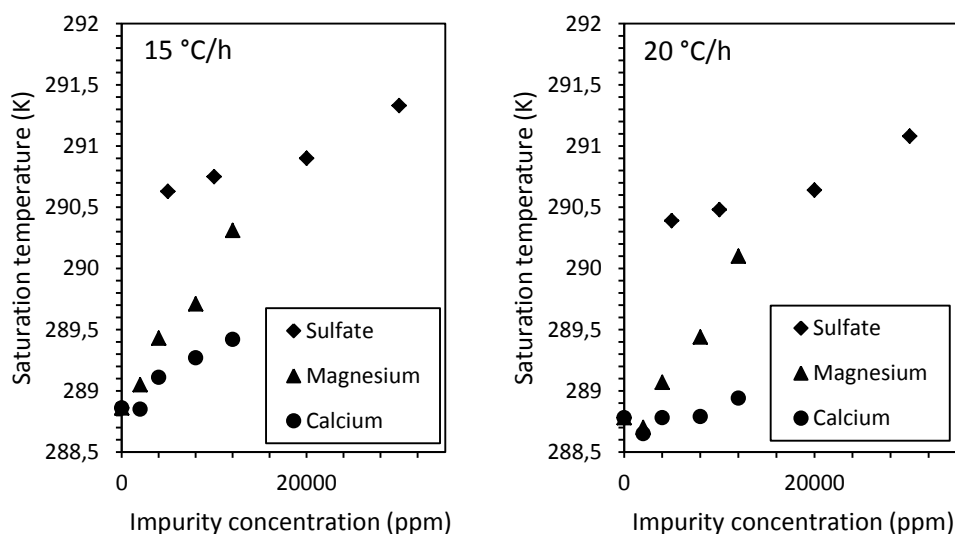


Figure 6. The effect of impurity concentration on saturation temperature of boric acid at 20 °C with 5, 10, 15, and 20 °C/h cooling rate

#### 4. CONCLUSION

MSZW of boric acid in aqueous media was measured in the presence of  $\text{Ca}^{+2}$ ,  $\text{Mg}^{2+}$  and  $\text{SO}_4^{2-}$  ions. In the presence of all used impurities the MSZW was reduced. The solubility of boric acid is much more influenced by the presence of  $\text{Ca}^{+2}$  in the solution. As expected, MSZW has been found to increase with increasing cooling rate. It appears that the nucleation order decreases with increasing amount of impurities.

#### ACKNOWLEDGMENT

The authors thank to the Etimaden Inc. for the financial support of this research (Project number: 400.02[TGD.2014/3]).

#### REFERENCES

- [1]. G. Jones, *Crystallization Process Systems*, Butterworth-Heinemann: Oxford, 2002.
- [2]. S.S. Kadam, et al., "A new view on the metastable zone width during cooling crystallization" *Chemical Engineering Science*, 72 (Supplement C): p. 10-19. 2012.
- [3]. W. Bogacz and J. Wójcik, "The Metastable Zone of Aqueous Solutions" *CHEMIK*, vol. 68, issue 3, pp. 198–201. 2014.
- [4]. J. W. Mullin, *Crystallization*, Fourth ed.; Butterworth-Heinemann: Oxford, 2001.
- [5]. Kuskay, and A.N. Bulutcu, "Design parameters of boric acid production process from colemanite ore in the presence of propionic acid". *Chemical Engineering and Processing: Process Intensification*, 50(4): p. 377-383. 2011.
- [6]. P. Sayan, and J. Ulrich, "Effect of Various Impurities on the Metastable Zone Width of Boric Acid". *Cryst. Res. Technol.*, 36: 4-5, 411–417. 2001.
- [7]. O. Sahin, H. Dolas, and H. Demir, "Determination of nucleation kinetics of potassium tetraborate tetrahydrate". *Cryst. Res. Technol.*, 42: 8, 766–772. 2007.
- [8]. J. Peng, N. Dong, Y. Dong, Z. Pan, and W. Li, "Solubility, Metastable Zone Width, and Nucleation Kinetics of Boric Acid in the NaCl–KCl–CaCl<sub>2</sub>–H<sub>2</sub>O System". *Journal of Chemical & Engineering Data* 60 (11), 3341-3346. 2015. J. Nyvlt, "Kinetics of nucleation in solutions". *J. Cryst. Growth*, 3/4, 377. 1968.
- [9]. Karakaya, A.N. Bulutcu, BIWIC 1991 (Ed. J. Ulrich), p.12, Verlag Mainz, Aachen, Germany 1991.
- [10]. N. Teodossiev, E. Kirkova, *Industrial Crystallization* 81, (Eds. S.J., Jancic, E.J. de Jong), p.155, North-Holland, Amsterdam 1982.

#### BIOGRAPHY

Muhammed Bora Akin was born 1975, in İstanbul and graduated from the Yildiz Technical University in 1999 with a bachelor of science in chemical engineering. He attended graduate school at the Yildiz Technical University, where he received a master of science in chemical engineering in 2005 and a Ph.D. in 2011.

From 2001 to 2004, Akin was worked as chemical engineer for different incorporations. He was a member of the chemical-metallurgical engineering faculty at Yildiz Technical University from 2005 until 2013, before coming to the Çankırı Karatekin University.

Akin' researches focused on additives and theirs inhibition effects in crystallization processes, and applications of metal oxide catalysts.



# Removal of the Water from Raw Biodiesel by Sunflower Hulls

Ayşe Dizman and Hakan Temur<sup>2</sup>

---

## Abstract

Basic catalytic biodiesel production is carried out by the reaction of vegetable oils with methanol and a basic catalyst such as NaOH and KOH. Following completion of transesterification reaction biodiesel is separated from the glycerid by gravitational settling. Biodiesel is then washed with water a couple of times in order to remove the impurities such as basic catalyst, excess methanol and soap. But, water content of the biodiesel increases during these washing cycles, which should be removed before using it as a diesel fuel substituent in a diesel engine. Vacuum evaporation of the water and methanol content of this crude biodiesel is the most common route applied in the production. A time and energy consuming step in the biodiesel production is removal of the water from the biodiesel by evaporation.

In this study, sunflower hulls were used to remove the water content of the raw biodiesel obtained from sunflower oil. Hulls were crushed, separated by size and mixed with raw biodiesel at specified experimental conditions. Sunflower hulls (shells) had already some water content as a result of open atmosphere by a ratio of 6.85 %. Even with this amount of water content, sunflower shells adsorbed about 20% of the water in the crude (after washed) biodiesel which was sufficient in terms of biodiesel standards defined by ASTM and EN.

In order to increase their water adsorption capacity sunflower hulls were dried at  $100 \pm 4$  °C and atmospheric pressure for different periods ranged from 1 to 3 hours in an ordinary laboratory oven. One hour later, 86% of the water content existed in the hulls was removed while it came up to almost all the water content in 3 hours. Dried sunflower hulls behaved as an effective water adsorbant for the raw biodiesel samples. As a result, it is safely suggested that most of the water content of raw biodiesel samples (>90%) could be removed by using predried sunflower shells as a water adsorption agent which makes it suitable for using as a diesel fuel substituent.

**Keywords:** biodiesel washing, purification, sunflower hulls, water content

---

## 1. INTRODUCTION

Biodiesel is an important alternative diesel fuel as a unique viable option so far. Its natural similarities to petroleum based biodiesel provide a wider usage area especially in transportation. Its technical and economic advantages have been proven as a trading liquid fuel in many countries in Europe, Asia and America. As a result, there is a growing interest for biodiesel production in the world wide [1].

Biodiesel is a mixture of fatty acid methyl esters (FAME) obtained from transesterification of vegetable oils with methyl alcohol in the presence of the sodium or potassium hydroxide as a catalyst. When transesterification is completed, FAMES and glycerol as products are formed as an immiscible binary mixture. Glycerol phase settles down as a result of its higher density at the bottom, while the FAME mixture stays as the upper part of the binary mixture in a couple of minutes [2]. After glycerol phase is removed, FAME phase is washed with warm distilled water in order to remove impurities such as soap, unreacted methanol and catalyst. Water phase is also separated at the bottom as a result of higher density. Water is an ideal solvent for this aim since impurities are mostly polar compounds and have a high solubility in water [3]. This washing treatment is mostly repeated several times. The final stage is removing of this wash water from the FAMES. After waiting for several hours, most of the water can be separated by simply pouring the bottom phase. But some water residue in the FAMES cannot be removed by simply gravitational settling and needs further separation treatments. In many commercial applications, water residue is evaporated under vacuum in one or several evaporation stages in order to be sure that all the

---

<sup>2</sup> Corresponding author: Ataturk University, Faculty of Engineering, Department of Chemical Engineering, 25200 Erzurum, Turkey. haktetur@yahoo.com

water and methanol is removed. To heat all the biodiesel content is an energy consuming step. New alternative drying processes are needed to decrease the production costs of the biodiesel production.

In this study, sunflower seed shells were used to remove water from biodiesel as an adsorbent agent. Reduced by size and pre-dried sunflower seed shells are mixed with the biodiesel. Adsorbed water amount in the biodiesel is analyzed under different adsorption conditions. It was seen that crushed and pre-dried sunflower seed hulls can be evaluated as an effective adsorbent to remove the washing water residue of the raw biodiesel.

## 2. EXPERIMENTAL

In the present study, sunflower seed shells are used as a water adsorption agent in biodiesel purification. Sunflower shells first were crushed, classified by size and dried in a laboratory oven. They are added into biodiesel samples in definite amounts and stirred in given periods. Water content of the biodiesel was measured before and after the mixing by a coulometric water analysis instrument. Removed water content from the biodiesel is given in graphs. Sunflower seed shell treatment is given as follows in detail.

### 2.1 Crushing

Sunflower oil seed shells are separated from the seeds by hand and left over the open atmosphere for a couple of days. Then they are crushed using a crossbeater mill into different size fractions. The moisture content of the shells were determined after crushing. Moisture content were measured between 5-7% in weight depending on the particle size (Figure 2). Table 1 shows the size fractions and average particle sizes obtained after sieving while in Figure 1 shell sizes used in the experiments are shown.

Table 1. Sizes of sunflower seed shells

| No                             | 1            | 2            | 3            | 4            | 5            | 6             | 7            |
|--------------------------------|--------------|--------------|--------------|--------------|--------------|---------------|--------------|
| <b>Sieve sizes (mm)</b>        | -<br>9.0+3.0 | -<br>3.0+2.0 | -<br>2.8+2.0 | -<br>2.0+1.0 | -<br>1.4+0.6 | -<br>0.63+0.0 | -<br>0.4+0.0 |
| <b>Mean particle size (mm)</b> | 6.0          | 2.9          | 2.4          | 1.7          | 1.02         | 0.52          | 0.3          |

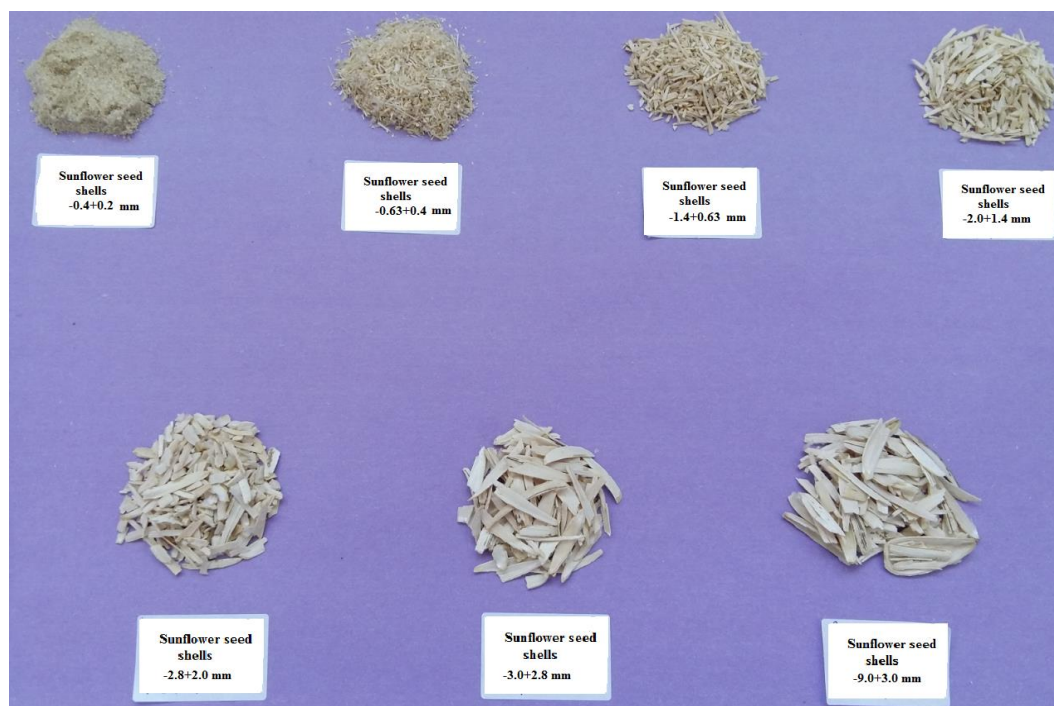


Figure 1. Classified sunflower seed shells into different particle sizes.

In order to investigate the effect of temperature on the water adsorption of sunflower seed adsorption was carried out at the temperatures of 15, 27, 40 and 50 °C. The temperature was kept constant by a constant temperature circulator.

## 2.2 Production of biodiesel

Biodiesel used in the experiments was produced from sunflower oil. In this way, it is aimed to show that sunflower oil biodiesel was purified from water with the shells of the same type oil's wastes. Methanol was used as alcohol and KOH as catalyst. Transesterification was carried out at 55 C and with 300 rpm stirring speed in a jacketted glass reactor. After transesterification reaction was completed, sunflower based biodiesel is left to separate the phases.

## 2.3 Water determination

Water content of the each sample was determined with a coulometric water determinator named Cou-Lo Aquamax KF Moisture Meter. About 1 mL of raw biodiesel sample is injected into instrument in every experiment and results were obtained percentage in weight. Measurements were taken at least twice.

## 3. Results and Discussion

It is aimed in the study to investigate the effects of adsorption temperature, particle size of the seeds and seed-to-biodiesel ratio of the mixture on the water percentage of the raw biodiesel. When the sunflower shells are used as an adsorption agent without drying, the adsorption capacity was quite low. In order to increase adsorption capacity sunflower shells are pre-dried in a laboratory oven. Figure 2 shows the weight loss of the different size distributions of the shells during pre-drying. As seen in the Figure 2, two hours later of the adsorption shells lost almost all their water content (maybe along with some volatile components) because weight loss became constant. The highest weight loss was seen for the 0.3 mm particle size because it is the thinnest one.

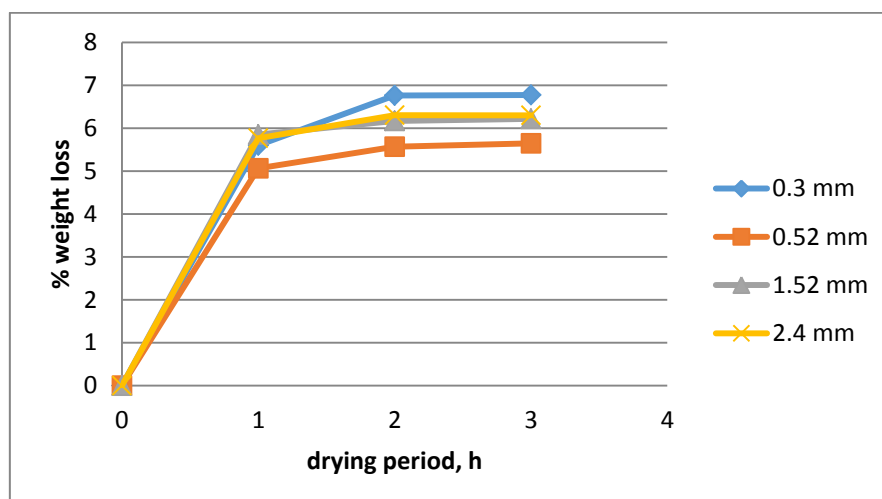


Figure 2. Weight loss when shells were pre-dried before the adsorption.

Pre-dried shells then used as adsorption an agent under different conditions. The effects of parameters are shown in detail as follows.

### 3.1 Effect of temperature

The effect of temperature on the adsorption of water by sunflower shells was given in Figure 3. As seen in the figure, as temperature decreases, adsorption capability of the shells is increased. The best water adsorption is observed at 15 °C. About 90% of the water in the raw biodiesel has been removed in less than 1 hour at this temperature.

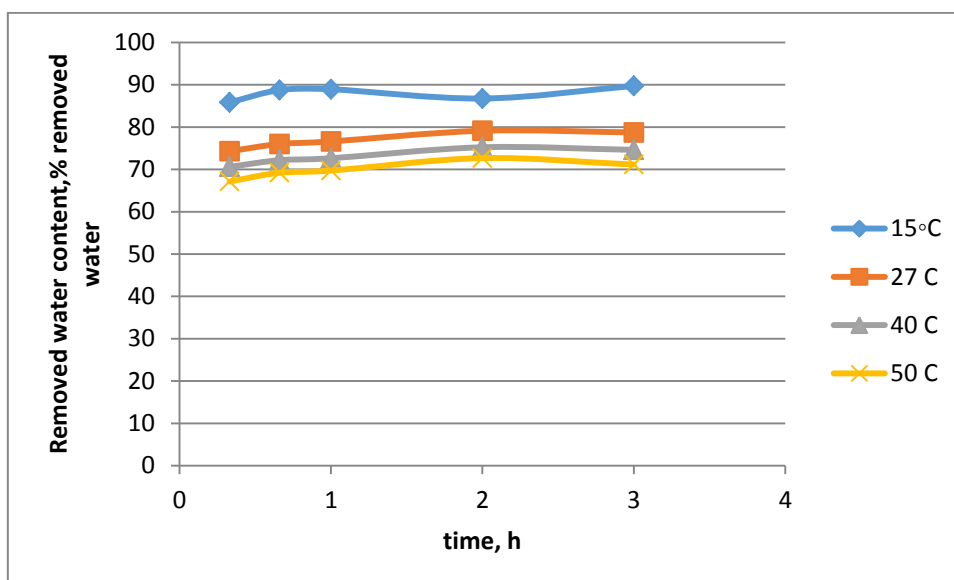


Figure 3. Effect of temperature on the adsorption.

### 3.2 Effect of particle size

Effect of particle size of sunflower shells on the adsorption is shown in Figure 4. As seen in figure 1.7 mm of particle size has held the water best. 0.3 mm of particle size has shown the least effective water adsorption.

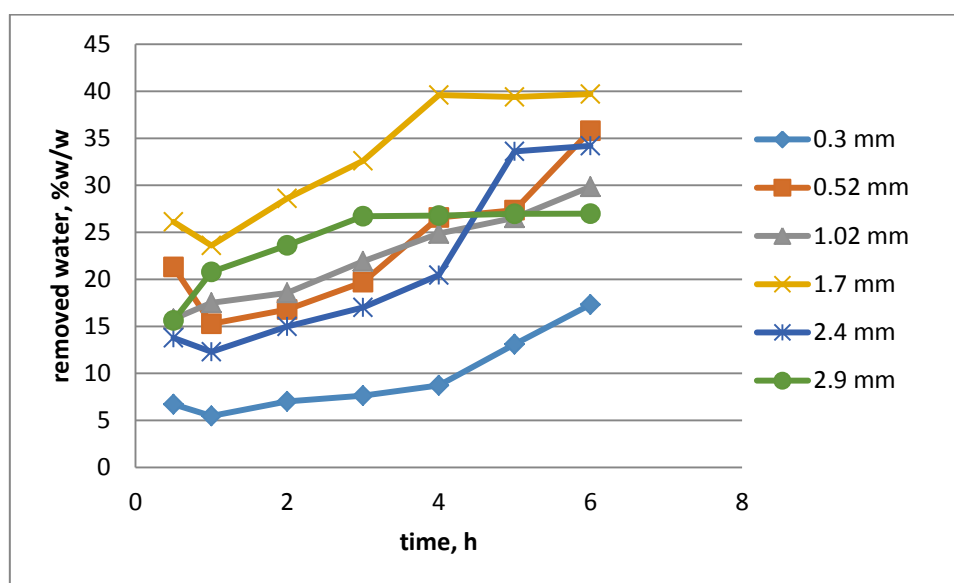


Figure 4. Removed water content with different particle sizes

It is an interesting result to see 1.7 mm particle size has given the best adsorption capacity for water in the raw biodiesel. The reason why is this needs more research on it. It may be attributed to the view that maybe this is a structurally favorable particle size for the sunflower oil shells which can provide better adsorption capability.

### 3.3 Effect of shell-to-biodiesel ratio

Amount of shell is observed as another important parameter in adsorption process. As seen in Figure 5, in 3 hours water adsorption reaches almost its maximum ratio for all the shell amounts. Shell-to-biodiesel ratios has been given in grams per 100 mLs in Figure 5. As the amount of sunflower shells increases, amount of adsorbed water increases as well until 15 grams per 100 mL. From this point there is no increase observed in the amount of adsorbed water. 20 grams of shells adsorbed the same as that of 15 grams adsorbed.

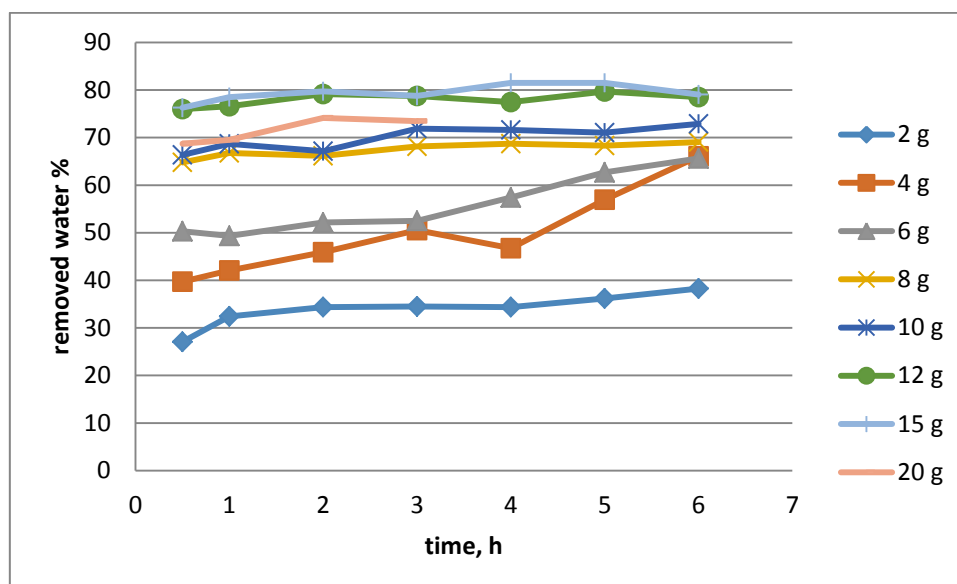


Figure 5. Effect of shell-to-biodiesel ratio

#### 4. CONCLUSIONS

It is investigated in the study if the sunflower oil shells can be used as a water adsorption agent in raw biodiesel purification. Water adsorption capacity of predried sunflower shells are observed at different conditions such as adsorption temperature, particle size and shell-to-biodiesel ratio. It has been observed that sunflower oil seed shells show a good adsorption capacity. After one hour predrying at about  $100 \pm 4$  °C temperature, shells can remove almost 90% of the water in the raw biodiesel in one hour mixing under appropriate conditions. As a result sunflower seed shells can be seen as a waste material which can be used as a water adsorption agent in the biodiesel purification.

#### REFERENCES

- [1] Çanakci, M and Sanli, H., *Biodiesel production from various feedstocks and their effects on the fuel properties*. J Ind Microbiol Biotechnol (2008) 35:431-441.
- [2] Ma, F. And Hanna, M.A., Biodiesel production: a review. Bioresource Technology 70 (1999) 1-15.
- [3] Hastie, M., Energy and Water Conservation in Biodiesel Purification Processes. MSc. Thesis, Department of Chemical and Biochemical Engineering Department, University of Ottawa, Canada, 2011.

#### BIOGRAPHY

Presenting author, Hakan Temur, is currently working as an Associated Professor at Atatürk University in Turkey. He is working on biofuels in particular biodiesel, its production, purification and improvement.



# A New Technique for the Measurement of Mixing Time

Özkan Aydın<sup>1</sup>, Sinan Yapıcı<sup>2</sup>

---

## Abstract

Mixing is defined as “the reduction of inhomogeneity in order to achieve a desired process result”. Mixing process has an important role in almost all industrial systems. Agitated liquid units are the most commonly encountered systems in the mixing operations with a wide range of applications. One of the indications for the degree of mixing in these units is the mixing time. The mixing time can be measured by applying a tiny pulse on a homogeneous agitated system and then measuring and recording the history of the medium until the system attains to a new homogeneity. The pulse can be a temperature, concentration, or a colouring agent, and generates a measurable tiny change in the physical properties of the system without causing a considerable change of the system properties.

Electrochemical limiting diffusion current technique (ELDCT) has been widely employed for the measurements of mass transfer, shear stress, fluid velocity, and turbulent fluctuations. The aim of the present work is to search whether the application of the ELDCT for the measurement of the mixing time in stirred vessels is possible, and to establish a new technique for the mixing time measurements in the systems consisting of liquid contents. A stirred vessel was designed according to the standards, and stirring speed, vane number, stirrer diameter, vane angle and liquid viscosity were chosen as parameters. Local mixing times and average mixing times were measured by using a local sensor, one of the baffles as sensor for average readings.

Comparisons with the results obtained from conductivity measurements showed that ELDCT can be practical, fast, simple and flexible mixing time measurement technique.

**Keywords:** Diffusion current, electrochemical limiting mixing time.

---

## 1. INTRODUCTION

Mixing processes are widely used in the industries such as chemical, biochemical, food, and pharmacy. In the mixing processes, many parameters such as minimum agitation speed, power consumption, circulation time, drop size distribution, breakup and coalescence, mixing time, interface area and phase change are used in determination of mixing effect [1].

Mixing time is one of the important parameters to define mixing effectiveness in the liquid-liquid mixing processes [2], [3]. It is also a degree of uniformity, desirable mixing and homogeneity throughout the vessel. The homogeneity of the system can be described by the gradient of properties such as concentration, temperature, viscosity, color and phase [4]. The time for the vessel content to become uniform, called the mixing time. Sizing and positioning of mixing equipment and flow characteristics are effective parameters to determine the mixing time [5], [6].

Several measurement techniques have been developed to measure the mixing time in stirred vessels. These techniques; conductivity techniques [7], thermal technique [8], planar laser-induced fluorescence (PLIF) [9], and colorimetric techniques [10], electrical resistance tomography technique [11], particle velocity imaging (PIV) technique [1] and acid - base neutralization reaction technique [12].

One of these techniques, colorimetric technique, is based on visual measurement. Therefore it depends on the person who is taking measurements. Second technique is conductivity technique; the measuring probe is immersed in the solution. This probe disrupts the flow hydrodynamics. If such measurement systems are used, the flow hydrodynamics will actually deviate from the intended and desired dynamics. Others need expensive devices and equipment.

Hence, Electrochemical Limiting Diffusion Current Technique (ELDCT) was used as a new technique to measure mixing time. This technique has been used to measure shear stress, mass and momentum transfer rates, fluid velocity [13]. Firstly, since the local mixing time values are obtained with conductivity meter in ELDCT, local cathode sensor was used to compare each other. Then, average mixing time values were obtained using one of the four baffles as a sensor.

## 2. MATERIALS AND METHODS

### 2.1. Theoretical Background of Method

The impeller Reynolds number is given by following equation:

$$Re = \frac{ND^2\rho}{\mu} \quad (1)$$

Three stirring flow regimes are described by impeller Reynolds number, namely laminar for  $Re \leq 10$ , transitional regime for  $10 \leq Re \leq 10^4$ , and turbulent for  $Re \geq 10^4$  [2].

In the electrochemical system, the ions are transferred from the bulk solution to the surface of the electrode principally by three driving forces; (1) migration due to potential field, (2) diffusion due to the concentration gradient, and (3) convection by the flow [3]. Assuming that the transfer is steady and unidirectional in the  $x$ - direction perpendicular to the surface of the electrode, the rate of transfer of a reacting species is expressed as;

$$N_A = (D + \varepsilon_\psi)c_A \left(\frac{n_0}{RT}\right) \left(\frac{\partial\psi}{\partial x}\right) - (D + \varepsilon_D)c_A \left(\frac{\partial c_A}{\partial x}\right) + v c_A \quad (2)$$

and the current density at the electrode can be written as;

$$N_A = \frac{i}{An_eF} \quad (3)$$

The three terms on the right side of Eq. (2) show us effect of the migration, diffusion, and convection, respectively. Since there is no bulk flow perpendicular to the electrode surface, the last term is neglected. The first term, migration, is vanished by adding inert electrolyte with excess amount into the system. In this case,

$$N_A = -Dc_A \left(\frac{\partial c_A}{\partial x}\right) \quad (4)$$

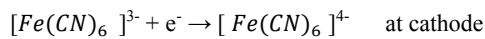
Eq. 4 can be written in a similar form as Newton's cooling law:

$$N_A = k_A(C_{Ab} - C_{As}) \quad (5)$$

Eq. 6 can be obtained by combining Eq. 3 and 5, so following equation can be written;

$$i_L = k_C C_{Ab} An_e F \quad (6)$$

In the above written equations,  $A$ , electrode area (cathode),  $m^2$ ;  $c_A$ , concentration of active ion,  $\text{mole}/m^3$ ;  $c_{Ab}$ , concentration of active ion in bulk solution,  $\text{mole}/m^3$ ;  $c_{As}$ , concentration of active ion at electrode surface (at cathode),  $\text{mole}/m^3$ ;  $D_A$ , diffusion coefficient of active ion in the electrolytic solution,  $m^2/s$ ;  $F$ , Faraday constant, ( $= 96485 \text{ C} \cdot (\text{e}^- \text{ mole})^{-1}$ );  $k_c$ , convective mass transfer coefficient,  $m/s$ ;  $I$ , electrical current,  $A$ ;  $i_L$ , limiting current,  $A$ ;  $(\partial c_A/\partial x)$ , concentration gradient,  $(\text{mole}/m^3)/m$ ;  $(\partial\theta/\partial x)$ , electrical potential gradient,  $V/m$ ;  $U_x$ , bulk flow velocity of the electrolytic solution in  $x$  direction,  $m/s$ ;  $z$ , transferred electron number. For the ELDCT, the most commonly and widely used electrolyte is the couple of potassium ferri-ferrocyanide and supported by the inert electrolyte of potassium carbonate. The reactions at the anode and the cathode are as follows;



## **2.2. Experimental Procedure**

For the mixing time measurements, the experimental setup was constructed according to the standard tank size given by Geankoplis (2003). The experiments were conducted in the vessel which was made of Plexiglas material with an inner diameter of 150 mm and the height of 200 mm having a cooling/heating jacket around it. Four baffles made of nickel were equally spaced into the tank. The each of electrolyte solutions was filled into tank until the liquid height was 150 mm. The temperature of solution was fixed to 20°C. Rushton turbine, having a diameter of 60 mm, six-vaned, 90° vane angled was concentrically orientated. The bottom clearance of the turbine was set to 50 mm (D/3). The electrochemical measurements were performed by GAMRY potentiostat-galvanostat (Interface 1000) with data acquisition and processing facility. The measurements based on conductivity were performed by using a conductivity probe made by HAMILTON, Conducell 4USF Arc 120 model. The stirring was carried out by Servodyne digital controlled stirrer equipped with a 50003-00 model tachometer. The electrolyte solution, which consists of 0.0002 M for ferricyanide, 0.0008 M ferrocyanide and 0.1 M K<sub>2</sub>CO<sub>3</sub> was used as basic electrolyte solutions.

At first, the concentration of electrolyte solution which would be used and the potential which the electrochemical limited diffusion current would be applied were determined for the measurements. Thus, the I-V measurements for basic solution (0.0002 M for ferricyanide, 0.0008 M ferrocyanide and 0.1 M K<sub>2</sub>CO<sub>3</sub>) was taken with Linear Sweep Voltammetry (LSV) method.

The stirring rate was set to 100 rpm. Four baffles made of nickel were equally spaced into the vessel. Three baffles in the vessel were used as anode and only one baffle in the vessel was used as cathode to obtain polarization curves for the determination of the limiting diffusion current conditions via LSV method with ELDCT.

At the second part, the mixing time was determined with ELDCT by using three baffles as anode and one baffle as cathode in the experimental setup given in Figure 1. Under the conditions of constant potential that gives the limiting diffusion current and at 60 rpm mixing rate, current change over time was recorded via chronoamperometry method with potentiostat device. While the measurement was going on, 5.6 mL concentrated electrolyte solution (0.1 M K<sub>3</sub>FCN<sub>6</sub>, 0.4 M K<sub>4</sub>FCN<sub>6</sub> and 0.1 M K<sub>2</sub>CO<sub>3</sub>) was added from the centre of tank at 60<sup>th</sup> second hence the change occurred in limiting current was recorded. Subsequent to the addition of concentrate solution at 60<sup>th</sup> second, the increment in current was observed in I-V graph and after a while mixing system became uniform again. This case is seen as two steps in ELDCT measurement graphs. The average values of these two steps were determined by applying Boltzmann fitting in Origin Pro 8 programme. The elapsed time between the 60<sup>th</sup> second and the second step was stated as mixing time.

Finally, the mixing time was simultaneously specified with ELDCT and conductivity measurement technique and the data were compared with each other. Basic electrolyte solution used in the experimental system was shown in Figure 1.

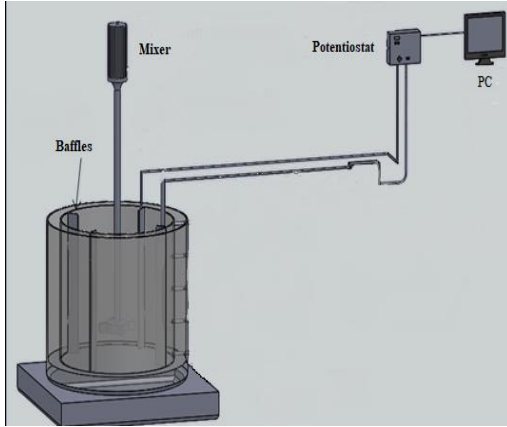


Figure 1. Experimental system.

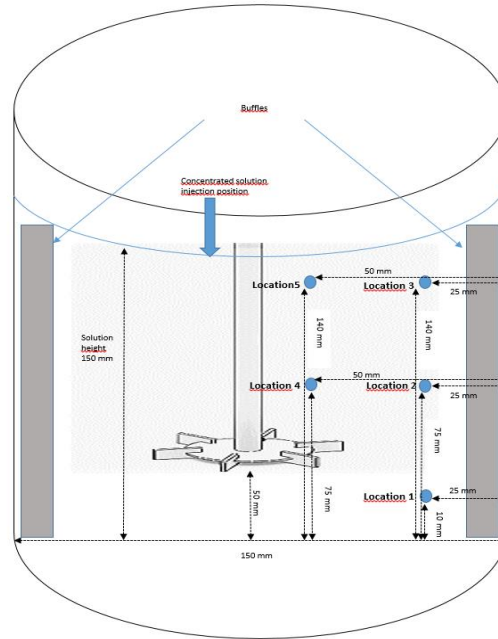


Figure 2. Positions for local measurements of mixing time

A local cathode was used for the measurements that were conducted with ELDCT because conductivity measurements were local. Therefore, the local cathode (10 mm diameter, 2 mm thickness) was placed to the same location with conductivity measurement probe. The other three baffles in the tank were used as anode. Local cathode and conductivity measurement probe were positioned in five different locations that can be seen in Figure 2.

### 3. RESULTS AND DISCUSSION

#### 3.1 Achievement Limiting Current Plateau for ELDCT

The potential that gives the value of limiting diffusion current must be specified in order to apply ELDCT. Accordingly, current-potential graph was obtained with LSV (Linear Sweep Voltammetry) method at the condition of 100 rpm constant mixing rate by using the measurement system which the one baffle was used as cathode and the other three ones were used as anode. The related graph was given in Figure 3.

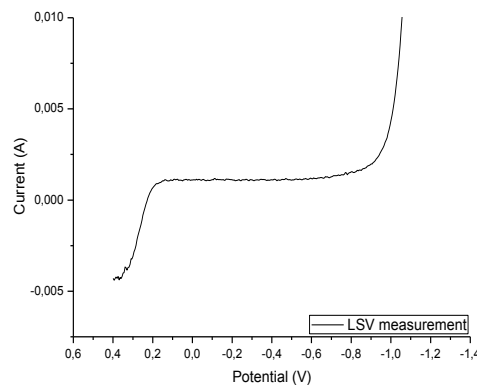


Figure 3. I-V values at constant 100 rpm mixing rate.

#### 3.2 Comparison of ELDCT and Conductivity Measurement Technique

Because the values obtained with conductivity measurement technique represent local mixing time values; the mixing time values obtained with ELDCT must be also local for comparison, therefore, a local cathode was used. This cathode and conductivity measurement probe were both positioned at five different locations as seen in Figure 2. Three nickel baffles

placed in the tank were used as anode with ELDCT measurement system. Measurements were conducted while the local cathode and conductivity measurement probe positioned at 'Location 1, 2, 3, 4 and 5'. The changes in both conductivity and limiting diffusion current were given in Figure 4, Figure 5, Figure 6, Figure 7, and Figure 8, respectively.

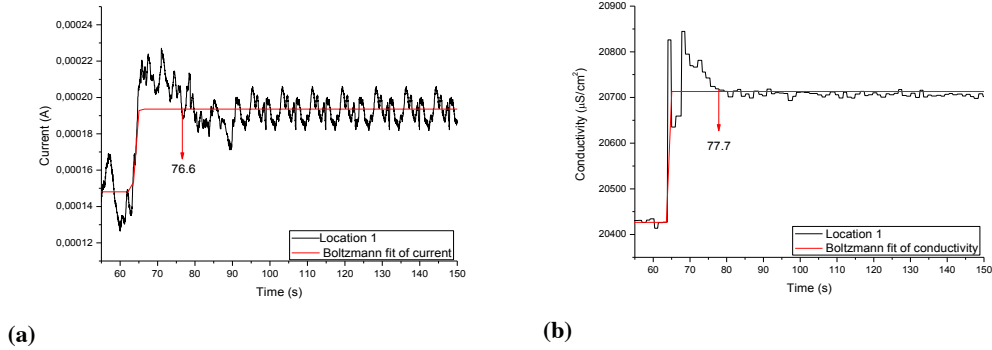


Figure 4. Mixing time recordings for Location 1 a) ELDCT b) Conductivity.

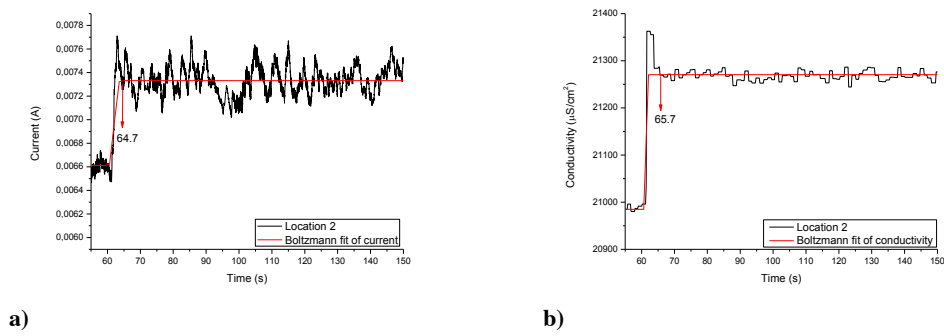


Figure 5. Mixing time recordings for Location 2 a) ELDCT b) Conductivity.

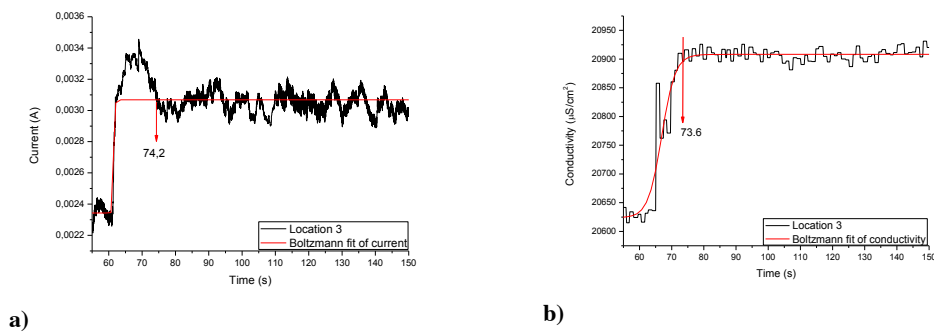


Figure 6. Mixing time recordings for Location 3 a) ELDCT b) Conductivity.

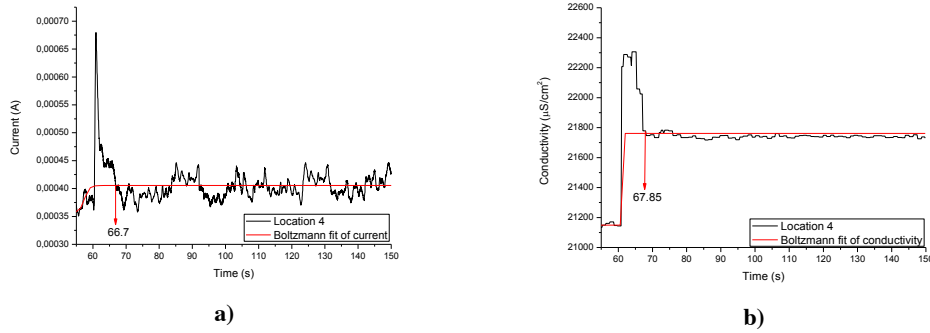


Figure 7. Mixing time recordings for Location 4 a) ELDCT b) Conductivity.

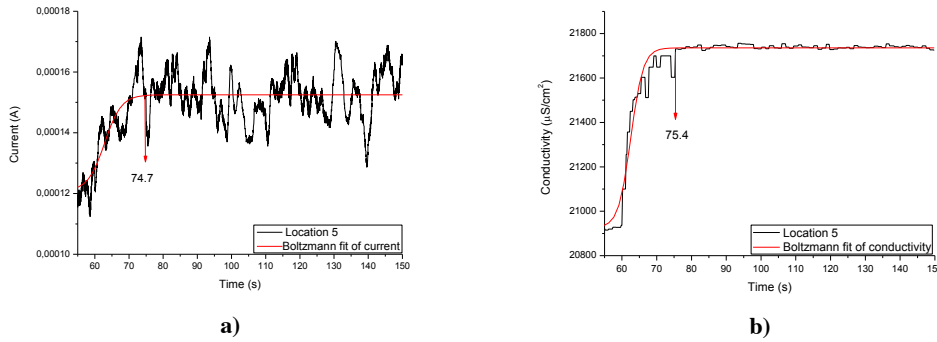


Figure 8. Mixing time recordings for Location 5 a) ELDCT b) Conductivity.

The mixing time values at each location were determined and given in Table 1.

Table 1. Average mixing time values obtained with ELDCT and conductivity measurement technique at five different locations.

| Mixing time (s)                       |         |         |         |         |         |       |
|---------------------------------------|---------|---------|---------|---------|---------|-------|
| Location                              | Loct. 1 | Loct. 2 | Loct. 3 | Loct. 4 | Loct. 5 | Mean  |
| <b>ELDCT</b>                          | 16.6    | 4.7     | 14.2    | 6.7     | 14.7    | 11.38 |
| <b>Conductivity</b>                   | 17.7    | 5.7     | 13.6    | 7.85    | 15.4    | 12.05 |
| <b>Deviation from conductivity, %</b> | 6.2     | 17.5    | -4.4    | 14.6    | 4.5     | 5.5   |

### 3.3 Determination of Average Mixing Time with ELDCT

The mixing time was determined with ELDCT method by using one of baffle as cathode and the other three ones as anode in the experimental system that is given in Figure 1. The basic electrolyte solution was used to obtain average mixing time. The current change over time was recorded by chronoamperometry method at 60 rpm mixing rate and at the constant potential which gives the limiting diffusion current. From the centre of tank, 5.6 mL concentrate electrolyte solution (0.1 M  $K_3FCN_6$ , 0.4 M  $K_4FCN_6$  and 0.1 M  $K_2CO_3$ ) was added at 60<sup>th</sup> second while the measurements were going on and the resultant change in the limiting current was recorded. Two repetitions of each experiment were conducted and the changes in limiting diffusion current were given in Figure 9. The average value of this two readings was taken as mixing time value, which was found to be 10.85 second.

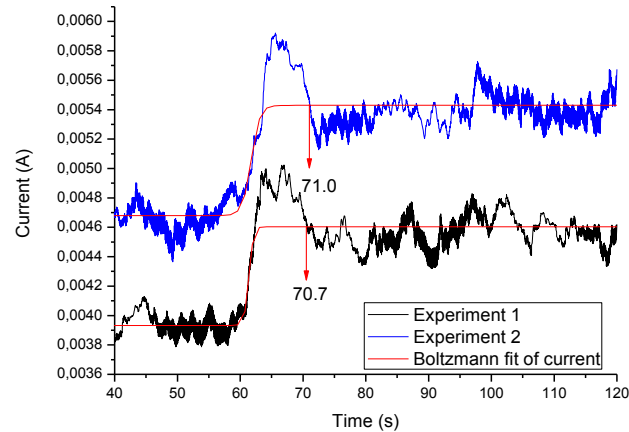


Figure 9. Records of limiting current changes at 60 rpm mixing rate for the base solution.

#### 4. CONCLUSIONS

In ELDCT, the potential which resembles the limiting diffusion current conditions was determined as  $-0.4$  V, which was the midpoint of plateaus for basic electrolyte solution at the constant mixing rate.

The average mixing time values for five different locations were obtained as 11.38 and 12.05 s respectively with ELDCT and conductivity measurement technique. The deviation between these averaged mixing times values is 5.50 %. This result shows us ELDCT is pretty much consistent with conductivity measurement technique in terms of average mixing time measurement.

The average mixing time value of the five local readings which were taken from the local cathode was 11.38 s while the corresponding value was 10.85 s for the readings from one baffle which was used as cathode. The deviation between these two values is 4.60 %. Hence, it can be claimed that the ELDCT can be used as a novel method for the determination of mixing time in the liquid mixing vessels.

#### ACKNOWLEDGEMENTS

The authors are gratefully acknowledged the financial support by Atatürk University [Grant Number: 2013/343].

#### REFERENCES

- [1]. R.A. Ghotli, A.A.A. Raman, S. Ibrahim, S. Baroutian, "Liquid-liquid mixing in stirred vessels: a review," Chem. Eng. Commun., vol. 200, pp. 595-627, 2013.
- [2]. Q.H. Zhang, Y.M. Yong, Z.S. Mao, C. Yang, C.J. Zhao, "Experimental determination and numerical simulation of mixing time in a gas-liquid stirred tank," Chem. Eng. Sci., vol. 64, pp. 2926-2933, 2009.
- [3]. G. Montante, M. Mostek, M. Jahoda, F. Magelli, "CFD simulations and experimental validation of homogenisation curves and mixing time in stirred Newtonian and pseudoplastic liquids," Chem. Eng. Sci., vol. 60, pp. 2427-2437, 2005.
- [4]. E.L. Paul, V.A. Atiemo-Obeng, K.S. M., Handbook of Industrial Mixing: Science and Practice, A John Wiley & Sons, Inc., Publication, United States of America, 2004.
- [5]. H. Jakobsen, Agitation and Fluid Mixing Technology, Chemical Reactor Modeling, Springer Berlin Heidelberg, pp. 679-755, 2008.
- [6]. P.M. Doran, Bioprocess engineering principles, Academic press, 1995.
- [7]. L. Manna, "Comparison between physical and chemical methods for the measurement of mixing times," Chem. Eng. J., vol. 67, pp. 167-173, 1997.
- [8]. J. Karcz, M. Cudak, J. Szoplik, "Stirring of a liquid in a stirred tank with an eccentrically located impeller," Chem. Eng. Sci., vol. 60, pp. 2369-2380, 2005.
- [9]. A. Cessou, U. Meier, D. Stepowski, "Applications of planar laser induced fluorescence in turbulent reacting flows," Measurement Science and Technology, vol. 11 pp. 887, 2000.

- [10]. M. Kraume, P. Zehner, "Experience with experimental standards for measurements of various parameters in stirred tanks: A comparative test," *Chem. Eng. Res. Des.*, vol. 79, pp. 811-818, 2001.
- [11]. L. Pakzad, F. Ein-Mozaffari, P. Chan, "Measuring Mixing Time in the Agitation of Non-Newtonian Fluids through Electrical Resistance Tomography," *Chemical engineering & technology*, vol. 31, pp. 1838-1845, 2008.
- [12]. D.J. Lamberto, F.J. Muzzio, P.D. Swanson, A.L. Tonkovich, "Using time-dependent RPM to enhance mixing in stirred vessels," *Chem. Eng. Sci.*, vol. 51, pp. 733-741, 1996.
- [13]. T. Mizushima, "The electrochemical method in transport phenomena," *Advances in Heat Transfer*, vol. 7, pp. 87-161, 1971.
- [14]. C.J. Geankoplis, *Transport Processes and Separation Process Principles: Includes Unit Operations*, Professional Technical Reference, Prentice Hall, 2003.

## **BIOGRAPHY**

Özkan AYDIN was born in Gümüşhane (Turkey) in 1981. After he graduated from Chemical Engineering Department in 2002, he got his master's degree in 2007 and got his PhD in 2017 at Atatürk University. He is currently working as a researcher at Osmaniye Korkut Ata University (Turkey).



# Optimization of Production of Boric Acid from Colemanite Ore with SO<sub>2</sub> Gas in Aqueous Medium

Mustafa Dağ<sup>1</sup>, M.Muhtar Kocakerim<sup>2</sup>

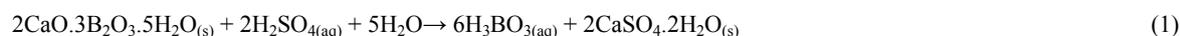
## Abstract

Boric acid can be produced with processes based on the reactions between acids and boron minerals such as colemanite, tincal and ulexite. At the present time, sulphuric acid is the most commonly used acid, although various mineral acids have been used for this purpose. In this study, firstly, optimum conditions have been determined in dissolution of colemanite with sulphur dioxide in aqueous medium. And then, levels of impurities such as magnesium, calcium, arsenic, sulphate and sulphite have been investigated in boric acid samples obtained in optimum conditions using a four stages process. A -150 µm ore, containing 81.25% colemanite and 18.75% gangue minerals from Espey, Kütahya, Turkey has been used in experiments in a 1 L-jacketted glass reactor. Chosen parameters are temperature (70-85°C), pH (3.5-4.5) and reaction time (90-150 min). Solid to liquid ratio was kept constant at 115 g/500 mL water, gas flowrate at 225 mL/min and stirring speed at 228 rpm. Optimum conditions have been found to be 4 for pH, 70°C for temperature and 60 min for reaction time. At these conditions, results of a 4-cycle study have been evaluated with regard to CaO, MgO, As<sub>2</sub>O<sub>3</sub>, SO<sub>4</sub><sup>2-</sup> and SO<sub>3</sub><sup>2-</sup> impurities. As a result, impurity levels of obtained boric acid samples have been found to be 430 ppm for CaO, 200 ppm for MgO, 0.97 ppm for As<sub>2</sub>O<sub>3</sub>, 1000 ppm for SO<sub>4</sub><sup>2-</sup> and 100 ppm for SO<sub>3</sub><sup>2-</sup>. When obtained boric acid is washed with 40 mL water for 40 g boric acid, impurities of CaO, MgO, As<sub>2</sub>O<sub>3</sub>, SO<sub>4</sub><sup>2-</sup> and SO<sub>3</sub><sup>2-</sup> drop off 110 ppm, 20 ppm, 0.29 ppm, 50 ppm and 30 ppm, respectively.

**Keywords:** Colemanite, impurity, optimization, sulphur dioxide

## 1. INTRODUCTION

Turkey is the country with the largest boron reserves in the world. 72% of the world boron reserves are in Turkey. Commercially important boron ores in Turkey are colemanite, tincal and ulexite. Colemanite is reacted with sulphuric acid to form boric acid, as follows;



One of the most important problems encountered in the production of boric acid is pollution of sulphate ions in boric acid produced. Sulphate in boric acid, especially used in optics and TV screens, is an undesirable compound. A few researches have been realized for the production of low sulphate boric acid.

Kocakerim and Alkan (1) studied the solubility of colemanite in SO<sub>2</sub>-saturated water and developed a mathematical model expressing the dissolution rate.

Çelikoyan (2) tried to reduce sulphate impurity by using propionic acid at different rates in the sulphuric acid process. But, an applicable method has been able to achieved until today.

In this study, obtaining boric acid by using SO<sub>2</sub> in aqueous media instead of sulphuric acid, which is currently available, and the determination of the level of sulphate and other impurities in obtained boric acid are investigated. For this purpose, an optimization study has been carried out using the Taguchi method.

<sup>2</sup>Corresponding author: Çankırı Karatekin University Department of Chemical Engineering, 18100 Çankırı, TURKEY

## 2. MATERIAL AND METHODS

### 2.1. Preparation of materials and methods

This study has been realized with -150  $\mu\text{m}$  ore samples, containing 81.25% colemanite and 18.75% gangue minerals from Espey, Kütahya, Turkey. Chemical analysis of ore samples used in experiments is given in the Table 1. Experimental set up is seen in Figure 1.

Table 1. Chemical Analysis of Used Colemanite Ores

| Ore   | Compounds (%)                 |       |      |                  |                                |                                |                                |          |
|---|-------------------------------|-------|------|------------------|--------------------------------|--------------------------------|--------------------------------|----------|
|   | B <sub>2</sub> O <sub>3</sub> | CaO   | MgO  | SiO <sub>2</sub> | Al <sub>2</sub> O <sub>3</sub> | As <sub>2</sub> O <sub>3</sub> | Fe <sub>2</sub> O <sub>3</sub> | Moisture |
| Espey<br>Conce. Ore (-<br>150 $\mu\text{m}$ ) | 41.44                         | 18.98 | 3.11 | 8.10             | 2.04                           | 0.18                           | 0.55                           | 1,54     |

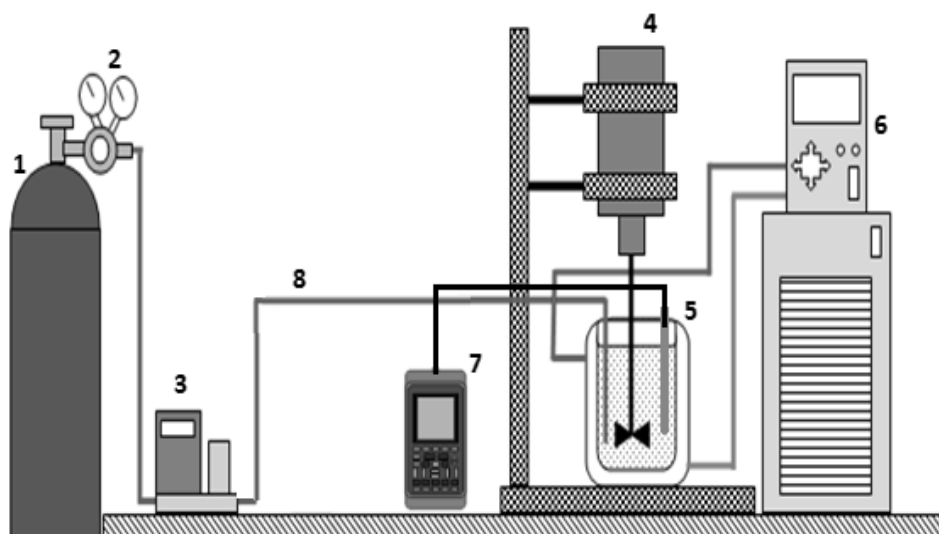


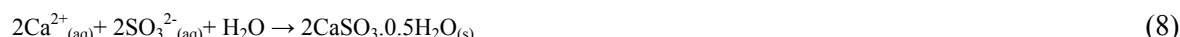
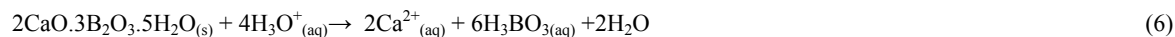
Figure 1. Experimental set up. 1-SO<sub>2</sub> cylinder, 2-Gas regulator, 3-Electrical flowmeter, 4- Mechanical stirrer, 5- Glass reactor, 6-Constant temperature circulator, 7- pH meter, 8- SO<sub>2</sub> transport line

## 2.2. Reactions

Sulfur dioxide is strong acid in aqueous solution and it has a 10<sup>-2</sup> range of acid constant. SO<sub>2</sub> gives following reactions in aqueous medium.



H<sub>3</sub>O<sup>+</sup> ions formed by above reactions dissolve colemanite and Ca<sup>2+</sup> ions formed take place CaSO<sub>3</sub>.0.5H<sub>2</sub>O with sulfite ions, according to the following reactions :



## 2.3. Preliminary Experiments and Parameters Determination of Levels

Preliminary experiments have been carried out to determine the levels of parameters considered to be effective in optimization studies. The determined parameters and their levels is given in Table 2. Also, experimental plan is seen in Table 3.

Table 2. Parameters and their levels

| Parameters |                 | Parameter levels |     |     |
|------------|-----------------|------------------|-----|-----|
|            |                 | 1                | 2   | 3   |
| A          | Temperature, °C | 70               | 80  | 85  |
| B          | pH              | 3.5              | 4.0 | 4.5 |
| C          | Time, min       | 90               | 120 | 150 |

Table 3. Experimental plan

| Experiment No | Parameter Levels |   |   |
|---------------|------------------|---|---|
|               | 1                | 2 | 3 |
| 1             | 1                | 1 | 1 |
| 2             | 1                | 2 | 2 |
| 3             | 1                | 3 | 3 |
| 4             | 2                | 1 | 2 |
| 5             | 2                | 2 | 3 |
| 6             | 2                | 3 | 1 |
| 7             | 3                | 1 | 3 |
| 8             | 3                | 2 | 1 |
| 9             | 3                | 3 | 2 |

## 3. RESULTS

### 3.1. Optimization study with concentrated Espey ore

These studies were carried out with 115-120 g of ore sample at a gas flow rate of 225 mL.min<sup>-1</sup> SO<sub>2</sub> and 228 rpm. Reactor taken 500 g water was brought to the desired temperature and then ore was added in it. Then SO<sub>2</sub> was passed through the mixture until the desired pH came. When wanted pH was arrived, SO<sub>2</sub> was cut. When the pH rises, SO<sub>2</sub> was again supplied. The results are given in Table 4.

Table 4. The results obtained with concentrated Espey colemanite ore

| Exp.No | Experimental Conditions                | Dissolution % |
|--------|--|---------------|
| 1      | Temperature:70°C, pH:3.5, Time:90 min  | 99.9          |
| 2      | Temperature:70°C, pH:4.0, Time:120 min | 99.1          |
| 3      | Temperature:70°C, pH:4.5, Time:150 min | 97.6          |
| 4      | Temperature:80°C, pH:3.5, Time:120 min | 99.7          |
| 5      | Temperature:80°C, pH:4.0, Time:150 m   | 98.9          |
| 6      | Temperature:80°C, pH:4.5, Time:90 min  | 97.5          |

|   |  |      |
|---|--|------|
| 7 | Temperature:85°C, pH:3.5, Time:150 min | 98.4 |
| 8 | Temperature:85°C, pH:4.0, Time:90 min  | 99.8 |
| 9 | Temperature:85°C, pH:4.5, Time:120 min | 97.0 |

By applying variance analysis to the results in Table 4, the effect level of the parameters was determined. The variance analysis results are given in Table 5. The most effective parameter according to these results is pH. Temperature and reaction time are not effective. Also, the effectiveness of the parameters on the larger better performance criterion is seen Figure 2. According to Fig. 2, optimum conditions are 70°C for temperature, 4.0 for pH and 90 min for reaction time.

Table 5. Variance analysis for concentrated Espey ore

| Parameters |                    | SS       | D <sub>f</sub> | MS       | F        |
|------------|--------------------|----------|----------------|----------|----------|
| A          | Temperature, °C    | 0.434689 | 2              | 0.217344 | 0.61027  |
| B          | pH                 | 7.432156 | 2              | 3.716078 | 10.43419 |
| C          | Reaction Time, min | 0.853756 | 2              | 0.426878 | 1.19861  |
| Error      |                    | 0.712289 | 2              | 0.356144 |          |

In order to determine the optimum value for the reaction time, in 70°C and pH 4, 45, 60 and 120 minutes of experiments were carried out. The results are given in Table 6. According to the results, it was understood that a 60 minute dissolution would suffice, and then, cycle experiments of 60 minutes were realized.

### 3.2. Cycle Experiments Made with Concentrated Espey and Impurity Analysis

In these experiments, the gas flow rate was 280 mL. min<sup>-1</sup> and the stirring speed was 228 rpm. 115 g concentrated colemanite was used in the first experiment and 70-75 g concentrated colemanite in subsequent experiments. Results are given in Table 7. Also, the obtained boric acid samples were washed with twice as much cold water as the wet mass. After washed and unwashed boric acid samples were dried, impurity analyzes were carried out on washed and unwashed samples. The results obtained are seen in Table 8.

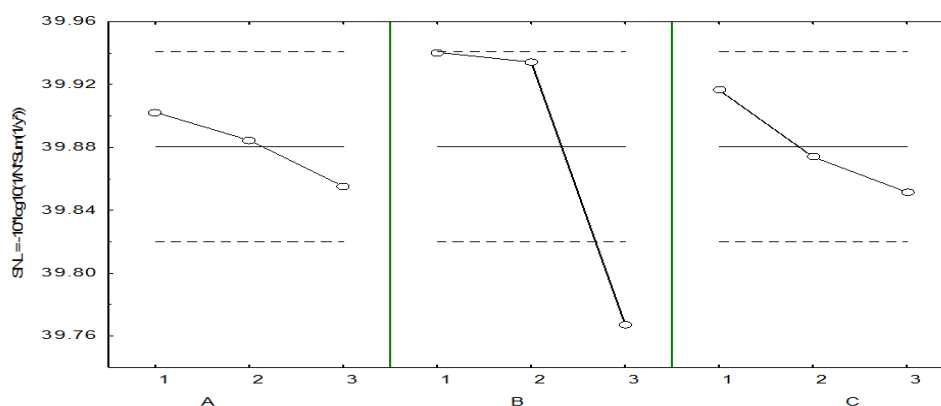


Figure 2. The effectiveness of the parameters on the larger better performance criterion for colemanite solubilized in studies with Espey concentrate colemanite

Table 6. The effect of reaction time on dissolution of concentrated Espey colemanite

| Exp. No | Experimental Conditions                | Dissolution % |
|---------|--|---------------|
| 1       | Temperature:70°C, pH:4.0, Time:120 min | 99.1          |
| 2       | Temperature:70°C, pH:4.0, Time:60 min  | 98.9          |
| 3       | Temperature:70°C, pH:4.0, Time:45 min  | 98.3          |

Table 7. The results of cycle experiments

| Cycle No | Experimental Conditions               | Dissolution % |
|----------|---------------------------------------|---------------|
| 1        | Temperature:70°C, pH:4.0, Time:60 min | 99.6          |
| 2        | Temperature:70°C, pH:4.0, Time:60 min | 99.7          |
| 3        | Temperature:70°C, pH:4.0, Time:60 min | 97.0          |

|   |                                       |      |
|---|---------------------------------------|------|
| 4 | Temperature:70°C, pH:4.0, Time:60 min | 99.5 |
|---|---------------------------------------|------|

Table.8. Impurities in boric acid obtained in cycle experiments

| Cycle No | Washing status | Compounds(ppm)                |                                |     |     |                               |                               |
|----------|----------------|-------------------------------|--------------------------------|-----|-----|-------------------------------|-------------------------------|
|          |                | B <sub>2</sub> O <sub>3</sub> | As <sub>2</sub> O <sub>3</sub> | CaO | MgO | SO <sub>4</sub> <sup>2-</sup> | SO <sub>3</sub> <sup>2-</sup> |
| 1        | Unwashed       | 56.23                         | 0.85                           | 470 | 110 | 900                           | <100                          |
|          | Washed         | 56.27                         | 0.37                           | 85  | 7   | 40                            | 30                            |
| 2        | Unwashed       | 55.97                         | 0.84                           | 445 | 202 | 1100                          | 100                           |
|          | Washed         | 56.24                         | 0.35                           | 125 | 6   | 50                            | 40                            |
| 3        | Unwashed       | 56.0                          | 0.91                           | 420 | 227 | 1100                          | 100                           |
|          | Washed         | 56.2                          | 0.29                           | 117 | 12  | 42                            | 35                            |
| 4        | Unwashed       | 55.96                         | 0.78                           | 430 | 285 | 700                           | 100                           |
|          | Washed         | 56.3                          | 0.29                           | 110 | 20  | 30                            | 30                            |

These results demonstrate that low sulphate boric acid can be obtained when reacting colemanite with SO<sub>2</sub> in aqueous medium under specified conditions. Also, another impurities such as CaO, MgO, SO<sub>4</sub><sup>2-</sup> and As<sub>2</sub>O<sub>3</sub> can be removed with this process.

## REFERENCES

[1]- B. K Çelikoyan, 2008, "Kolemanitten Propiyonik Asit Varlığında Borik Asit Üretim Prosesinin Geliştirilmesi", Ph.D, Thesis, Sciences Institute, ITU, Istanbul, Turkey.

[2]- M.M. Kocakerim, and M. Alkan,, "Dissolution Kinetics of Colemanite in SO<sub>2</sub>-Saturated Water", Hydrometallurgy, vol. 19, pp 385-392, 1998.

## BIOGRAPHY

Dr. M.Muhtar Kocakerim is lecturer at Chemical Engineering Dep. of Çankırı Karatekin University in Turkey. He graduated from Chemical Engineering Dept. of Istanbul University. He received Ph.D degree from Atatürk University in 1975.



# Removal of Sulfate Anions from Borax Solution by Purolite A 400 MB

Mehmet Çopur<sup>1</sup>, Mehtap Özekmekçi<sup>\*1</sup>, Habibe Yetkin<sup>1</sup>, M. Muhtar Kocakerim<sup>2</sup>

---

## Abstract

*Tincal is the main mineral among the various boron minerals for the production of borax decahydrate and pentahydrate salts. Tincal ore contains some clay minerals (mainly montmorillonite), dolomite, other calcium and magnesium borate minerals. Although the production processes of borax salts are very simple, the impurities coming from the raw material (tincal ore) cause many problems in the processes. These impurities exist especially in the final salt products and consist mostly of calcium, magnesium and sulfates ions. In this study, Purolite A 400 MB, an ion exchange resin was used to remove sulfate ions. It has high operating capacity, excellent regeneration efficiency and good rinse characteristics. Temperature, borax concentration and sulfate concentration were chosen as parameters in the experiments and effects of these parameters on sulfate removal were investigated. Experiments were carried out on an ion exchanger column. A solution of borax containing sulfate was fed onto the top of column at the known flow rate using peristaltic pump. Eluate samples were collected at intervals and analyzed by ICP OES. The results of analysis of samples collected showed that Purolite A 400 MB can efficiently remove sulfate anions in borax solutions.*

**Keywords:** Borax, ion exchanger, sulfate

---

## 1. INTRODUCTION

Boron is the most important element in the world. Turkey has approximately 70% of the world's total boron reserves. Boron compounds, which are used in a very broad range of industrial application such as glass, polymer, refractory materials, steel and etc. Most of the commercially recoverable boron reserves are colemanite, ulexite and tincal [1]. Tincal, which contains dolomite and various clay minerals (mainly montmorillonite) and small amounts of other boron minerals such as ulexite colemanite, inyoite, tunellite, hydroboracite, tincalkonite, kurnakovite and meyerhofferite, is a mineral with a chemical formula of  $\text{Na}_2\text{O} \cdot 2\text{B}_2\text{O}_3 \cdot 10\text{H}_2\text{O}$ .

Borax decahydrate and borax pentahydrate, which are the starting materials in the production of many other boron compounds, are produced from tincal. Although the production process of borax hydrates are simple, due to the calcite, dolomite, sulfates minerals and clay minerals and small amount of calcium and magnesium borate which are present in the tincal ore, some impurities exist especially in the final products and effect the product quality negatively.

---

Corresponding author: <sup>1</sup>Department of Chemical Engineering, Bursa Technical University, Bursa, Turkey, [mehtap.ugur@btu.edu.tr](mailto:mehtap.ugur@btu.edu.tr)

<sup>2</sup>Çankırı Karatekin University, Department of Chemical Engineering, 18100 Çankırı, Turkey. [mkocakerim@yahoo.com](mailto:mkocakerim@yahoo.com)

Tincal contains approximately 25-28 % B<sub>2</sub>O<sub>3</sub>. In the production of borax pentahydrate, tincal ore is first dissolved with the necessary amount of water or mother liquor containing about 18% Na<sub>2</sub>B<sub>4</sub>O<sub>7</sub> with %2 Na<sub>2</sub>CO<sub>3</sub> at 92-95 °C. Then the saturated borax solution is separated from the undissolved particles by filtration. After the solution density is brought to 1.24-1.25 g/cm<sup>3</sup> and then crystallized by cooling up to 65°C to obtain borax pentahydrate [2].

The most important impurity components encountered during ore dissolution are CaO, MgO, sulfate, SiO<sub>2</sub>, Cl. While only CaO and sulfate are problems in the tincal ore, SiO<sub>2</sub>, CaO and sulfate impurities in the calcined ore are greatly increased. This indicates that the gypsum is in the clay matrix and is not much dissolved with water due to the fact that clay swollen with water in tincal ore. In calcined tincal, more sulfates have been found in the solution since ore has been milled, structure of clay has been decomposed and the gypsum has become more solubility semihydrate or anhydrate structures.

There are several methods for removal of sulfate anions from waste water. The removal of this anion by means of adsorption with active carbon [3], chemical precipitation method [4], membrane technologies such as reverse osmos and dialysis, biological treatment [5, 6] and ion exchange [7] method were studied. The selection of the wastewater treatment method generally depends on the wastewater type, removal rate, waste concentration and cost of treatment. The essential requirement of sulfate removal process from solution is that it has the ability to meet regulatory. Chemical precipitation by adding lime is the simplest and lower cost alternative method to remove sulfate, but it can only remove sulfate to the gypsum saturation level nearly 1800 mg/l. For this reason, it is more convenient to use a pretreatment stage. Membrane technology is an efficient method for removal of sulfate, however some of the technical and economical limitations prevents its usage. Sulfate is removed from water or solution using semipermeable membrane. Concentration difference is used as driving force. Due to the organic pollutants, membranes are clogged continuously in a short time and since they need to be changed, it is a costly method. In Biological treatment, temperature of the solution must be high in order to allow growth of the bacteria that reduce the amount of sulfate. In this case, too much energy is needed. The process requires a large input of a relatively cost organic reagent for sulfate removal. For these reasons, biological treatment is not highly preferred method [8].

Ion exchange resin has been important method for the removal of ions from water or aqueous solution [9-14]. Process for removal ions by using ion exchange have been studied by different authors [15-17]. It was observed that ion exchange resin has good potential for sulfate removal. Ion exchange removes unwanted ions from solution by transferring them to a solid material called ion exchange resin. The sulfate anions are exchanged with hydroxyl ions in the anion exchange resins to adsorb the anion exchanger. It has several advantages compared to other sulfate removal methods. The process has based on low cost and there are varieties of resins that can be found easily. Operating cost is also low due to low power consumption compared to membrane and biological method on sulfate removal. Because of these reasons, the ion exchange method is the most suitable for sulfate removal.

Purolite A 400 MB, an ion exchange resin was used to remove sulfate ions. This resin is a strong base type 1 anion exchange resin with gel polystyrenic matrix specially designed for use in mixed bed systems. In fact it has a special particle size distribution to enhance separation from the cation component. It has high operating capacity, excellent regeneration efficiency and good rinse characteristics. The chemical structure of resin is RN<sup>+</sup>(CH<sub>3</sub>)<sub>3</sub>Cl<sup>-</sup> and when washed with water, Cl<sup>-</sup> ions exchange with OH<sup>-</sup> ions. According to the authors' knowledge, up to now there is not a comprehensive study on the removal of sulfate anions from borax solutions with Purolite A400 MB ion exchange resin. In this study, Purolite A 400 MB, an ion exchange resin was used to remove sulfate ions from borax solution in a fixed bed column. The parameters that influence ion exchange such as temperature, borax concentration and sulfate concentration were investigated.

## 2. MATERIALS AND METHOD

In the experiment after 50 gram of resin was washed with distilled water, it was packed into a water jacket glass column of internal diameter 2.5 cm and a length of 80 cm. (given figure 1). A solution of borax containing different temperature and sulfate concentration was fed onto the top of column at the 170 ml/min flow rate using peristaltic pump. Samples were collected at the end of the each minute and analyzed by ICP OES. The average sulfate concentrations versus time were plotted in the obtained results.

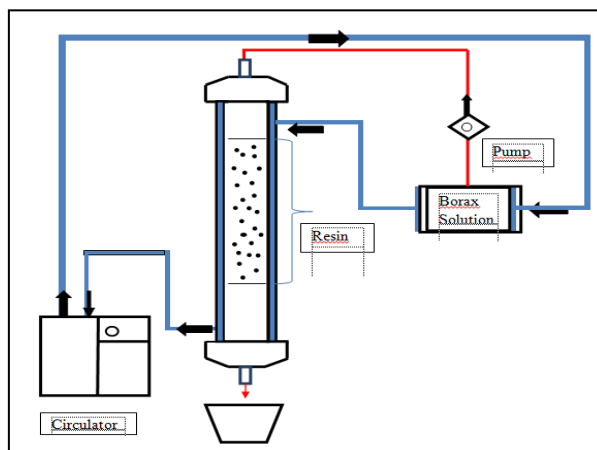


Figure 1. Experimental set up used in sulfate removal experiments

### 3. RESULTS AND DISCUSSION

Temperature, borax concentration and sulfate concentration were investigated in this study.

#### 3.1 Effect of Temperature

Figure 2 shows the effect of temperature on removal of the sulfate from solution at a concentration of 27.08 g/L  $\text{Na}_2\text{B}_4\text{O}_7$  containing 5000 ppm sulfate. The cumulative mean sulfate concentration of the solution taken from the column was given against time in the graph. It was observed that the best sulfate removal occurs at 35 °C and 55 °C. It is needed to be fed water for a longer time in order to increase the desired value of sulfate concentration of solution taken from column as the temperature increased. It is meant to be obtained water having the more than required amount of sulfate concentration.

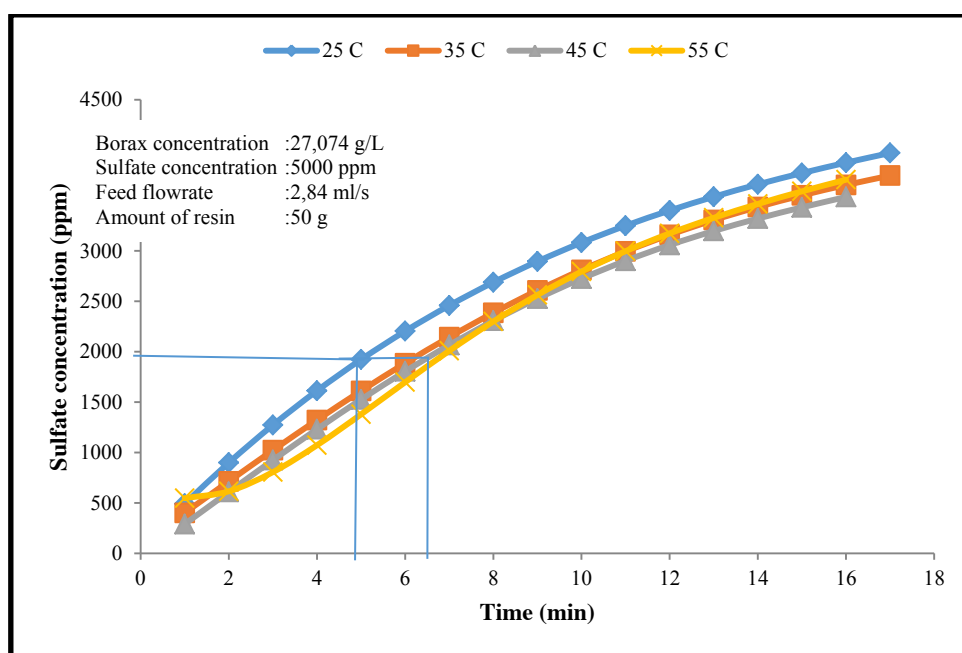


Figure 2. The cumulative mean sulfate concentration of the solution taken from the column at different temperature.

The effect of temperature for sulfate removal from 51.874 g/L concentration of borax solutions which contains 5000 ppm sulfate was investigated at 42 °C, 50 °C and 60 °C in figure 3. According to the graph, the sulfate removal at 42 °C and 50 °C were nearly the same results.

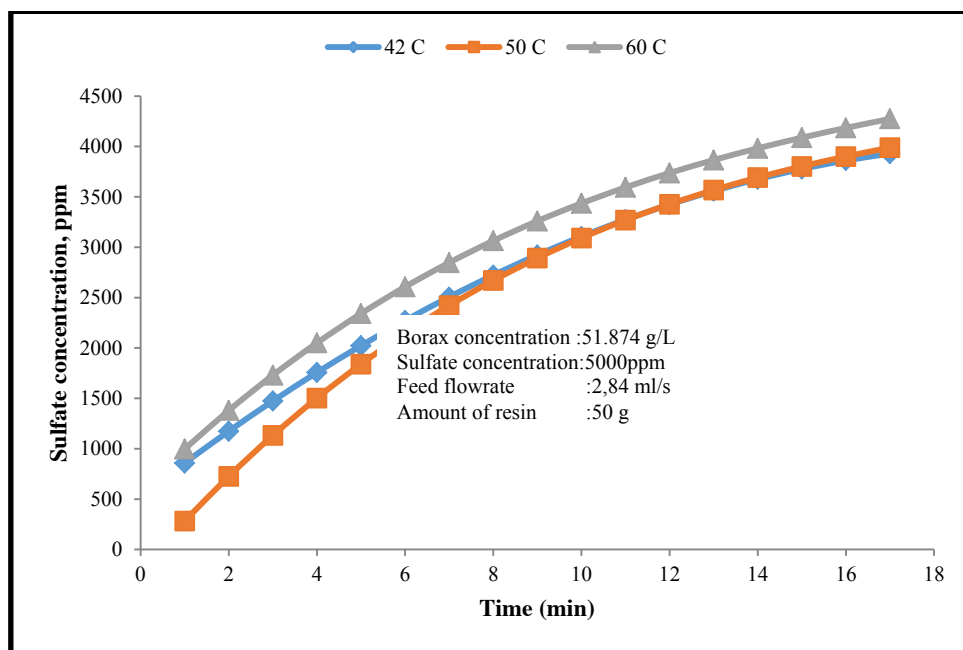


Figure 3. The effect of temperature on the removal of sulfate by A400 ion exchange resin

### 3.2 Effect of Sulfate Concentration

Figure 4 shows the effect of sulfate concentration on removal of sulfate from solution containing 27,074 g/l  $\text{Na}_2\text{B}_4\text{O}_7$  and different amount of sulfate at 25 °C. As the sulfate concentration of the solution increases, the less purified water will be obtained at the same time. However, as the sulfate concentration is increased, the amount of sulfate removed is also increased.

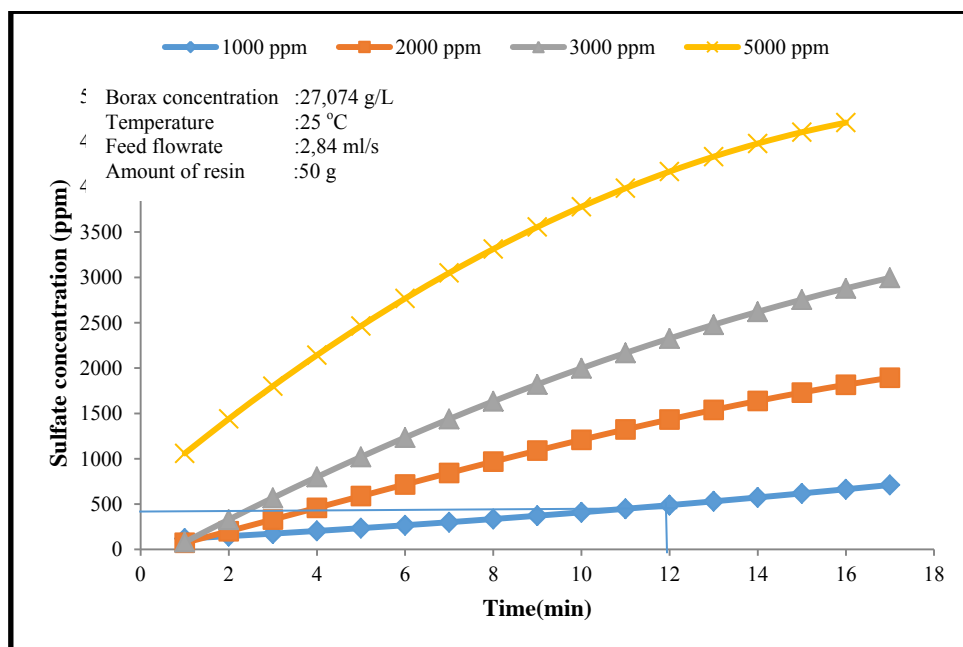


Figure 4. The effect of sulfate concentration on the removal of sulfate by A400 ion exchange resin

### 3.3 Effect of Borax Concentration

To investigate the effect of boron concentration on the sulfate removal, solution containing 5000 ppm sulfate were prepared at three different borax concentrations (0 g/l  $\text{Na}_2\text{B}_4\text{O}_7$ , 13,537 g/l  $\text{Na}_2\text{B}_4\text{O}_7$ , 27,074 gram  $\text{Na}_2\text{B}_4\text{O}_7$ ) and the experiments were carried out at 25 °C. The result was given figure 5. It was observed that, borax concentration was not an important effect on the sulfate removal.

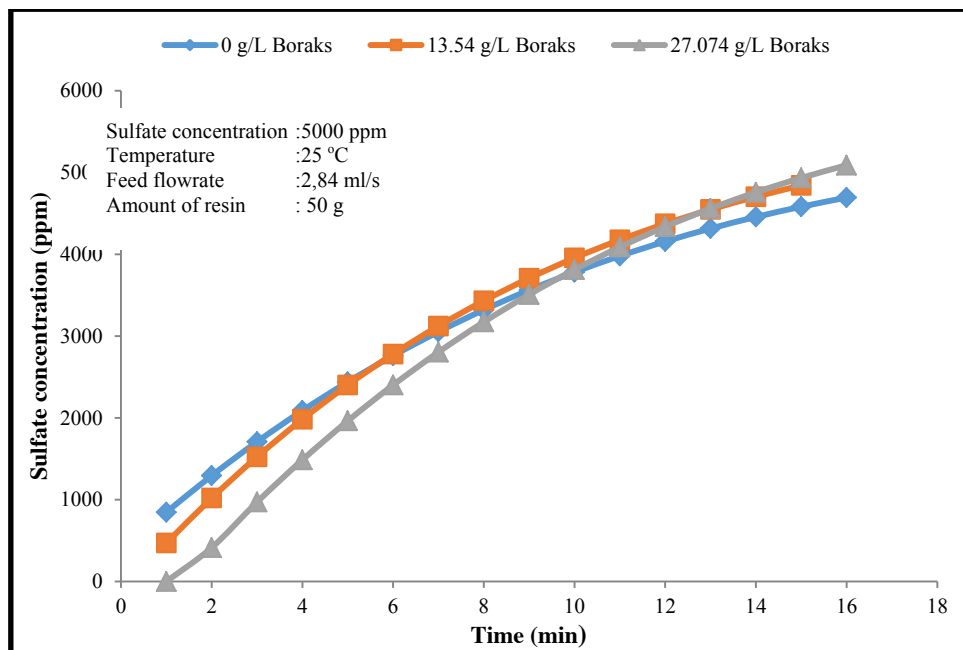


Figure 5. The cumulative mean sulfate concentration of the solution taken from the column at different borax concentration

## 4. CONCLUSION

In this study, Purolite A400 MB resin was used for sulfate removal ions from borax solution for the first time. According to the results show that Purolite A400 MB resin can efficiently remove sulfate anions concentration in the ranges of 1000-5000 mg/l.

## REFERENCES

- [1] Ö. Küçük, M. M. Kocakerim, A.Yartaşı, M. Çopur, "Dissolution of Kestelek's colemanite containing clay minerals in water saturated with sulfur dioxide", *Industrial and Engineering Chemistry Research*, vol. 41, pp.2853-2857, 2002.
- [2] A. Biyikoglu, E. Yeksan, "Production of anhydrous borax from pentahydrate", *International Journal of Hydrogen Energy*, vol. 33, pp. 7103-7109, 2008.
- [3] C. Namasivayam, D. Sangeetha, "Application of coconut coir pith for the removal of sulfate and other anions from water", *Desalination*, vol. 219, pp. 1-13, 2008.
- [4] J.P Maree., H.A. Greben, M. De beer, "Treatment of acid and sulfate-rich effluents in an integrated biological/chemical process", *Water SA*, vol. 30 (2), pp.183-190,2004.
- [5] L.A Du Preez, J.P. Odendaal, J.P. Maree, M. Ponsonby, "Biological removal of sulfate from industrial effluents using producer gas as energy source", *Environmental Technologies*, vol. 13, pp. 875-882, 1992.
- [6] J.P. Maree, G. Hulse, D. Dods, Schutte C.E., "Pilot plant studies on biological sulfate removal from industrial effluent", *Water Science and Technologies*, vol. 23, pp.1293-1300, 1991.
- [7] Schoeman J.J., Steyn A., "Investigation into alternative water treatment technologies for the treatment of underground mine water discharged by Grootvlei Proprietary Ltd. into the Blesbokspruit in South Africa", *Desalination*, 133, 13-30, 2001.
- [8] D. Kratochvíl, B. Marchant, M. Bratty, R. Lawrence," Innovations in ion exchange technology for removal of sulfate", *Annual International Water Conference*, 2008.
- [9] S. Rengaraj, Y. Kim, C.K. Joo, K. Choi, J. Yi, "Batch adsorptive removal of copper ions in aqueous solutions by ion exchange resins: 1200H and IRN97H", *Korean Journal of Chemical Engineering*, vol. 21, pp.187-194, 2004.

- [10] Ö. Yavuz, Y. Altunkaynak, F. Güzel, "Removal of copper, nickel, cobalt and manganese from aqueous solution by kaolinite", *Water Research*, vol. 37, pp. 948-952, 2003.
- [11] D. Muraviev, V. Gorshkov, A. Warshawsky, *Ion Exchange*, Decker, New York, 2000.
- [12] G.M. Tillman, *Water Treatment Troubleshoot and Problem Solving*, Lewis Publishers, New York, 1996.
- [13] J.P. Rawat, A. Ahmad, A. Agrawal, "Equilibrium studies for the sorption of Cu<sup>2+</sup> on lanthanum diethanolamine—a chelating material", *Colloids and Surface*, vol. 46, pp. 239-253, 1990.
- [14] R. Haghsheno, A. Mohebbi, H. Hashemipour, S. Sarrafi, "Study of kinetic and fixed bed operation of removal of sulfate anions from an industrial wastewater by anion exchange resin", *Journal of Hazardous*, vol. 166, pp. 961-966, 2009.
- [15] A.U. Beas, S.J.P. Umali, R.L. Mercado, "Ion exchange and adsorption of some heavy metals in a modified coconut coir cation exchanger", *Water Science and Technology*, vol. 34, pp. 193-200, 1996.
- [16] J. Lehto, R. Harjula, H. Leino-nen, A. Paajanen, T. Larila, K. Mononen, L. Saarinen, "Advanced separation of harmful metals from industrial waste effluents by ion exchange", *J. Journal of Radioanalytical and Nuclear Chemistry*, vol. 208, pp. 435, 1996.
- [17] C. Simpson, S.H. Laurie, "Ion exchange studies on zinc-rich waste liquors", *Hydrometallurgy*, vol. 51, pp. 335-344, 1996.

## **BIOGRAPHY**

Dr. M. Muhtar Kocakerim is lecturer at Chemical Engineering Dep. of Çankırı Karatekin University in Turkey. He graduated from Chemical Engineering Dept. of Istanbul University. He received Ph.D degree from Atatürk University in 1975.



# Removal of Boron from Aqueous Solution Using Tannins from Turkish Acorns (Valonia)

*Nalan Erdöl Aydın<sup>1</sup>, Yaren Barutçu, Gülhayat Nasün Saygılı*

---

## Abstract

*Adsorption has been proved as an efficient process to remove a multiplicity of solutes from aqueous solution. Various biosorbents have found promising applications in wastewater treatment and in the recovery of critical metals that is, nowadays, the spotlight due to the promotion of environmental and economic sustainability. Tannins are excellent candidates to produce biosorbents.*

*In this study, valex which has natural tannens was produced from Turkish acorns (valonia) by extraction process and then, valex was used for adsorption studys of boron from aqueous solutions. Boron concentrations were measured using the ICP. Produced valex was also characterized by using FTIR and SEM. The results was showed that boron can be removed from aqueous solution by tannins by yield of 88%.*

**Keywords:** Boron removal, Bioadsorbents, Tannins, Turkish acorns

---

## 1. INTRODUCTION

In the recent years a significant increase in the concentration of boron in surface waters has been observed. The increase as well as concentration fluctuations at different areas are caused by many natural and anthropogenic factors. For the natural source one can count weathering of rocks and leaching of salt deposits. The deposits of natural boron appear on the shoreline mostly. Because of the high volatility of this element, boron is found in the rainfall at coastal areas. The same component can be found in the "acid rain" also resulted from industrial activities [1]. The industrial activities are the next reason in increase of boron amount in surface waters as well. Boric acid and boron salts are very widely used in many branches of industry and used as a preservative [2],[3]. Recently, some boron compounds are used in manufacturing of high-energy fuels, coolants and catalysts [4].

Because of all these factors, the concentration of boron in surface water at industrial and urban areas still increases. Therefore, the problem of removing boron from water is not only related to the countries with natural deposits of this element but it has also become the critical issue for highly developed countries [2].

Boron is also an essential element for plants, animals and human being. For plants, boron plays a role in carbohydrate metabolism, sugar translocation, hormone action, normal growth and functioning of the apical meristem, nucleic acid synthesis, and biological membrane structure and function [5]. Boron deficiency can cause a series of damage to plants, such as retardation of root and leaf growth, bark splitting, retardation of enzyme reactions and leaf photosynthesis, and even can lead to a death of plants [6], [7]. For animals and human beings, boron relates to immune function of organisms [8], it also has effects on bone metabolism and central nervous system function [9]. Lack of boron may lead to malformations of embryos grown for vertebrates [10] and cause low absorption efficiency for nutrient elements such as calcium, magnesium and phosphorus [11], [12].

However, the concentration range between boron deficiency and its toxicity is very narrow, it becomes hazardous for organisms when boron amount is slightly higher, and toxicity effects caused by excess boron is more common than boron deficiency in the environment [12]. For human and animals, although the mechanism is not clear for toxicity by excessive boron, a long-term effect on environment can't be ignored with chronic exposure of boron. Adverse effects of boron can lead to problems with cardiovascular, coronary, nervous and reproductive systems [2]. In addition, it results in a change in blood composition, development retardation of children and a higher risk of birth pathology for pregnant women [13].

In the past few decades, numerous of separation technologies have been applied in the boron removal from aqueous solutions, including adsorption, reverse osmosis [2], ion exchange [13], electrocoagulation [14], chemical coagulation [15], hybrid process [16].

Adsorption is an extremely effective way for boron removal from aqueous solutions. Various sorbents are utilized in adsorption processes for boron removal, including activated carbon, fly ash, clays, natural minerals, layered double hydroxides, biological materials, oxides, mesoporous silica, nanoparticles, complexing membranes and selective resins. According to different material characteristics, natural material sorbents can be divided into two major parts. One is natural minerals like sepiolite, red mud, cristobalite, alunite, etc. The other is plant materials, such as seeds of plants, natural polymers. Extensive source and lower price are main advantages of natural material sorbents, which is confirmed to be the requirement of low cost boron removal processes for water treatment [12].

Recently, bioadsorbents mostly have been utilized in adsorbent process for water purification. Tannins are naturally occurring phenolic compounds, which have been a subject of extensive research leading to development of a wide range of industrial applications. Tannins, are high molecular weight polycyclic aromatic compounds widely distributed through the plants. They are found in the leaves, fruits, barks, roots, and wood of trees like oak, walnut, mimosa, and mahogany. Tannins are water-soluble compounds, so to use tannins as adsorbents; they need to be modified to insoluble tannin gels [2], [17].

There are no universal condition for extracting tannins from vegetable sources. The yield and the composition of extracts depends on the source, type of solvent, extraction time, temperature, solid-liquid ratio, and preparation of the sample, which is commonly milled, used in fresh, frozen or dried state. The extraction procedure should be optimized in a case-specific basis. The polar nature of water makes it possible for use as an extraction solvent for many compounds [17].

In this study, valex which has natural tannens was produced from Turkish acorns (valonia) by extraction process, and removal of boron from aqueous was investigated by adsorption process. Produced valex was used as adsorbent in adsorption studys

### **1.1. The Standart of Boron**

Since a series of environmental and health issues have been found caused by boron, WHO established guideline for boron limit in drinking water. In 2011, WHO revised the guideline value of boron to 2.4 mg/L [18]. However, only a few of countries follow the WHO recommendation. Because the value of 2.4 mg/L exceeds the tolerate concentration of many crops, especially in the low annual rainfall regions, such as South and South West Asia, and Africa, where a large quantity of irrigation water is provided by desalination plants [19]. The boron regulations are 1.0 mg/L in European Union, UK, South Korea and Japon. There are no federal regulations of boron in the USA, while the boron regulations differ from state to state in the range of 0.6 to 1.0 mg/L [12]. Canada, Brazil and Australia have set the recommended content of boron as high as 5 mg/L, 5 mg/L, 4 mg/L, respectively, much higher than the WHO guideline [11]. Also, boron discharge limit value is 500 mg/L in the Turkish water pollution control regulation.

### **1.2. Acorns (Valonia), Valex and Tannin-containing Plants**

Acorns (oak acorn) is a hard, toothed fruit that is oval. It is called "valonia" in the form of chestnut. It is also very rich in carbohydrate, protein and sterols, which are common in Mediterranean countries such as Italy, Spain, Greece, and Turkey [20]. It should be noticed that oak acorns have a structure that accumulates waste and are not affected by agricultural chemicals and chemical wastes. The main elements of acorns are; gallic acid, ellagic acid, starch, sugar and tannins [21]. The tannin content of valonia is about 35%. Turkish oak is a source of valonia which grows in 260,000 hectare areas in Turkey.

Acorns (Valonia) extracts, commercially know as "valex", are rich in tannin and are widely used in many fields; essentially, in the leather trade, pharmaceuticals and painting. Valex produced by the extraction of valonia is used in the leather industry as a filler material. Valonia is utilized either in the form of its extract or direct powder. In the tanning of leather, valonia can be used either alone or mixed with the other tanning material. Valex is a natural tannin, an acorn extract, and a bio adhesive that does not pollute the environment during application [20].

Tannins have a wide distribution in the plant world. There are many plants in the world that contain tannins. Oak, chestnut, birch tree, acacia, pomegranate, pine, beech and their different varieties are among the richest plants. They include tea leaves, coffee seeds, apples and grapes as well as tannins. The acorns, the fruit peels of the pomegranate and sumac leaf contain plenty of tannins [21]. As the tree grows older, the amount of tannins in its crust increases. Mimosa and kebrako, which are a type of tanning material used extensively in the world, are used in Turkey, sumac and acorn tannins (valex). Commercial quantities of tannins can only be obtained from some plants, and tannins are found intensely in different parts of each plant, including crust, wood, fruit and leaves [20].

## 2. MATERIALS AND METHODS

In this study, the valex was produced from the acorns obtained from Artu Chemical Company. The adsorbent which is then to be used in the adsorption experiment of the valex was prepared.

The produced adsorbent was added to the boron solution of the specific concentration and left to stir at 175 rpm in the shaken water bath for 24 hours. At last the solution was analyzed by ICP analysis to determine the concentration after adsorption and the adsorption yield for the boron removal of the produced adsorbent was calculated.

### 2.1. Valex Production from Turkish Acorns (*Valonia*)

The production of valex in classical method, firstly acorns were broken and then the grain sizes were reduced to 2 – 0.85 mm. Grinded acorns pellets taken in a beaker were added to 1/3 of water and stirred at 90°C for 8 hours. The solid phase was removed and water and fresh oak pellets were added. In this way, the enrichment was carried out by the addition of gradually ground solid and water. The enriched liquid phase was further concentrated on a rotary evaporator, then centrifuged to remove impurities from the impurities. The pH of the resulting solution was measured as 3.3 and the density as 1.12 g/cm<sup>3</sup>. At the last stage, the concentrated solution was fed to the spray drier at 180°C to complete the valex production. The valex yield from the oak acorn is calculated by the following Equation 1.

$$\text{Efficiency (\%)} = (\text{amount of valex obtained} / \text{acorn amount used}) \times 100 \quad (1)$$

### 2.2. Preparation of Adsorbent from Produced Valex

Before starting the production of the adsorbent, the water solubility of the valex obtained by extraction from the acorns was checked. For this purpose, 1 g of produced valex was weighed and mixed with 200 mL distilled water for 5-10 minutes on a magnetic stirrer and the entire valex was dissolved. In this way, it is made possible to convert the valex into a water-insoluble adsorbent as a modified gel with formaldehyde.

11.5 g of the produced valex and 50 mL of 13.3 N NH<sub>3</sub> solution were stirred in a beaker for 5 minutes, and this solution was stirred for another 5 minutes at room temperature with addition of 65 mL of 37% formaldehyde. At the end of mixing, a yellowish precipitate was formed in the beaker and the solution was again stirred in a magnetic stirrer for 30 minutes and centrifuged. The pH of this liquid phase was measured as 6.55. On top of the precipitate formed by the solid phase, 50 mL distilled water was added and stirred at 70 °C for 3 hours in a magnetic stirrer. The resulting solution was centrifuged, the precipitate was added to 100 mL of 0.1 N HNO<sub>3</sub> solution and stirred for 30 minutes. Subsequently, it was centrifuged again and the adsorbent production was completed by drying the solid phase at 80°C for 12 hours.

### 2.3. Adsorption Experiments

1 g of the dehumidified adsorbent was weighed and the particle size was reduced to about 0.1 mm. The adsorbent was mixed with 50 mL of 8 ppm boric acid solution, and the pH of the solution was recorded as 5.63. Then, 10.7 mL of 0.1 N HNO<sub>3</sub> solution was added as buffer solution to bring the solution pH to 3. Finally, the prepared solution and the adsorbent at pH 3 were kept in a shaking water bath for 24 hours at 175 rpm at 35 °C. The solution from the water bath was centrifuged and the liquid phase was analyzed in ICP. The adsorption yield (%) was calculated from Equation 2.

$$\text{Adsorption \%} = (1 - C_t / C_0) \times 100 \quad (2)$$

C<sub>0</sub>: Ion concentration in solution before adsorption (ppm)

C<sub>t</sub>: Ion concentration in solution after adsorption (ppm)

## 3. RESULTS AND DISCUSSION

### 3.1. Extraction Experiment Results

In the extraction study, the yield of valex production from the acorns was calculated to be 13.86%. The photograph of the commercial valex-1, commercial valex-2 and the valex produced from the Turkish acorns by the conventional method after extraction and spray drier is shown in the Figure 1.



Figure 1. Produced valex (a), commercial valex-1 (b), commercial valex-2 (c)

### 3.2. Results of Adsorption Experiments

The adsorbent prepared with the valex produced from Turkish acorns was used for the removal of boron from 8 ppm boric acid solution. In the ICP analysis of the liquid phase, the boron concentration decreased from 8 ppm to 0.960 ppm after adsorption. The adsorption yield is calculated as 88% from Equation 2.

### 3.3. Results of FT-IR Analysis

After the valex was obtained, FT-IR analysis was carried out to examine the general bond structure and to compare it with the commercial valex-1 and commercial valex-2 examples. The results of the analysis are shown in Figure 2.

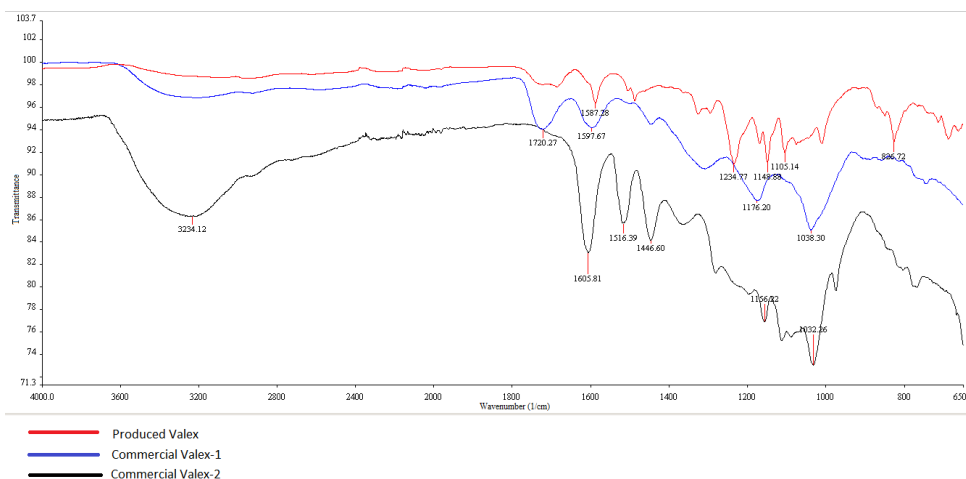


Figure 2. FTIR analysis

The peaks formed in the spectrum obtained by FTIR were investigated in four regions. The first region has a wavelength between 4000 and 2500  $\text{cm}^{-1}$ , between 2500 and 2000  $\text{cm}^{-1}$  in the second region, between 2000 and 1500  $\text{cm}^{-1}$  in the third region, and between 1500 and 400  $\text{cm}^{-1}$  in the fourth region, or fingerprint region [22]. Both of the commercial valex-1 and commercial valex-2 valex did not peak in the first and second regions. This region is due to peak O-H bonds at 3234  $\text{cm}^{-1}$  in the spectrum of commercial-2 valex [21].

In the third region, there is a peak at 1720  $\text{cm}^{-1}$  for commercial valex-2. This peak is due to the C = O bond in the tannic acid structure of the valex. The peaks seen in the range of about 1600-1400  $\text{cm}^{-1}$  wavelength in the three valex are caused by the aromatic C = C bonds, whereas the peaks seen between 1200 and 1000  $\text{cm}^{-1}$  are due to the C=O bonds.

In the fourth zone, called the fingerprint region, there was a pike with a wavelength of 826  $\text{cm}^{-1}$  for the produced valex, but commercial valex-2 was not found. The peaks formed in this region are mostly due to the characteristic bonds. Because of

the three valex do not have the same characteristics, it is unlikely that the peaks in this area will be exactly same in this region.

### 3.4. SEM Results

Figure 3 illustrates the SEM micrographs of the valex samples obtained from the Turkish oak acorn. The surface of the valex appears to be composed of highly uniform and homogeneous distributed curves. This is shown as an important parameter that positively affects the efficiency of adsorption.

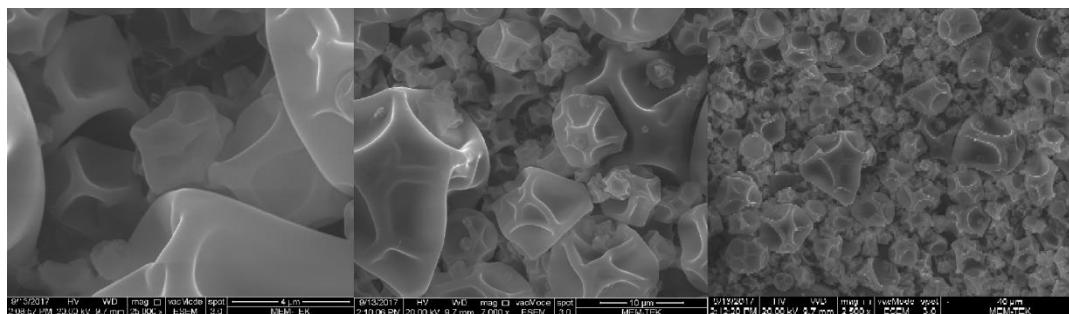


Figure 3. SEM micrographs of the valex samples obtained from the Turkish acorns

## 4. CONCLUSIONS

The yield of valex production from acorn was found to be in the range of 10-15% in literature, it was found to be 13.86% in this study. This is an acceptable value. In order to increase the yield, the extraction stage can be increased and the extract phase concentration can be increased by the advanced enrichment method. Furthermore, after extraction, the concentrate of the solution will increase the efficiency of feeding the spray dryer. It has been seen that the adsorbent produced from valex has a good result with 88% efficiency in boron removal [17].

The pH value of the solution is an important parameter for the amount of boron adsorbed, since it affects the ionization of boric acid. In this study, pH value was determined as 5.3 after adsorbent solution was added to boric acid solution and pH value was adjusted to 3 by nitric acid solution according to optimum conditions and solution was adsorbed. The experiment can be repeated at different pH values to increase adsorption efficiency. However, higher pH should not be preferred as they may cause degradation of the grain structure [23].

## ACKNOWLEDGMENT

The authors acknowledge the valonia supply of the Artu Chemical Company, Manisa, Turkey.

## REFERENCES

- [1]. A.J. Wynes, R.H.Parkaman, C.Neal, "A summary of boron surface water quality data throughout the European Union", *Sci. Total Environ.*, vol.314-316, pp. 255-269, 2003.
- [2]. J.Wolska, M.Bryjak, "Methods for boron removal from aqueous solutions – A review", *Desalination*, vol.310, pp.18-24, 2013.
- [3]. M.Badruk, N.Kabay, M.Demircioğlu, H.Mordoğan, U, İpekoğlu, "Removal of boron from wastewater of geothermal power plant by selective ion-exchange resins. I.Batch sorption-elution studies", *Sep.Sci.Technology*, vol.34 (13), pp.2553-2569, 1999.
- [4]. S.Sarp, "A mathematical relationship for the explanation of ion exchange for boron removal, *Desalination*, Vol.43, pp. 35-43, 2002.
- [5]. P.D.Howe, "A review of boron effects in the environment", *Biol.Trace.Elem.Res.*, Vol.66, pp.153-166,1998.
- [6]. N.Kabay, E.Guler, M.Bryjak, "Boron in seawater and methods for its separation – a review", *Desalination*, vol.262, pp.212-217, 2010.
- [7]. H.E.Goldbach, M.A. Wimmer, "Boron in plants and animals: is there a role beyond cell-wall structure", *Plant.Nutr.Soil.Sci.*, vol.170, pp.39-48, 2007.
- [8]. C.D.Hunt,"Dietary boron: an overview of the evidence for its role in immune function", *J.Trace Elem.Exp.Med.*, vol.16, pp.291-306, 2003.
- [9]. F.H.Nielsen, B.J.Stoecker, J.G.Penland, "Boron as a dietary factor for bone microarchitecture and central nervous system function", *Advances in Plant and Animal Boron Nutrition*, pp.277-290, 2007.
- [10]. D.J.Fort, E.L.Stover, P.L.Strong, F.J.Murray, C.L.Keen, "Chronic feeding of a low boron diet adversely affects reproduction and development in *Xenops laevis*", *J.Nutr.*, vol.129, pp.2055-2060, 1999.
- [11]. B.Wang, X.Guo, P.Bai, "Removal technology of boron dissolved in aqueous solution – a review", *Colloids Surf. A Physicochem.Eng.Adv.*, vol.444, pp.338-344, 2014.
- [12]. Z.Guan, J.Lv, P.Bai, X.Gou, "Boron removal from aqueous solutions by adsorption – a review", *Desalination*, vol.383, pp.29-37, 2016.
- [13]. I.A.B.L.A. Melnik, V.V.Goncharuh, "Sorption-membran removal of boron compound from natural waste waters: ecological economic aspects," *J.Water Chem.Technology*, vol.30, pp.167-169, 2008.
- [14]. M.A.Sari, S.Chellam, "Mechanisms of boron removal from hydraulic fracturing wastewater by aluminum electrocoagulation", *J.Colloid Interface Sci.*, vol.458, pp.103-111, 2015.
- [15]. E.Yoshikawa, A.Sasaki, M.Endo, "Removal of boron from wastewater by the hydroxyapatite formation reaction using acceleration effect of ammonia", *J.Hazard.Mater.*, vol.237-238, pp.277-282, 2012.

- [16]. S.Samatya, P.Köseoğlu, N.Kabay, A.Tuncel, M.Yüksel, "Utilization of geothermal water as irrigation water after boron removal by monodisperse nanoporous polymers containing NMDG in sorption-ultrafiltration hybrid process", *Desalination*, vol.364, pp.62-67, 2015.
- [17]. H.A.M.Bacelo, C.R.Santos, C.M.S.Botelho, "Tannin-based biosorbents for environmental applications - a review", vol.303, pp.575-587, 2016.
- [18]. WHO; *Guidelines for Drinking-Water Quality*, 4th ed., World Health Organization, 2011.
- [19]. N.Hilal, G.J.Kim, C.Somerfield, "Boron removal from saline water: a comprehensive review", *Desalination*, vol.273, pp. 23-35, 2011.
- [20]. M.Dıđrak, A.İlçim, M.H.Alma, S.Şen, "Antimicrobial activities of the extracts of various plants", *Turkish J.Biology*, Tübitak, vol.23, pp.241-248, 1999.
- [21]. M.Özacar, İ.A.Şengil, "The use of tannin from Turkish acorns (valonia) in water treatment as a coagulant and coagulant air", *Turkish J. Eng.Env.Sci.*, Tübitak, vol.26, pp.255-263, 2002.
- [22]. H.Cedeno, "Removal of boron from aqueous solutions using biopolymers and composites", Ph.D Thesis, Polytechnic University of Catalonia, Barcelona, Spain, 2014.
- [23]. P. Erdem, E.Bursali, and M. Yurdakoç, "Preparation and characterization of tannic acid resin: study of boron adsorption", Dokuz Eylül University, Graduate School of Natural and Applied Sciences, İzmir, 2012.

## BIOGRAPHY

Nalan Erdöl Aydın is graduated from Chemical Eng. Dept. of İstanbul Technical University in 1990 and she received her M.Sc. and Ph.D. degree from İstanbul Technical University. She teaches undergraduate Unit operations, Transport Phenomena. Her research areas of interest include hazardous waste treatment in aqueous systems, mineral processing and biomaterials.



# Evolution of Boric Acid Crystal Size Distribution and Shape in a CMSMPR Crystallizer-the Effect of Residence Time, Stirring Speed, Feed Flow Rate and Amount of Supersaturation

*Sinan Kutluay<sup>1</sup>, Ömer Şahin, A. Abdullah Ceyhan, M. Sait İzgi*

---

## **Abstract**

*In industrial crystallization processes, Crystal size Distribution (CSD), crystal size and the shape of crystal product are important characteristics for both process efficiency and further use of the crystals. In this study, the effect of residence time, stirring speed, feed flow rate and amount of supersaturation both on the crystal size distribution and the shape of boric acid crystals were investigated in a CMSMPR (Continuous Mixed-Suspension Mixed-Product Removal) crystallizer. The crystal size distribution and kinetic data were determined experimentally using CMSMPR crystallizer running at steady state. Sieve and light microscope analyzes were performed to determine the effects of important parameters (residence time, stirring speed, feed flow rate and amount of supersaturation) for the crystallization process of boric acid. The population density of nuclei, the nucleation rate and the crystal growth rate of boric acid were determined from the experimental population balance distribution when the steady state was reached.*

**Keywords: Boric Acid, CMSMPR, CSD, Crystallization**

---

## **1. INTRODUCTION**

The crystallization process is applied as a separation and purification technique for the production of different substances from basic chemical compounds to specific chemicals [1]. Crystallization is used in a wide range of fields such as biotechnology, mineral processing, waste treatment, pollution control, energy storage, new building materials and electronic chemicals [2]. Crystallization, an important industrial process, is the process of nucleation in supersaturated solutions, followed by growth of these nuclei and eventual separation of the solid phase from the liquid phase. Although the industrial crystallization process has been in use for many years, unfortunately no solution has been found for most of the problems in this process. The most important reason for this is that the effects of parameters affecting the crystallized material are not fully understood and optimized. The industrial crystallization parameters such as residence time in the crystallizer, feed flow rate, stirring speed and amount of supersaturation are influential on the crystal habit and crystal size distribution.[3]. In this study, the industrial crystallization parameters affecting the crystallization process of boric acid were determined and optimized in the CMSMPR type crystallizer. In the crystallization process, the effects of pure environment parameters such as residence time, stirring speed, feed flow rate and amount of supersaturation on crystal size distribution and habit change of boric acid crystals were determined. The population density of nuclei, the nucleation rate and the crystal growth rate of boric acid were determined from the experimental population balance distribution when the steady state was reached.

---

<sup>1</sup> Corresponding author: Siirt University, Faculty of Engineering and Architecture, 56100 Siirt, Turkey. kutluays2012@gmail.com

## 2. MATERIALS AND METHODS

Boric acid with purity of 99.92-101.07% used in this study was procured from Eti Mine Enterprises (ETIMINE) in Turkey. Experiments were performed with pure boric acid solution at different residence times (60-240 min), stirring speeds (150-450 rpm), feed flow rates (40-100 mL/min) and the amount of supersaturation (90-60°C, 90-50°C, 90-40°C and 90-30°C) in the CMSMPR system. In continuous crystallization experiments, a crystallizer of the CMSMPR type with continuous feed and continuous product draw was used. In the study, the schematic representation has been worked steadily with the CMSMPR system given in Figure 1. The so-called coated crystallizer used in the experiments is a continuous stirred 10 L tank with 5 liters active working volume, made of stainless steel and equipped with a three flow breakers.

The control of the inner temperature of the crystallizer was measured with a Pt-100 thermocouple placed in the crystallizer and was provided with a cooled cryostat. The boric acid solutions to be crystallized were prepared in a hot and continuous stirred tank (30 L) made of stainless steel at a temperature (95°C) higher than the saturation temperature (90°C). The internal temperature of the tank is kept constant with a heated thermostat. The supersaturated boric acid solutions were continuously drawn into the CMSMPR type crystallizer from the solution feed tank using a peristaltic pump set to work. The boric acid solutions withdrawn are crystallized in the CMSMPR crystallizer, cooling to the desired temperature. To ensure constant active working volume in the CMSMPR crystallizer, the mixture was withdrawn from the crystallizer back to the dissolution tank throughout the experiment using a second peristaltic pump with a suitable gradient set. The 300 mL mixture withdrawn from the crystallizer vacuum pump was filtered through the filtration unit and the volume and weight of the drained main solution were recorded. The boric acid crystals obtained from the filtration unit were dried in the air (24 hours). Sieve analysis of completely dried boric acid crystals were carried out using a Retsch ASTM E11 model sieve range of 180-850 µm. Photographs of boric acid crystals obtained after sieve analysis were determined by microscope. Then, the mixture sent to the recycle tank from the crystallizer during the test was quickly transferred to the feed tank after dissolving in the tank, ready for the next test. Measurements made in the CMSMPR system were performed at least twice and showed good reproducibility.

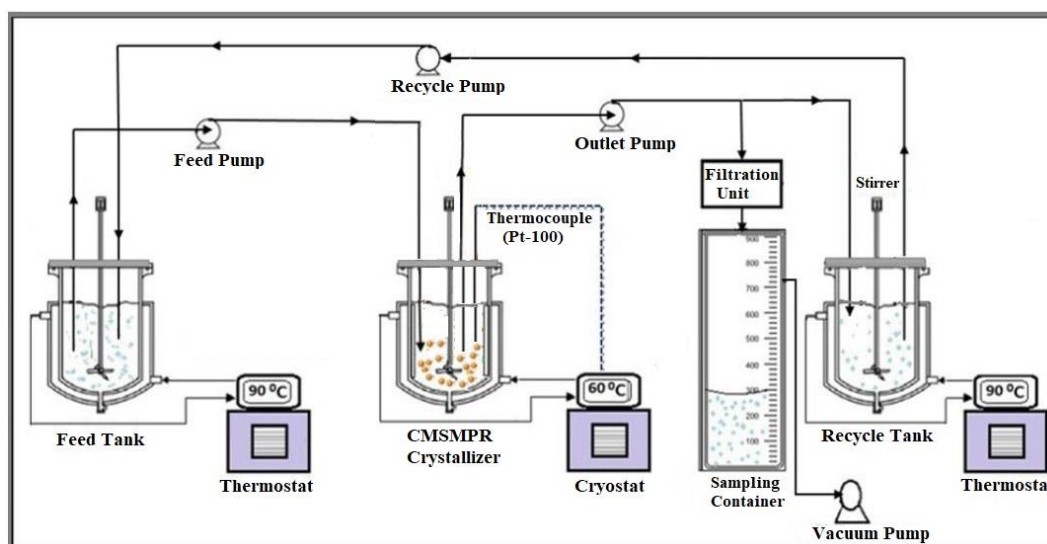


Figure 7. Schematic representation of the experimental setu

## 3. RESULTS AND DISCUSSION

Continuous crystallization studies on boric acid have been carried out with the experimental setup described in Figure 1. The active volume of the CMSMPR type crystallizer used in the boric acid studies was approximately 5 liters. In the CMSMPR type crystallizer, the crystal size range of the microscope images obtained for boric acid crystals obtained in pure medium was chosen as the range (-600 + 500) µm where the crystal habit change was best observed and compared.

### 3.1 Effect of Residence Time Both on the CSD and the Shape of Boric Acid Crystals

In the first step of the experimental work on boric acid in the CMSMPR type crystallizer system, the crystallization time required to reach steady state conditions in which the crystal size distribution has not changed is determined. For this purpose, at 90°C the saturated pure boric acid solution was crystallized at 60°C by feeding CMSMPR type crystals adjusted to a stirring rate of 250 rpm at a feed flow rate of 80 mL/min. In this case, the average crystallizer residence time of the solution was calculated as 60 min taking into account the active volume of 5 liters. Boric acid crystals drawn by vacuum from the system were filtered after 60, 120, 180 and 240 minutes crystallizer residence time to determine steady-state conditions, and then dried in the air for 24 hours. The crystal size distribution determined from the analysis of dried boric acid crystals is given in Figure 2. As can be seen in Figure 2, the crystal size distribution of the boric acid crystals is also increased due to the increase in crystallizer residence time. In addition, it is seen that the crystal size distributions of boric

acid crystals obtained as a result of 180 and 240 minutes crystallizer residence times are very close to each other. This result indicates that steady-state conditions have been reached after 180 minutes of residence time. Based on this result, the crystallizer residence time was selected as 180 minutes in boric acid studies conducted in pure medium.

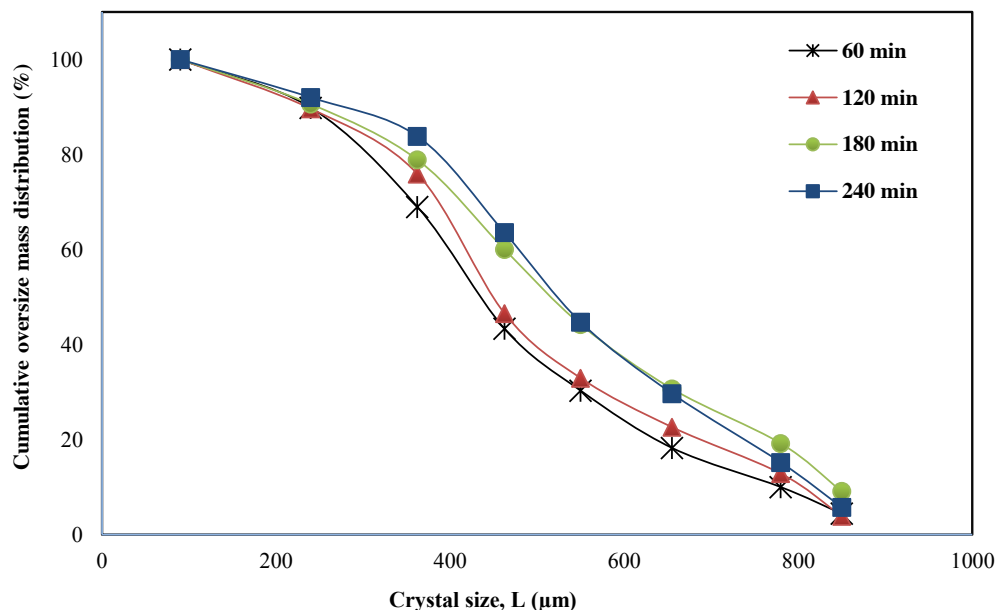


Figure 2. Change of CSD of crystals for different residence times at 90-60°C, 80 ml min<sup>-1</sup>, 250 rpm

### 3.2 Effect of Stirring Speed Both on the CSD and the Shape of Boric Acid Crystals

One of the most important parameters that are effective in the crystallization of boric acid is the speed of solution stirring. The speed of stirring is also one of the most important parameters affecting energy expenditure, especially in industrial production, as well as on the metastatic region [4, 5]. The main reason why this parameter is important is; the secondary nucleation in the crystallization of boric acid and thus the breakage are effective. Because the boric acid crystals grow dendritically and become a main body in a new crystal by the effect of the mixture and the breakdown of each protrusion in the dendritic structure. If each piece in the resulting dendritic structure is weak and thin, the resulting crystal size distribution may increase the number of crystals with a small crystal size. Crystal size distribution (a) and microscope images (b) of boric acid crystals obtained at CMSMPR type crystallizer at 90-60°C amount of supersaturation, 80 mL/min feed flow rate, 180 min crystallizer residence time and 150-450 rpm stirring speed conditions are given in Figure 3. As seen in Figure 3a, 60% of these crystals obtained at a stirring speed of 450 rpm, but 90% of boric acid crystals obtained at a stirring speed of 150 rpm are above 300 µm. Two possible reasons for this behavior are; it may be that the dendritic structure formed at low stirring speeds protects itself by the effect of stirring and forms a crystal structure with a larger particle size but with a distorted structure or with the effect of high stirring speeds and separating the crystals formed in the dendritic structure into smaller pieces to reduce the crystal size distribution of the crystals formed. Moreover, according to the mechanism of "collisional debris", one of the theories introduced to explain the secondary nucleation, the nuclei broken from the edges and weak points of the growing crystals at high stirring speeds are separated from the parent crystal. Such crystals behave like nuclei [6, 7]. This evaluation supports the reduction of the crystal size distribution of boric acid crystals at high stirring speeds. Examination of the microscope images in Figure 3b, reveals that habit disorders are intensively observed in boric acid crystals obtained at different stirring speeds. Moreover, these crystals have been found to carry formations originating from one or several points and have no form that can be expressed as standard. The main reason for this is that the starting crystals formed in the dendritic structure are not sufficiently broken by the effect of stirring. Boric acid crystals obtained at a stirring speed of 450 rpm have a more uniform habit than crystals obtained at a stirring speed of 150 rpm. However, breaks due to the high mixing speed can be explained by the breaks that occur during the growth of the crystals, which are broken only in the dendritic structure and not in the first dendritic structure, and are likely to be the main bodies of the new crystals.

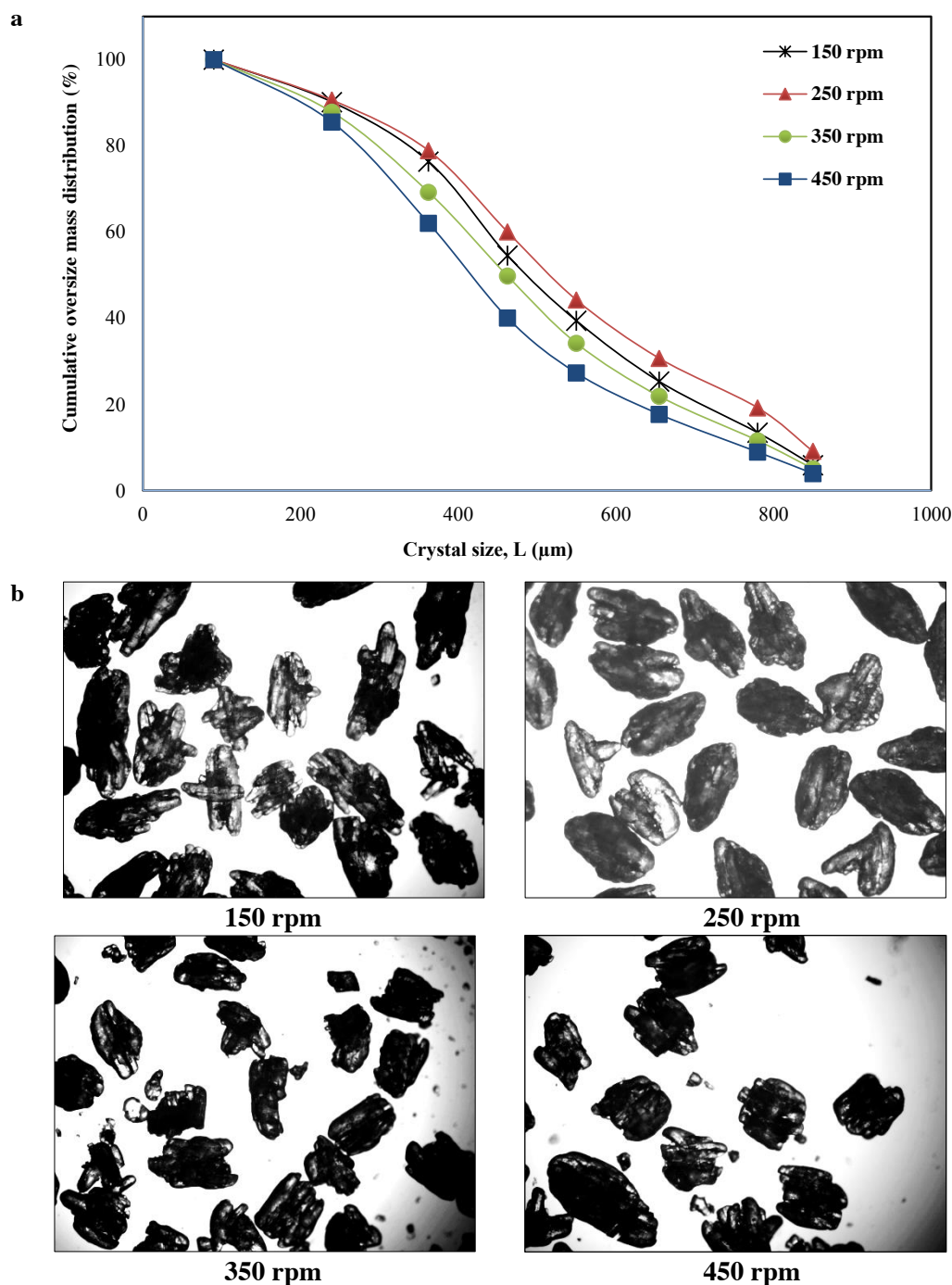


Figure 3. Change of CSD (a) and shape (b) of crystals for different stirring speeds at 90-60°C, 80 ml min<sup>-1</sup>, 180 min

### 3.3 Effect of Feed Flow Rate Both on the CSD and the Shape of Boric Acid Crystals

Another parameter that is effective in boric acid crystallization is the feed flow rate. Crystal size distribution (b) and microscope images (b) of the boric acid crystals obtained in the CMSMPR type crystallizer at 250 rpm stirring speed, 90-60°C amount of supersaturation, 180 min crystallizer residence time and 40-100 mL/min feed flow rate conditions are given in Figure 4. A decrease in crystal size distribution is expected as the residence time in the crystallizer will decrease as the feed flow rate increases. Because, as the volumetric feed flow rate of the solution increases, the residence time in the crystallizer decreases, so that the crystals do not have enough time for growth [3]. As seen in Figure 4a, 80% of the boric acid crystals obtained at the feed flow rate of 80 mL/min are above 300 µm and 80% of these crystals are at the feed flow rate of 100 mL/min but above 300 µm. An increase in the solution feed flow rate indicates that the crystal size distribution results in a more pronounced transition due to the crystals having less time for particle-particle, particle-mixer and particle-wave breaker-wall interaction. This change in particle size distribution is said to be a consequence of such interactions in the crystallizer residence time [3]. Examining the microscope images given in Figure 4b, it was observed that the boric acid crystals obtained in the different solution feed flow rates had little habit change. However, boric acid crystals obtained in different feed flow rates have not been found to have uniform habits.

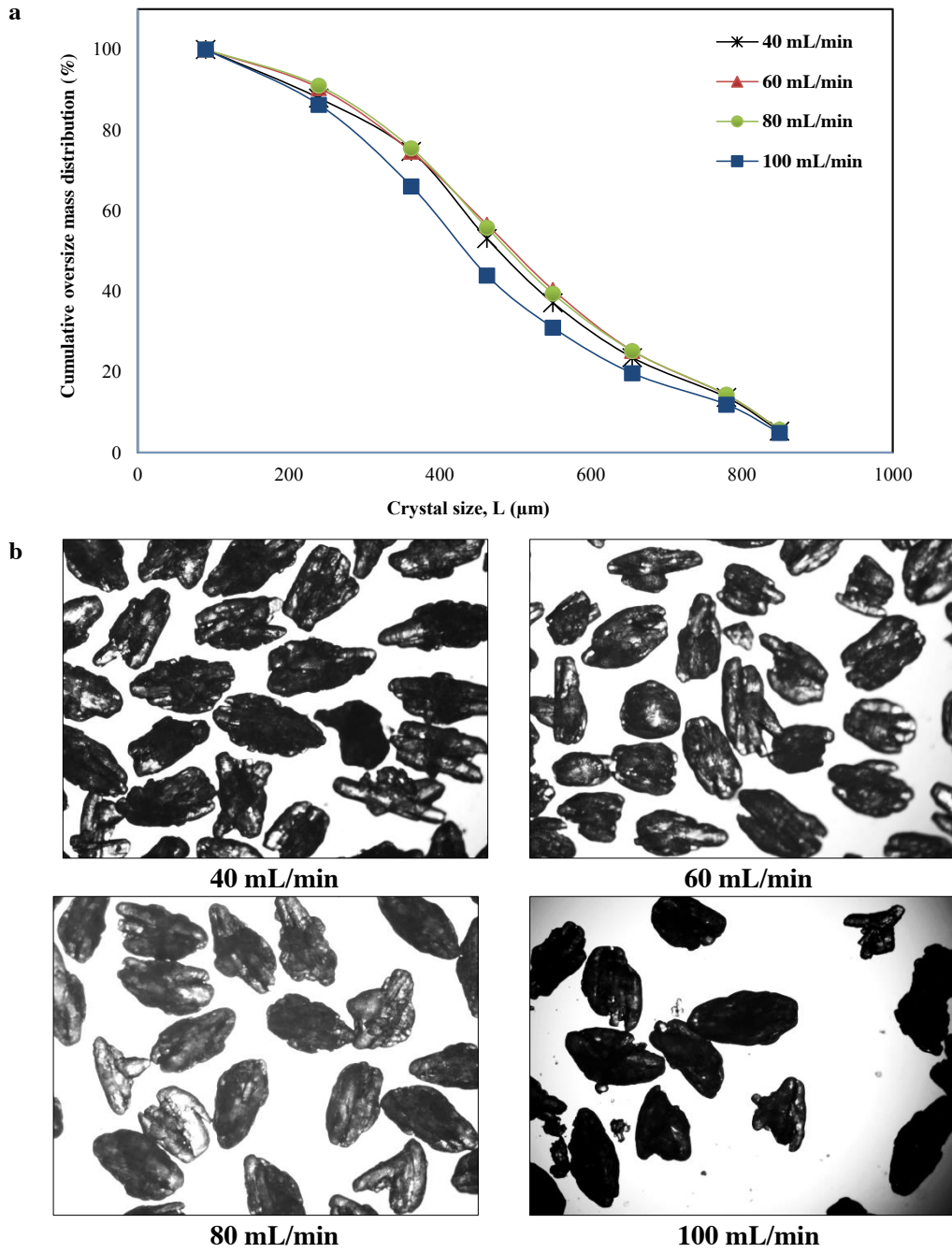


Figure 4. Change of CSD (a) and shape (b) of crystals for different feed flow rates at 90-60°C, 250 rpm, 180 min

### 3.4 Effect of Supersaturation Both on the CSD and the Shape of Boric Acid Crystals

One of the most important parameters affecting nucleation and crystal growth in industrial crystallization processes is the amount of supersaturation of the solution in the CMSMPR system. Because of the supersaturation obtained by the difference between the two temperatures, nucleation and crystal growth processes occur [8].

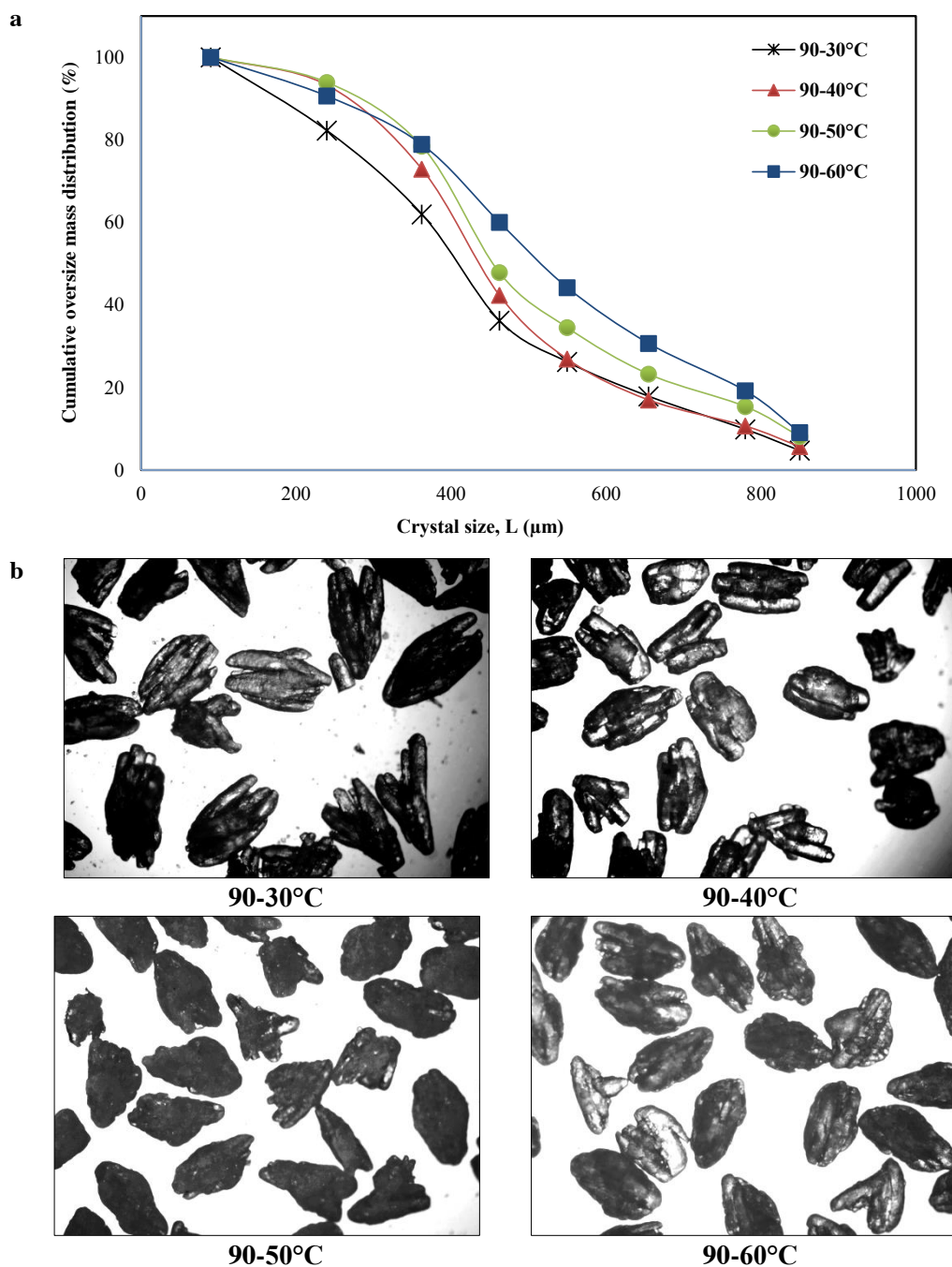


Figure 5. Change of CSD (a) and shape (b) of crystals for different supersaturations at 80 ml min<sup>-1</sup>, 250 rpm, 180 min

Crystal size distribution (a) and microscope images (b) of the boric acid crystals obtained in the CMSMPR type crystallizer at 250 rpm stirring speed, 80 mL/min feed flow rate, 180 min residence time and 90-30°C, 90-40°C, 90-50°C and 90-60°C amount of supersaturation conditions are given in Figure 5. As seen in Figure 5a, the crystal size distribution of boric acid crystals decreases due to the increase in the number of nuclei formed as the amount of supersaturation increases. Furthermore, boric acid is considered to have a narrow crystal size distribution due to secondary nucleation in the high hyper-sensitivities given that the metastable region interval is very narrow. Because, in the supersaturated solution medium, the formation of new nuclei with secondary nuclei and the presence of crystals make it possible for the nucleation to take place at lower saturation, as it shrinks the metastable region. Examination of the microscope images given in Figure 5b, reveals that the boric acid crystals obtained in different supersaturated solutions have almost the same habit. But the most interesting result in microscope images is that boric acid crystals obtained at 90-60°C amount of supersaturation have more uniform habits. It is seen that the boric acid crystals obtained in this condition have a higher crystal size distribution, although they are low in amount of supersaturation given at 90-60°C. It can also be said that boric acid crystals with the desired uniformity of habits in industrial production are obtained in this amount of supersaturation compared to other extreme saturations. Studies on boric acid crystallization have shown that boric acid crystals grow dendritically in pure saturation with all the supersaturation [9].

### 3.5 Application of Population Balance for Boric Acid Crystals

The most important issue in industrial crystallization processes is crystal size distribution. Because the crystal properties (crystal size and habit and agglomeration tendency) are of vital importance for both process efficiency and product quality. When the crystallization processes involve a large number of crystals of different sizes, a crystal size distribution is required to completely characterize the system. The theory that best characterizes the crystal size distribution is the population balance theory. The best application of number density theory is on CMSMPR type crystallizers [10]. In the characterization of crystal size distribution, the basic equation between number density,  $n$  and particle size,  $L$  is given below:

$$n = n_0 \exp\left(-\frac{L}{G\tau}\right) \quad (1)$$

Equation  $n_0$  is the number density in the nucleus size, and  $G$  is the growth rate. After the continuously running laboratory type CMSMPR crystallizer is brought to equilibrium, the crystal suspension taken is filtered and the crystals are sieve analysis. In the sieve analysis,  $\Delta L$  is the difference in openness between two sieves.  $L$  is the mean sieve clearance. If the cumulative sieve fraction  $\Delta W$  at the end of a sieving operation is taken as the suspension density  $M_T$ , then the numerical intensity expression is defined as [11]

$$n = \frac{\Delta M M_T}{\Delta L \alpha \rho L^3} \quad (2)$$

Where  $\alpha$  is the volume shape factor, and  $\rho$  is the crystal density. A plot of  $\ln(n)$  versus  $L$  should give a straight line with an intercept at  $L = 0$  equal to  $n_0$  and a slope of  $-\frac{1}{G\tau}$  (Figure 6). The number density of crystals in the nucleus size refers to  $n_0$  parameter and is related to nucleation kinetics.  $G$  expresses the crystal growth rate, the nucleation rate,  $B_0$  is calculated from the following equation.

$$B_0 = n_0 G \quad (3)$$

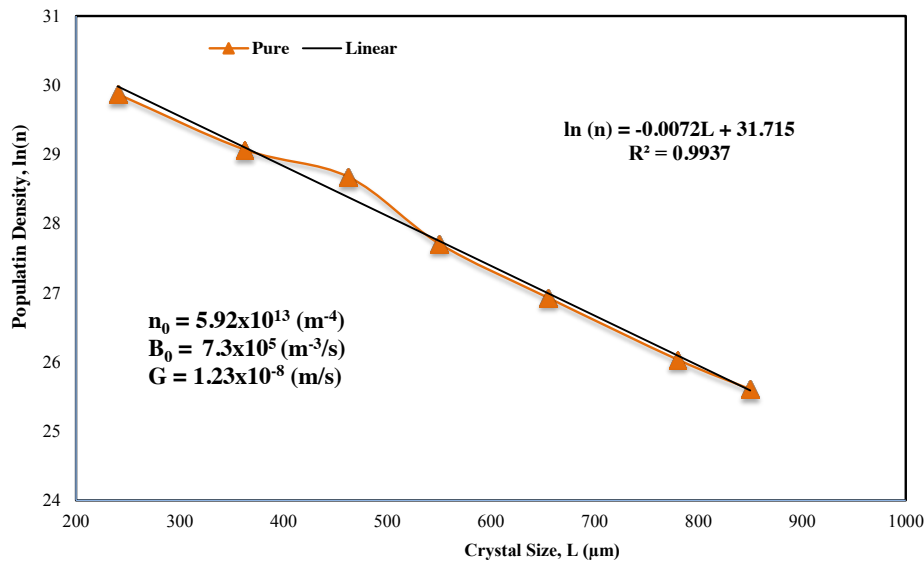


Figure 6. Population density versus crystal size for boric acid at 90-60°C, 80 ml min<sup>-1</sup>, 250 rpm, 180 min

## 4. CONCLUSIONS

In the present work, the effects of residence time, stirring speed, feed flow rate and amount of supersaturation both on the crystal size distribution and the shape of boric acid crystals were observed in a CMSMPR crystallizer. However, the population density of nuclei and the nucleation and the crystal growth rates of boric acid were determined from the experimental population balance distribution using the CMSMPR crystallizer running at the steady state. In the CMSMPR type crystallizer, crystals obtained in the residence time range of 60-240 minutes were determined to be stable conditions after 180 minutes of crystallization in the crystal size distribution determined after sieve analysis to determine the conditions under which steady-state conditions are satisfied. It was found that the stirring speed was very effective on the crystal size distribution and the crystal habit change and that the secondary nucleation was effective at stirring speeds above 250 rpm. The parameters of solution feed flow rate and amount of supersaturation, which are important in the CMSMPR type crystallizer, were also found to be very effective on the particle size distribution. When there is an increase in the solution feed flow rate, it has been shown that the crystal size distribution results in a more pronounced transition due to the particles having less time. The results of studies in pure medium have revealed that boric acid crystals grow completely dendritic and developed nicely after the nuclear phase and that the crystals formed are capable of allowing amorphous and secondary nucleation.

## ACKNOWLEDGMENTS

This work was supported by the Eti Mine Enterprises [ETIMINE, project number: 400.02(TGD.2014/3)].

## REFERENCES

- [1] A. Moreno, M.E. Mendoza, 31-Crystallization in gels., 2 ed., Boston, Elsevier, 2015.
- [2] S.N. Tavare, Industrial crystallization: Process simulation analysis and design, New York, Plenum Pres, 1995.
- [3] B.S. Choi, T.A. Ring, Evolution of crystal size distributions in a CMSMPR—the effect of temperature, flow rate, and mixing speed with time, *Fluid Phase Equilibria* 228 (2005) 99-107.
- [4] J.W. Mullin, Crystallization, 3 ed., London, Butterworth-Heinemann, 1993.
- [5] J. Nyvlt, O. Sohnel, M. Matuchova, M. Broul, The kinetics of industrial crystallization, New York, Elsevier Science Publishing Company, Inc., 1985.
- [6] R.E.A. Mason, R.F. Strickland-Constable, Breeding of crystal nuclei, *Transactions of the Faraday Society*, 1966.
- [7] A.S. Myerson, Handbook of industrial crystallization, New York, Butterworth-Heinemann, 1993.
- [8] A. Mersmann, C. Heyer, A. Eble, Crystallization technology handbook, 2 ed., Garching, Germany, Technische Universitat München, 2001.
- [9] P. Sayan, Polielektrolitlerin borik asit kristalizasyonuna etkisi, İstanbul Teknik Üniversitesi Fen Bilimleri Enstitüsü, İstanbul, 1995, pp. 16.
- [10] A.D. Randolph, M.A. Larson, Theory of particulate processes: Analysis and techniques of continuous crystallization, 2 ed., New York, Academic Press, 1988.
- [11] J.W. Mullin, Crystallization, 4 ed., Oxford, Butterworth-Heinemann, 2001.

## BIOGRAPHY

Sinan KUTLUAY was born in 1988 in Tutak/Ağrı. He graduated from Yıldız Technical University, Faculty of Chemistry-Metallurgy, Department of Chemical Engineering in 2010. Between the years 2010-2012, he completed his master's degree at Yıldız Technical University, Graduate School of Natural Sciences, Division of Chemical Engineering. The doctorate education that he started in 2014 is going on at Selçuk University, Graduate School of Natural Sciences, Division of Chemical Engineering. In 2011, he was appointed as research assistant at Siirt University, Faculty of Engineering and Architecture, Department of Chemical Engineering, Division of Process and Reactor Design, and still serves as research assistant in the same department. Sinan KUTLUAY is married and has one child.



# Determination of Borax Pentahydrate Crystal Size Distribution and Shape in a CMSMPR Crystallizer-the Effect of Supersaturation, Feed Flow Rate and Stirring Speed with Time

*Sinan Kutluay<sup>1</sup>, A. Abdullah Ceyhan, Halil Demir, Ömer Şahin*

---

## Abstract

*In this study, the effect of residence time, stirring speed, feed flow rate and amount of supersaturation both on the CSD (Crystal size Distribution) and the shape of borax pentahydrate crystals were investigated in a CMSMPR (Continuous Mixed-Suspension Mixed-Product Removal) crystallizer. In industrial crystallization processes, crystal size distribution and the shape of crystal are important characteristics for both process efficiency and further use of the crystals. The crystal size distribution and kinetic data were determined experimentally using CMSMPR crystallizer running at steady state. Sieve and light microscope analyzes were performed to determine the effects of important parameters (residence time, stirring speed, feed flow rate and amount of supersaturation) for the crystallization process of borax pentahydrate. The population density of nuclei, the nucleation rate and the crystal growth rate of borax pentahydrate were determined from the experimental population balance distribution when the steady state was reached.*

**Keywords: Borax Pentahydrate, CMSMPR, CSD, Crystallization**

---

## 1. INTRODUCTION

Crystallization has become a technique used in a wide range of fields such as biotechnology, mineral processing, waste treatment, pollution control, energy storage, new building materials and electronic chemistry [1]. The crystallization process is applied as a separation and purification technique for the production of different substances from basic chemical compounds to specific chemicals [2, 3]. Crystallization, an important industrial process, is the process of nucleation in supersaturated solutions, followed by growth of these nuclei and eventual separation of the solid phase from the liquid phase. Crystallization is also a complex process that is simultaneously effected by mass and heat transfer events and is influenced by factors such as impurities, hydrodynamic conditions in the solution [3]. Crystallization, an important industrial process, is the process of nucleation in supersaturated solutions, followed by growth of these nuclei and eventual separation of the solid phase from the liquid phase. Although the industrial crystallization process has been in use for many years, unfortunately no solution has been found for most of the problems in this process. The most important reason for this is that the effects of parameters affecting the crystallized material are not fully understood and optimized. The industrial crystallization parameters such as residence time in the crystallizer, feed flow rate, stirring speed and amount of supersaturation are influential on the crystal habit and crystal size distribution.[4]. In this study, the industrial crystallization parameters affecting the crystallization process of borax pentahydrate were determined and optimized in the CMSMPR type crystallizer. In the crystallization process, the effects of pure medium parameters such as residence time, stirring speed, solution feed flow rate and amount of supersaturation on crystal size distribution and habit change of borax pentahydrate crystals were determined. The population density of nuclei, the nucleation rate and the crystal growth rate of borax pentahydrate were determined from the experimental population balance distribution when the steady state was reached.

---

<sup>1</sup> Corresponding author: Siirt University, Faculty of Engineering and Architecture, 56100 Siirt, Turkey. kutluays2012@gmail.com

## 2. MATERIALS AND METHODS

Borax pentahydrate with purity of 99.92-103.24% used in this study was procured from Eti Mine Enterprises (ETIMINE) in Turkey. Experiments were performed with pure borax pentahydrate solution at different residence times (30-150 min), stirring speeds (150-450 rpm), feed flow rates (70-230 mL/min) and amount of supersaturation (90-65°C, 90-70°C and 90-75°C) in the CMSMPR system. In continuous crystallization experiments, a crystallizer of the CMSMPR type with continuous feed and continuous product draw was used. In the study, the schematic representation has been worked steadily with the CMSMPR system given in Figure 1. The so-called coated crystallizer used in the experiments is a continuous stirred 10 L tank with 5 liters active working volume, made of stainless steel and equipped with a three flow breakers. The control of the inner temperature of the crystallizer was measured with a Pt-100 thermocouple placed in the crystallizer and was provided with a cooled cryostat. The borax pentahydrate solutions to be crystallized were prepared in a hot and continuous stirred tank (30 L) made of stainless steel at a temperature (95°C) higher than the saturation temperature (90°C). The internal temperature of the tank is kept constant with a heated thermostat. The supersaturated borax pentahydrate solutions were continuously drawn into the CMSMPR type crystallizer from the solution feed tank using a peristaltic pump set to work. The borax pentahydrate solutions withdrawn are crystallized in the CMSMPR crystallizer, cooling to the desired temperature. To ensure constant active working volume in the CMSMPR crystallizer, the mixture was withdrawn from the crystallizer back to the dissolution tank throughout the experiment using a second peristaltic pump with a suitable gradient set. The 300 mL mixture withdrawn from the crystallizer vacuum pump was filtered through the filtration unit and the volume and weight of the drained main solution were recorded. The borax pentahydrate crystals obtained from the filtration unit were washed with approximately 5 mL of ethanol and then dried at 60°C (2 minutes). Sieve analysis of completely dried borax pentahydrate crystals were carried out using a Retsch ASTM E11 model sieve range of 180-850 µm. Photographs of the crystals obtained after sieve analysis were determined by microscope. Then, the mixture sent to the recycle tank from the crystallizer during the test was quickly transferred to the feed tank after dissolving in the tank, ready for the next test. Measurements made in the CMSMPR system were performed at least twice and showed good reproducibility.

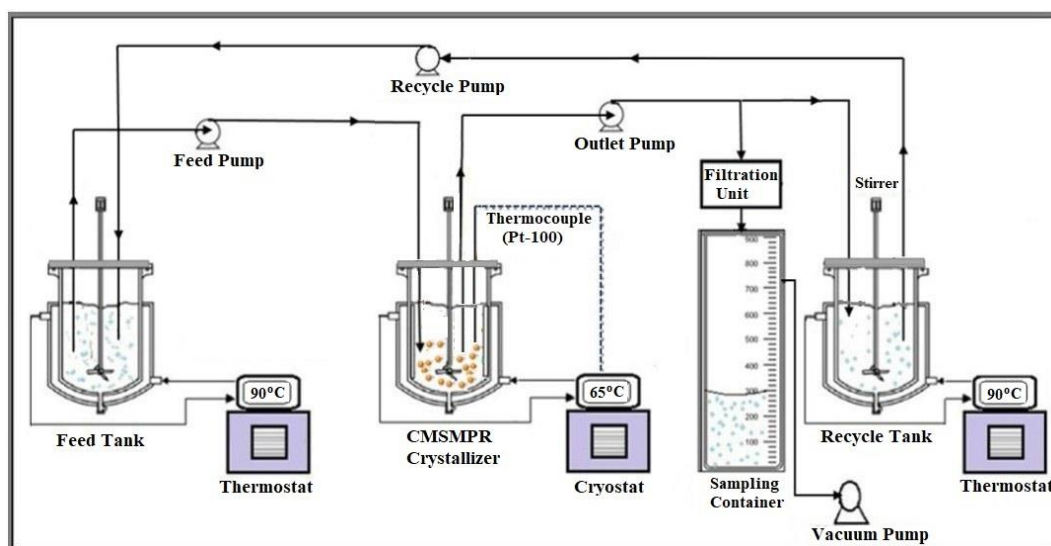


Figure 8. Schematic representation of the experimental setup

## 3. RESULTS AND DISCUSSION

Continuous crystallization studies on borax pentahydrate have been carried out with the experimental setup described in Figure 1. The active volume of the CMSMPR type crystallizer used in the borax pentahydrate studies was approximately 5 liters. In the CMSMPR type crystallizer, the crystal size range of the microscope images obtained for borax pentahydrate crystals obtained in pure medium was chosen as the range (-425+300) µm where the crystal habit change was best observed and compared.

### 3.1 Effect of Residence Time Both on the CSD and the Shape of Borax Pentahydrate Crystals

In the first step of the experimental work carried out in the CMSMPR type crystallizer system related to borax pentahydrate, the residence time required to reach steady state conditions in which the crystal size distribution did not change was determined. For this purpose, at 90°C, the saturated pure borax pentahydrate solution is crystallized at 65°C by feeding CMSMPR type crystals adjusted at a feed rate of 175 mL/min with stirring speed of 350 rpm. According to these conditions, the average crystallizer residence time of the solution was calculated to be 30 minutes taking into account the active volume of 5 liters. In order to determine steady-state condition, borax pentahydrate crystals vacuum drawn from the system were filtered after 30, 60, 90, 120 and 150 minutes crystallizer residence time, and then dried at 60-70°C. The crystal size distribution determined by sieve analysis of dried borax pentahydrate crystals is given in Figure 2. As can be seen in Figure 2, the crystal size distribution of the borax pentahydrate crystals increases with the increase in the crystallizer residence time.

Moreover, it is seen that the crystal size distributions of the borax pentahydrate crystals obtained as a result of the residence times of 120 and 150 minutes crystallizers are very close to each other. This result shows that after 120 minutes the crystallizer is in steady state condition. Based on this result, the crystallization time of the borax pentahydrate studies carried out in pure medium was chosen as 120 minutes.

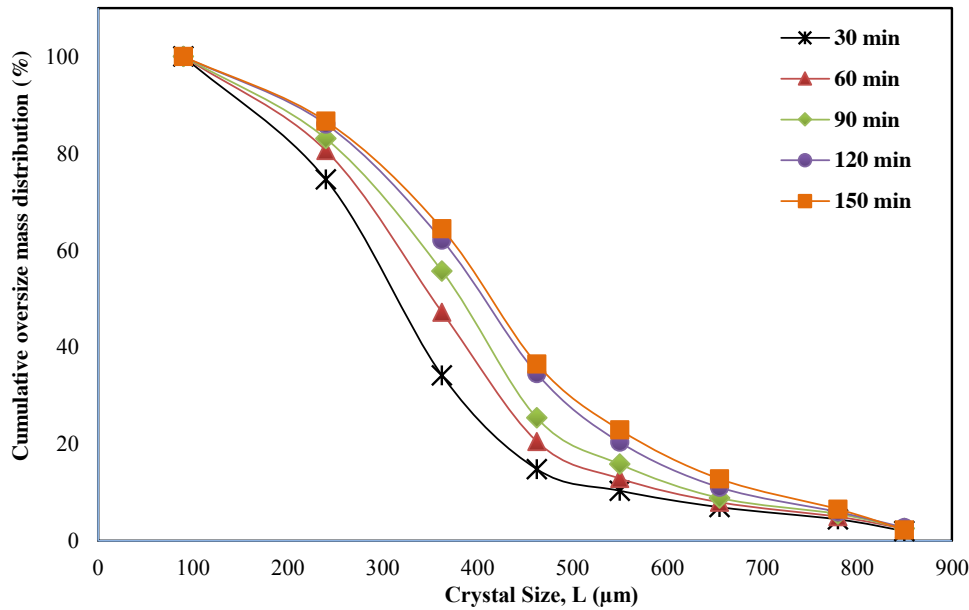
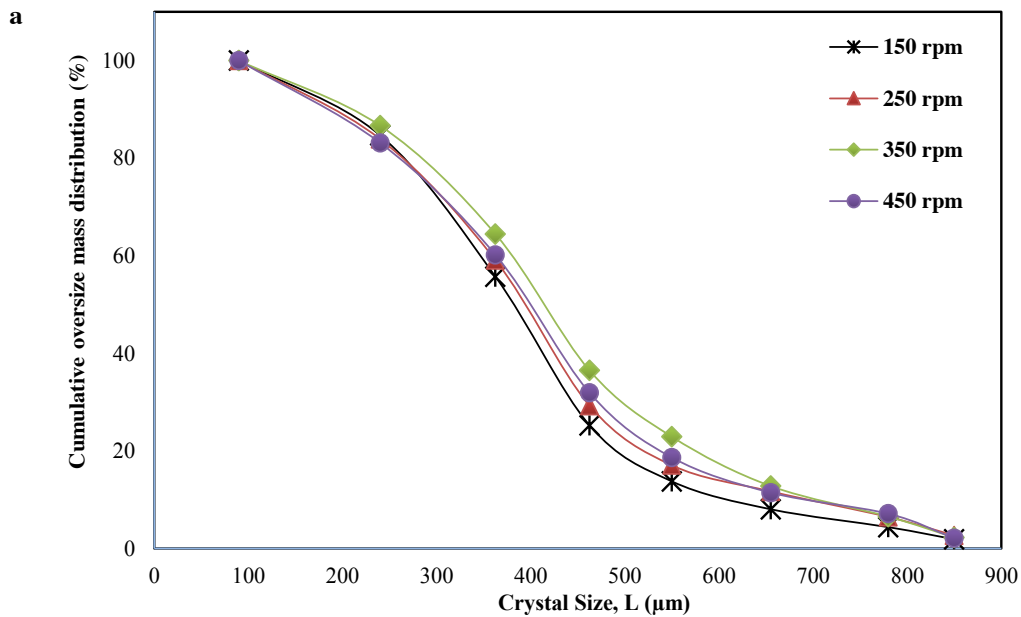


Figure 2. Change of CSD of crystals for different residence times at 90-65°C, 175 ml min<sup>-1</sup>, 350 rpm

### 3.2 Effect of Stirring Speed Both on the CSD and the Shape of Borax Pentahydrate Crystals

One of the parameters that affect the crystallization of borax pentahydrate is the rate of solution mixing. The crystal size distribution (a) and microscope images (b) of the borax pentahydrate crystals obtained in the CMSMPR type crystallizer at 90-65°C supersaturation, 175 mL/min feed flow rate, 120 min residence time and 150-450 rpm stirring speed conditions are given in Figure 3. As shown in Figure 3a, 72% of the borax pentahydrate crystals obtained at a mixing speed of 150 rpm are above 300 µm, while 76% of these crystals are above 300 µm at a mixing speed of 350 rpm. Therefore, it appears that there is no significant difference in the crystal size distribution of the borax pentahydrate with the effect of the blend. Examination of the microscope images given in Figure 3b, shows no significant change in the habit of the borax pentahydrate crystals obtained at stirring speeds of 150-450 rpm. However, borax pentahydrate crystals obtained at high stirring speeds appear to have a smoother habit. These results show that secondary nucleation in borax pentahydrate crystallization is not as effective. Because, according to the mechanism of "collision crumbling" in the secondary nucleus, the nuclei breaking from the edges and weak points of the growing crystals at high stirring speeds are separated from the parent crystal, and such crystals are regarded as acting like nuclei [5, 6]. However, it can be said that such a state does not exist in borax pentahydrate crystals.



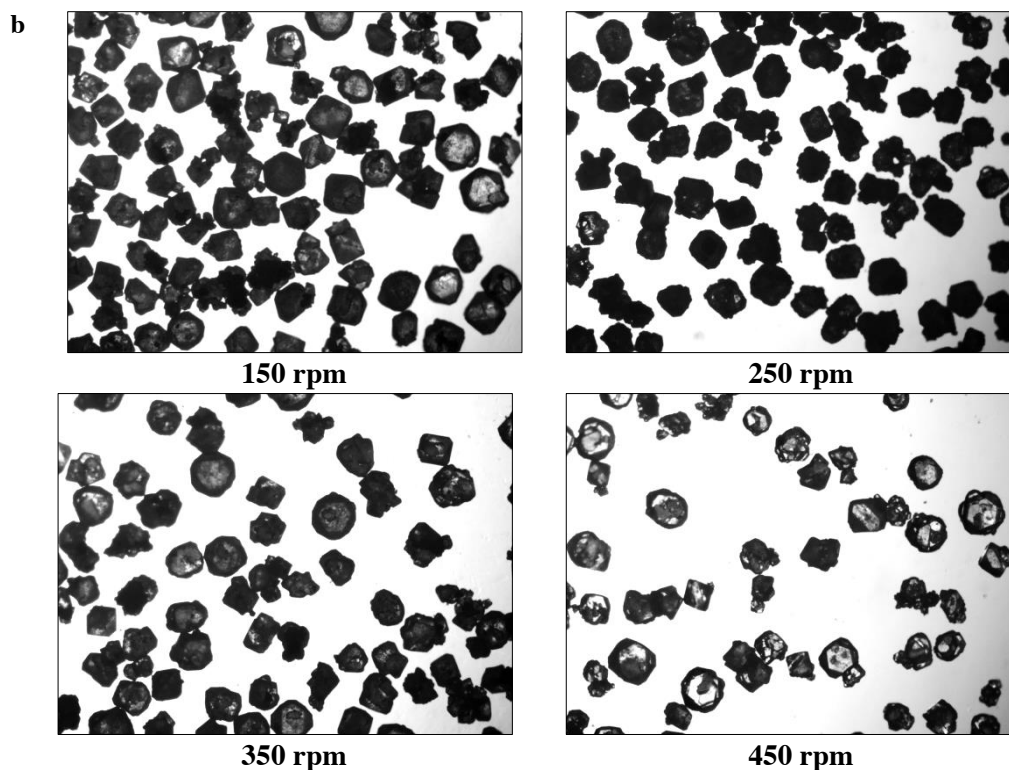
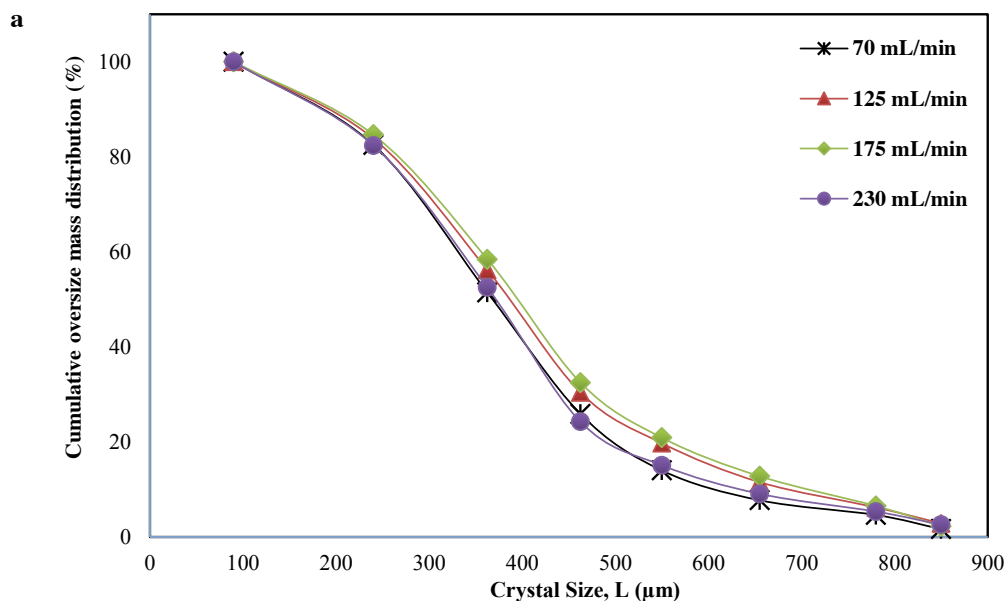


Figure 3. Change of CSD and shape of crystals for different stirring speeds at 90-65°C, 175 ml min<sup>-1</sup>, 120 min

### 3.3 Effect of Feed Flow Rate Both on the CSD and the Shape of Borax Pentahydrate Crystals

Another parameter that influences the crystallization of borax pentahydrate is the solution feed flow rate. The crystal size distribution (a) and microscope images (b) of the borax pentahydrate crystals obtained in the CMSMPR type crystallizer at 350 rpm stirring speed, 120 min residence time at 90-65°C and 70-230 mL/min feed flow rate conditions are given in Figure 4. As seen in Figure 4a, there is no significant change in the crystal size distribution of the borax pentahydrate crystals obtained in the different feed flow rates. Under normal conditions, crystals need to have enough time in the crystallizer to grow. Therefore, a decrease in crystal size distribution is expected in the high feed flow rate. However, borax pentahydrate crystals did not seem to have much effect. The probable cause of this is the habit disorder observed in the crystals obtained in the high feed flow rate. The correctness of this situation is shown in the microscope images shown in Figure 4b.



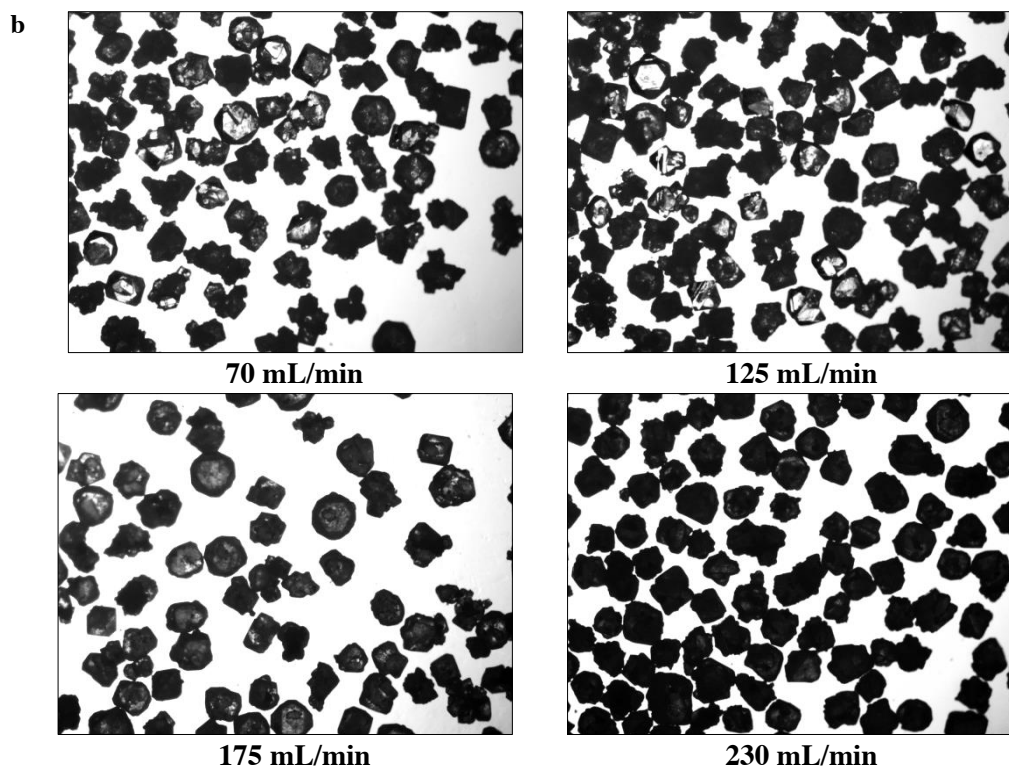


Figure 4. Change of CSD and shape of crystals for different feed flow rates at 90-65°C, 350 rpm, 120 min

### 3.4 Effect of Supersaturation Both on the CSD and the Shape of Borax Pentahydrate Crystals

One of the most important parameters affecting the nucleation and crystal growth kinetic processes in industrial crystallization is the supersaturation that the solution has in the CMSMPR system. The crystal size distribution (a) and microscope images (b) of the borax pentahydrate crystals obtained in the CMSMPR type crystallizer at 350 rpm stirring speed, 175 mL/min feed flow rate, 120 min residence time and 90-65°C, 90-70°C and 90-75°C supersaturation conditions are given in Figure 5. As shown in Figure 5a, the crystal size distribution of the borax pentahydrate crystals increased as the supersaturation increased to the solution in the CMSMPR type crystallizer. This result shows that the borax pentahydrate solutions tend to be supersaturation. Because, in the crystallization process, if the solution has a tendency to supersaturation, the supersaturation given to the solution grows faster with the effect of supersaturation in the formed nuclei, and as a result, the crystal size distribution increases [7]. The reason why the borax pentahydrate crystals are not studied at higher supersaturation than the 90-65°C supersaturated in the CMSMPR system is that borax decahydrate transforms when the borax solution is cooled and cooled below the critical temperature of 60.2-60.8°C [8]. Therefore, the lower temperature of the optimum supersaturation value for borax pentahydrate was chosen as 65°C. Examination of the microscope images shown in Figure 5b, shows that the borax pentahydrate crystals obtained in different supersaturation of the solution are habitually defective. However, the most interesting result in microscope images is that borax pentahydrate crystals obtained at 90-65°C supersaturation have a relatively uniform habit.

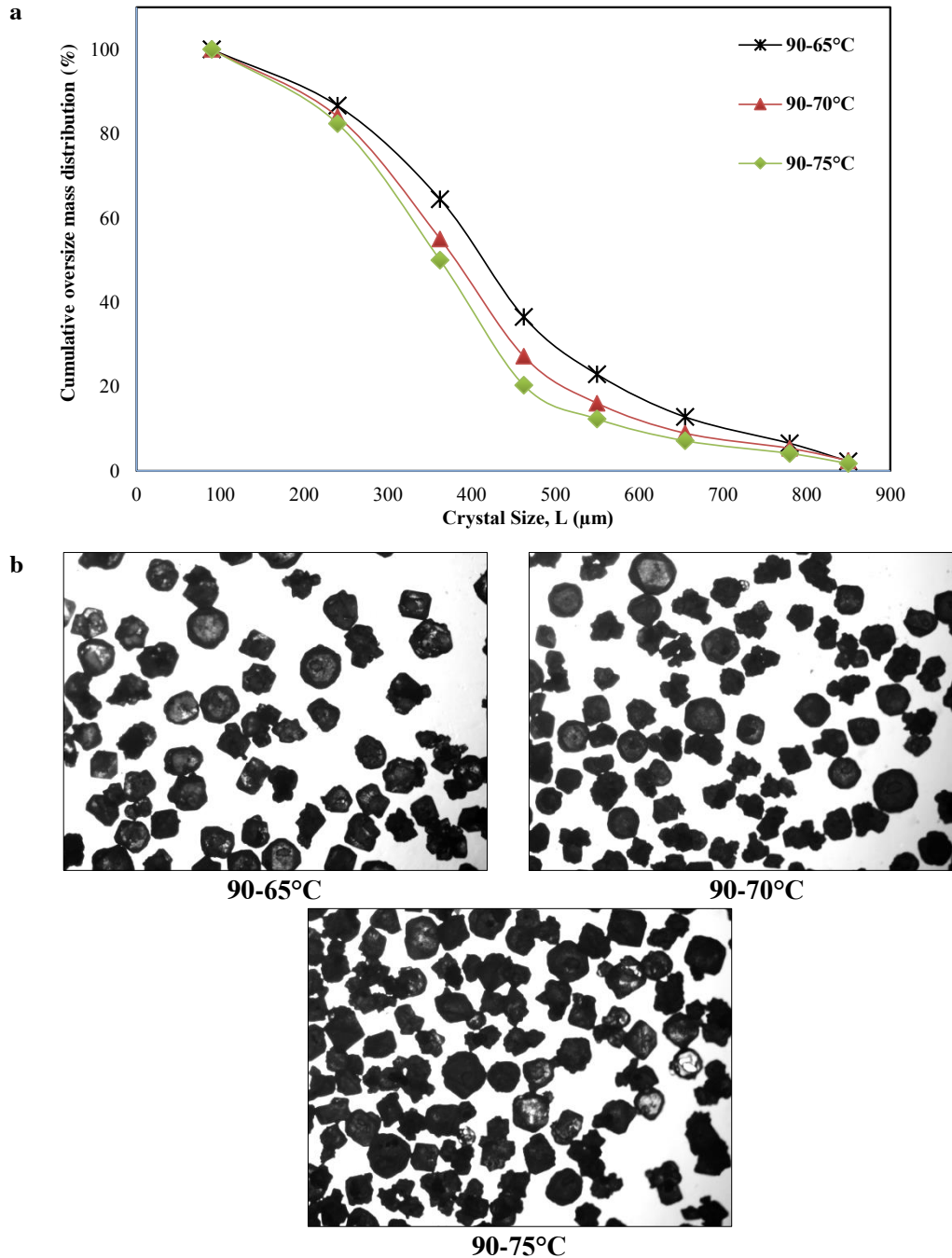


Figure 5. Change of CSD and shape of crystals for different supersaturations at 175 ml min<sup>-1</sup>, 350 rpm, 120 min

### 3.5 Application of Population Balance for Borax Pentahydrate Crystals

The most important issue in industrial crystallization processes is crystal size distribution. Because the crystal properties (crystal size and habit and agglomeration tendency) are of vital importance for both process efficiency and product quality. When the crystallization processes involve a large number of crystals of different sizes, a crystal size distribution is required to completely characterize the system. The theory that best characterizes the crystal size distribution is the population balance theory. The best application of number density theory is on CMSMPR type crystallizers [9]. In the characterization of crystal size distribution, the basic equation between number density,  $n$  and particle size,  $L$  is given below:

$$n = n_0 \exp\left(-\frac{L}{G\tau}\right) \quad (1)$$

Equation  $n_0$  is the number density in the nucleus size, and  $G$  is the growth rate. After the continuously running laboratory type CMSMPR crystallizer is brought to equilibrium, the crystal suspension taken is filtered and the crystals are screened. In the sieve analysis,  $\Delta L$  is the difference in openness between two sieves.  $L$  is the mean sieve clearance. If the cumulative sieve fraction  $\Delta W$  at the end of a sieving operation is taken as the suspension density  $M_T$ , then the numerical intensity expression is defined as [10]

$$n = \frac{\Delta MM_T}{\Delta L \alpha \rho L^3} \quad (2)$$

Where  $\alpha$  is the volume shape factor, and  $\rho$  is the crystal density. A plot of  $\ln(n)$  versus  $L$  should give a straight line with an intercept at  $L = 0$  equal to  $n_0$  and a slope of  $-\frac{1}{Gt}$  (Figure 6). The number density of crystals in the nucleus size refers to  $n_0$  parameter and is related to nucleation kinetics.  $G$  expresses the crystal growth rate, the nucleation rate,  $B_0$  is calculated from the following equation.

$$B_0 = n_0 G \quad (3)$$

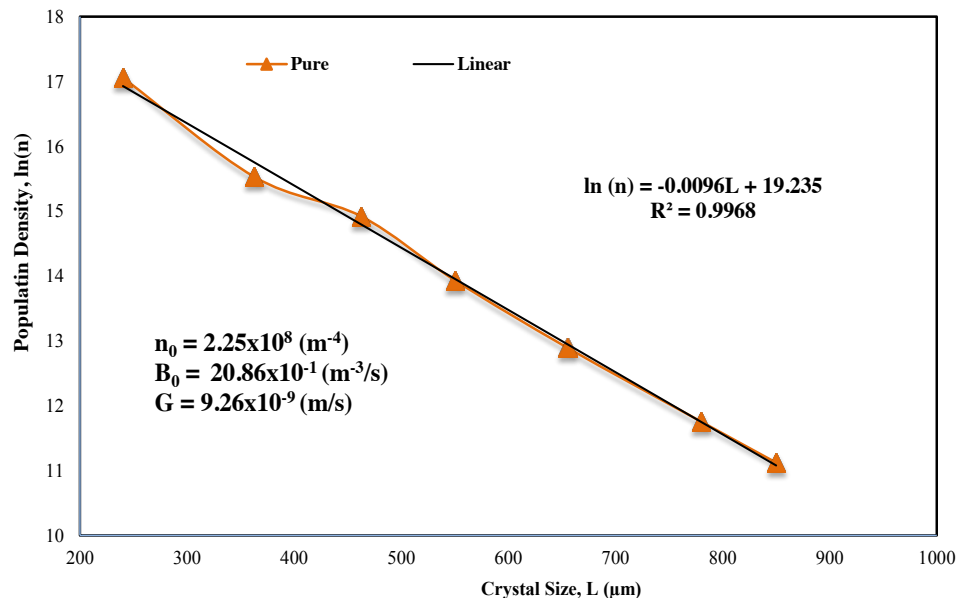


Figure 6. Population density versus crystal size for borax pentahydrate at 90-65°C, 175 ml min<sup>-1</sup>, 350 rpm, 120 min

#### 4. CONCLUSIONS

In this study, the effects of residence time, stirring speed, feed flow rate, amount of supersaturation on the crystal size distribution and the shape of borax pentahydrate crystals were determined in the CMSMPR crystallizer. However, the population density of nuclei, the nucleation rate and the growth rate of borax pentahydrate were determined from the experimental population balance distribution using the CMSMPR crystallizer running at the steady state. In light of the results obtained from this study, in the CMSMPR type crystallizer, crystals obtained in the residence time range of 30-150 minutes to determine the condition that steady-state conditions are satisfied were found to have stable state conditions after 120 minutes of residence time in the crystal size distribution determined after sieve analysis. It has been stated that in the CMSMPR system experiments with stirring speeds of 150-450 rpm, the stirring speed is effective on the crystal size distribution and that the crystal size distribution is reduced at a speed greater than the stirring speeds of 350 rpm, the probable cause is the stirring speed effect and the breaking of borax pentahydrate crystals is the resultant triggering of the secondary nucleation. In the experiments with pure borax pentahydrate solution in CMSMPR type crystallizers, the results were obtained in the range of feed flow rate of 70-230 mL/min, whereas the feed flow rate on the 175 mL/min, bag showed optimum conditions and the nucleation was increased in the ones above. In the CMSMPR system, microscopic photographs show that the average particle size decreases as the amount of supersaturation decreases and the resulting crystal quality increases, in the results obtained at the 90-65°C, 90-70°C and 90-75°C supersaturations. In addition, microscopic photographs of borax pentahydrate crystals obtained as a result of pure medium parameters are observed near the hexagonal structure.

#### ACKNOWLEDGMENTS

This work was supported by the Eti Mine Enterprises [ETIMINE, project number: 400.02(TGD.2014/3)].

#### REFERENCES

- [1] S.N. Tavare, Industrial crystallization: Process simulation analysis and design, New York, Plenum Pres, 1995.
- [2] R.M. Kellogg, M. Leeman, 9.16 Crystallization as a tool in industrial applications of asymmetric synthesis, Elsevier, 2012.
- [3] A. Moreno, M.E. Mendoza, 31-Crystallization in gels., 2 ed., Boston, Elsevier, 2015.
- [4] B.S. Choi, T.A. Ring, Evolution of crystal size distributions in a CMSMPR—the effect of temperature, flow rate, and mixing speed with time, Fluid Phase Equilibria 228 (2005) 99-107.
- [5] R.E.A. Mason, R.F. Strickland-Constable, Breeding of crystal nuclei, Transactions of the Faraday Society, 1966.
- [6] A.S. Myerson, Handbook of industrial crystallization, London, Butterworth-Heinemann, 1993.
- [7] A. Mersmann, Crystallization technology handbook, 2 ed., New York, Marcel Dekker, Inc., 2001.

- [8] A.H. Gülçek, A. Meriç, Boraks Pentahidrat Prosesinde Yapılan İyileştirme Çalışmalar, 1.Uluslararası Bor SempozyumuKütahya/Türkiye, 2002, pp. 70-83.  
[9] A.D. Randolph, M.A. Larson, Theory of particulate processes: Analysis and techniques of continuous crystallization, 2 ed., New York, Academic Press, 1988.  
[10] J.W. Mullin, Crystallization, 4 ed., Oxford, Butterworth-Heinemann, 2001.

## **BIOGRAPHY**

Sinan KUTLUAY was born in 1988 in Tutak/Ağrı. He graduated from Yıldız Technical University, Faculty of Chemistry-Metallurgy, Department of Chemical Engineering in 2010. Between the years 2010-2012, he completed his master's degree at Yıldız Technical University, Graduate School of Natural Sciences, Division of Chemical Engineering. The doctorate education that he started in 2014 is going on at Selçuk University, Graduate School of Natural Sciences, Division of Chemical Engineering. In 2011, he was appointed as research assistant at Siirt University, Faculty of Engineering and Architecture, Department of Chemical Engineering, Division of Process and Reactor Design, and still serves as research assistant in the same department. Sinan KUTLUAY is married and has one child.



# Effect of Processing Time on High Temperature Carbonization of Tea Plant Wastes

Elif ARANCI ÖZTÜRK<sup>1</sup>, Mustafa BOYRAZLI

## Abstract

*In this study, carbonization of tea plant wastes, which was done at relatively low temperatures and durations, was carried out at higher temperatures and was examined the effect of the transaction time on the carbonization process. The sample to be carbonized was placed in a crucible with the screw and processed in a muffle type furnace at different temperatures of 400-800 °C for 30-2160 minutes. The carbon and sulphur content in the sample treated at 1400 minutes at 800 °C was 94.68% and 0.03%, respectively, while the heat value of the same sample was 8823 cal/gr. In the samples subjected to the carbonization process, it was determined that as the temperature increased, the sulphur ratio decreased by 92% in parallel with the increase of the carbon ratio.*

**Keywords:** Tea plant waste, Carbonization

## 1. INTRODUCTION

Increased agricultural production and the development of agro-based industries in many countries of the world have brought about the production of large quantities of agricultural wastes, most of which are not adequately managed and utilized [1]. Agricultural wastes were used for animal feed, fertilizer and fuel for energy production, but any work hasn't been carried out to develop utilization of these wastes in the production of reduction technologies. Tea industries are one of the most important agro based contributors to the economy of a Nation. Processed tea wastes in tea industries can be used as a raw material for the production of Bio-oil, Bio-char and producer gas using pyrolysis and gasification technologies [2].

In our country, tea plant wastes reach considerably large amounts as the basic waste material of tea processing factories, especially as a result of non-standard harvesting of black tea leaves produced in the Eastern Black Sea Region. This ratio is between 3-5% in normal standards, but it is up to 17-18% due to improper harvest. Having a very large potential, the tea waste causes environmental problems because it cannot be evaluated in any way and is destroyed by being burned and decayed [3-5]. Tea wastes are used both as compost fertilizers and as an adsorbent in the recent years to remove heavy metals in waste water [6-8]. Many methods have been developed to remove metal ions such as Cd, Zn, Pb, Cr, Cu and Ni in abundant quantities in industrial wastewater. One of these methods is the adsorption process. In adsorbents used for adsorption, the cost is an important place. There are studies in the literature on the use of tea plant wastes as adsorbents to remove heavy metal ions such as Cd, Zn, Pb, Cr, Cu and Ni, which are intensively present in industrial waste water [9-15].

In this study, the carbonization processes of tea plant wastes, which were carried out at different temperatures and at lower temperatures, the effect of treatment period on the carbonization process carried out at high temperatures has been investigated.

## 2. EXPERIMENTAL STUDIES

Tea plant wastes obtained from Rize-Çaykur facilities and containing 49,15% C and 0,39% S were used in the studies. The tea plantings containing 2% moisture were dried at 105 °C for 4 hours and then weighed 5 gr into a metal pot (Figure 1) and subjected to a carbonization process in a muffle type furnace. As a result of the experiment, it was observed that weight loss occurred at a rate of approximately 60-76% of the material.

<sup>1</sup> Corresponding author: Firat University, Faculty of Engineering, Department of Metallurgy and Materials Engineering, 23119 Elazığ, Turkey. earanci@firat.edu.tr

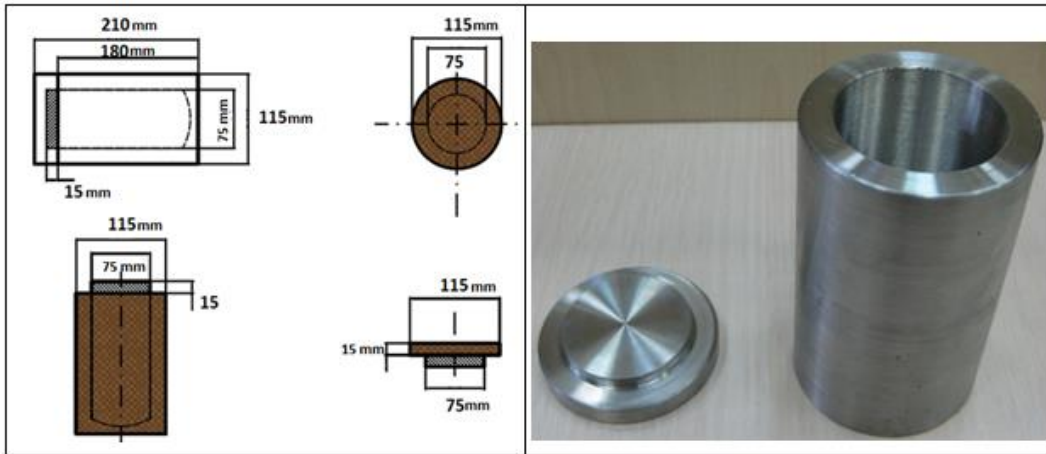


Figure 1. Metal pot used in carburization processes

### 2.1 Experimental Results

5 g of the sample placed in the crucible was subjected to carbonization at 400, 500, 600, 700, 800 and 900 °C for 30, 60, 90, 120, 240, 360, 720, 1440, 2160 minutes and the fixed carbon-sulphur content was examined. At temperatures above 800 °C, a high rate of scaling occurred in the metal pot and the gas outlet which was opened on the pot was clogged and occasionally small bursts occurred in the pot. In addition, the carbon content of the sample in the crucible was increased in the range of thousandths and the carbonization processes above 800 °C were cancelled.

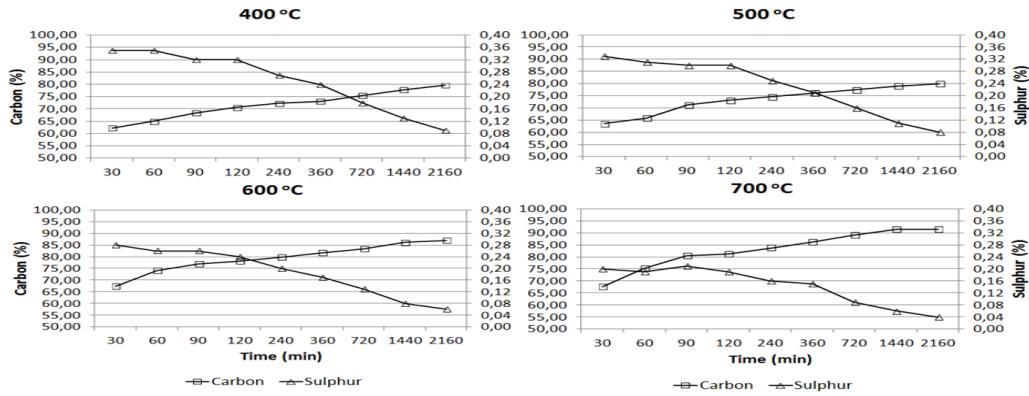


Figure 2. Carbon and sulphur content in the samples subjected to carbonization between 30-2160 minutes at temperatures of 400, 500, 600 and 700 °C.

In the samples which were carbonized at different times in the range of 30-2160 minutes in the temperature range of 400-700 °C, a decrease of about 87% in the sulphur ratio was observed in parallel with the increase of the carbon ratio as the temperature increased (Figure 2). At 400 °C temperature, while the carbon content is 62,24% and the sulphur content is 0,35%, in the sample treated at 800 °C, the carbon and the sulphur content is 72,14% and 0,19% respectively.

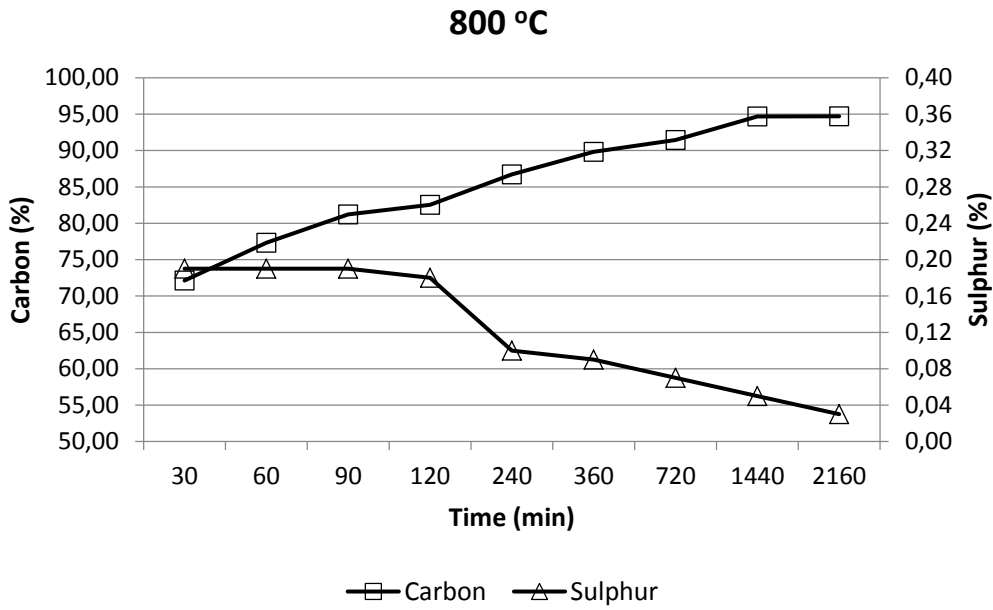


Figure 3. Carbon and sulphur content in samples subjected to carbonization for 30-2160 minutes at 800 °C.

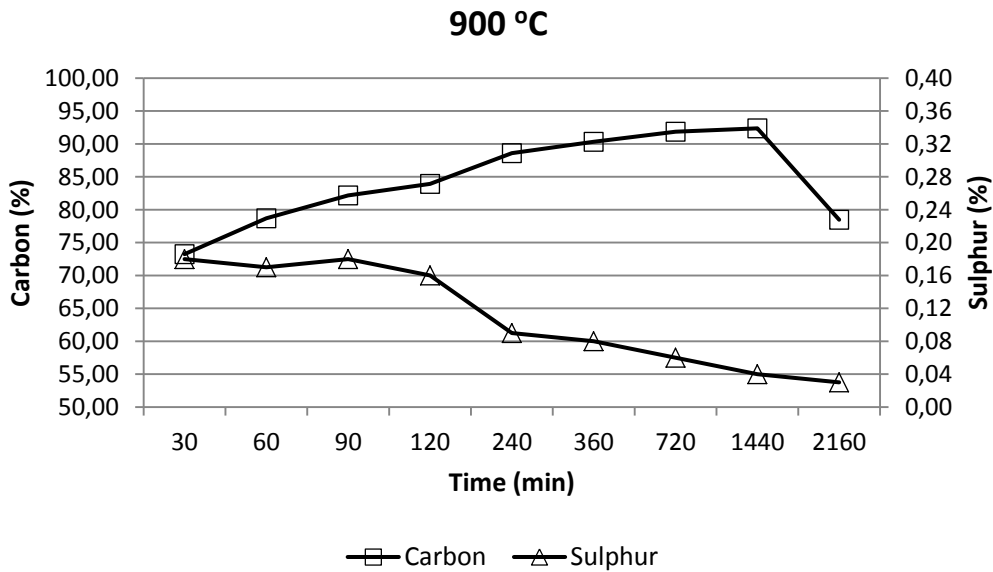


Figure 4. The contents of carbon and sulfur in samples subjected to carbonization at 900 °C for 30-2160 minutes.

In samples subjected to carbonization at different temperatures in the range of 30-2160 minutes at 900 °C, there was an increase in carbon content up to 1440 minutes parallel to the increase in temperature and time, and a sharp decrease was observed after 1440 minutes (Figure 4). While the decrease in sulphur was partly continued, the ash ratio was increased during carbonization over 1440 minutes. The reason for this increase in ash ratio can be explained by the clogging of the holes in the cap of the metal pot due to formation of the scale. The clogging of the holes on the cap of the pot and the partial opening of the cap by the gas pressure in the pot, the carbonized product reacts with oxygen and becomes the combustion products CO and CO<sub>2</sub>. At 1000 °C and 1100 °C, the cap of pot was fully opened due to the burst occurring in the pot and a large part of the sample completely turned into ash.

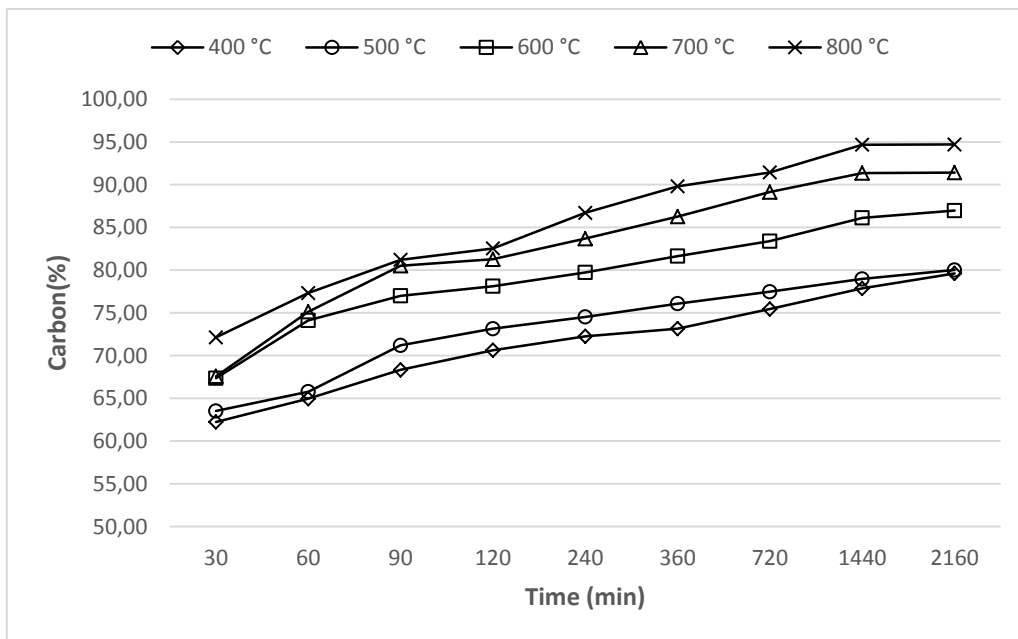


Figure 5. Carbon content in the sample subjected to carbonization at 400-800 °C temperature and 30-2160 minutes.

Carbon content was increased from 49.15% to 94.68% at the sample which was carbonized 1440 minutes at 800 °C (Figure 5). The thermal value of this sample is measured as 8823 cal/gr. Similarly, the amount of sulphur after carbonization was reduced from 0.39% to 0.03% by eliminating approximately 92% and the weight loss was measured between 60% and 76% (Figure 6). The SEM images of this sample are shown in Figure 7 A and B.

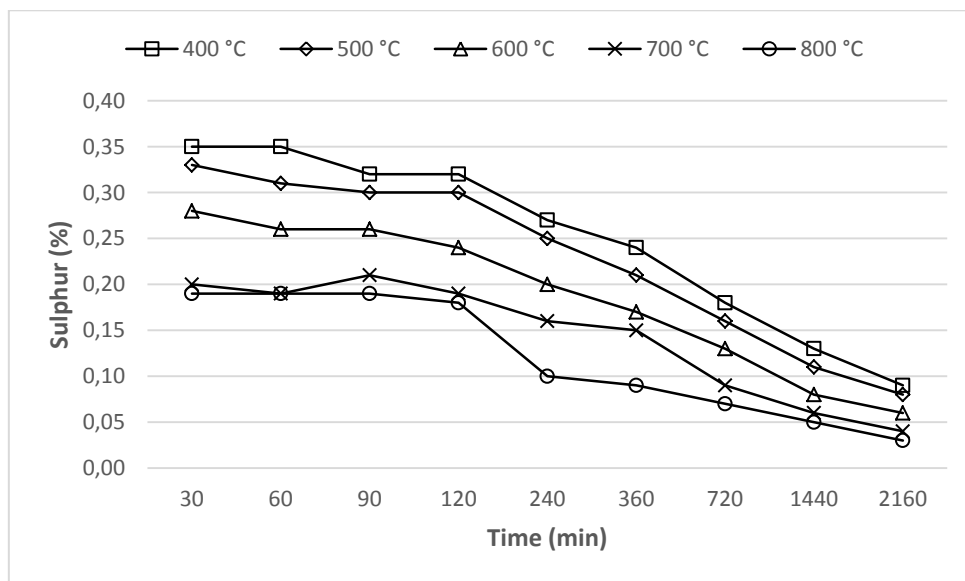


Figure 6. Sulphur content in the sample subjected to carbonization at 400-800 °C temperature and 30-2160 minutes.

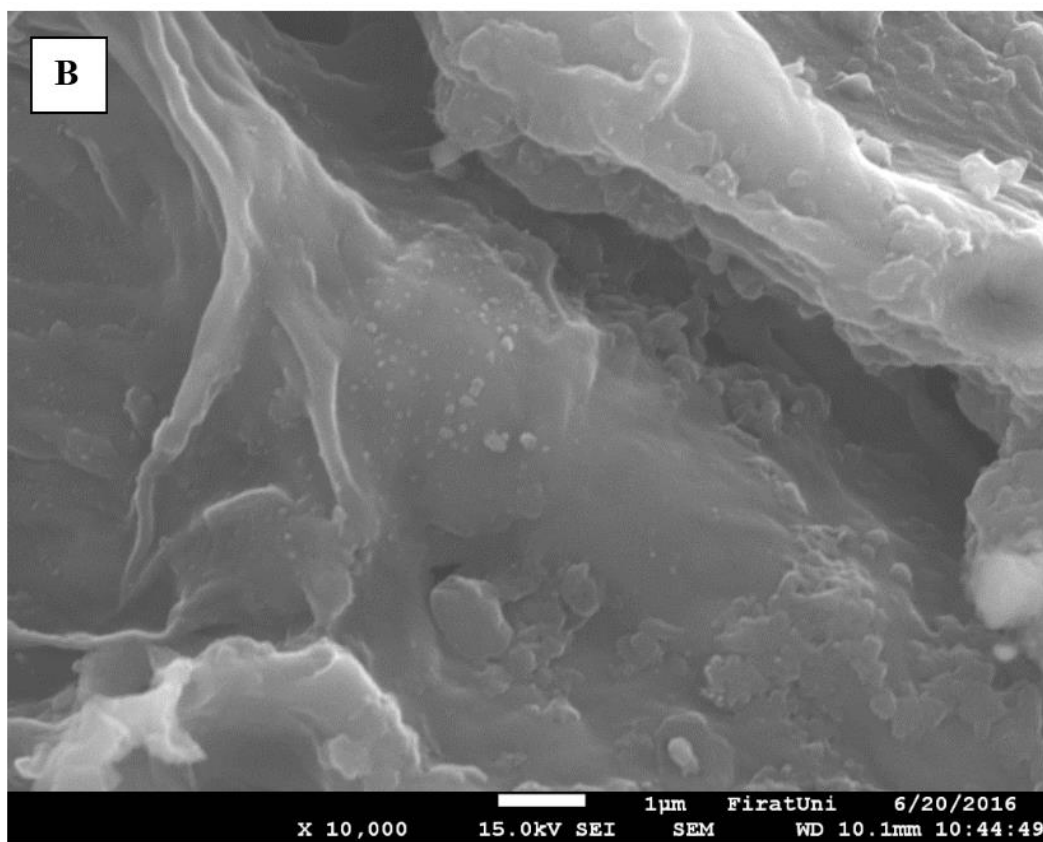
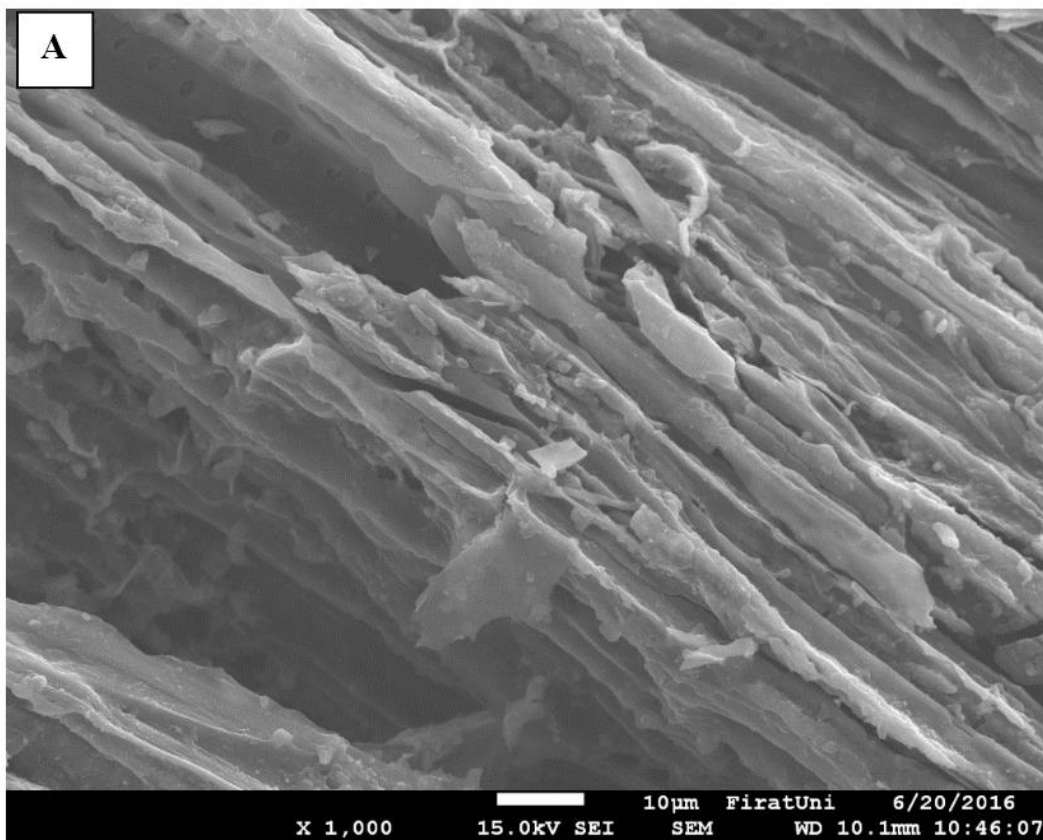


Figure 7. SEM image of this sample processed at 800 °C for 1440 minutes.

### 3.RESULTS

In this study, carbonization of tea plant wastes containing 49.15% C, 0.39% S, which was done at lower temperatures and durations before, was carried out at higher temperatures and was, examined the effect of the transaction time on the carbonization process.

In the samples subjected to 30, 60, 90, 120, 240, 360, 720, 1440 and 2160 minutes carbonization at 400-800 °C temperature range, a decrease of about 92% in sulphur ratio was observed as the temperature increased. While the carbon and sulphur content of the sample were 62.24% and 0.35% at 400 °C, the carbon content was 72.14% and the sulphur content was 0.19% at the sample treated at 30 minutes at 800 °C. Carbon and sulphur contents in the sample treated at 1400 minutes at 800 °C were 94.68% and 0.05% respectively. In the sample treated at 1400 minutes at 800 °C temperature, about 76% mass loss was observed and the calorimetric analysis of the same sample was found to be 8823 cal/gr.

This study was conducted to determine the availability of carbonized tea wastes as a carbon source in the reduction of metal oxide components. After the carbonization process, the carbon, sulphur and ash content of the product obtained shows that this product can be used both in the reduction of metal oxides and in the production of nano carbon tubes. Reduction of iron oxides with carbonized tea waste is done as continuation of current work.

### REFERENCES

- [1] Demir İ., 2006, An investigation on the production of construction brick with processed waste tea, *Building and Environment* 41 (2006) 1274–1278
- [2] Nagaraja M., Charles I., Sundaresan R., Natarajan R., and Srinivas T., 2013, Energy and by Products Recovery from Tea Waste, *International Journal of Electrical Energy*, Vol.1, No.1
- [3] Malkoc, E. and Nuhoglu, Y., 2006, Removal of Ni(II) ions from aqueous solutions using waste of tea factory: Adsorption on a fixed-bed column. *Journal of Hazardous Materials*, 135, 328-336.
- [4] Gurten İ., I., 2008, Çay Atığından Adsorbent Üretimi ve Üretilen Adsorbentin Adsorbsiyon Özelliklerinin İncelenmesi, Yüksek Lisans Tezi, Ankara Üniversitesi, Fen Bilimleri Enstitüsü, Kimya Mühendisliği Anabilim Dalı.
- [5] <http://dergi.cayeksperi.com.tr/index.php?islem=haber&id=36>
- [6] Yaman, S. 2004, Pyrolysis of biomass to produce fuels and chemical feedstocks, *Energy Conversion & Management*, 45, 651-671.
- [7] Gurav M., Sinalkar S., 2013, Preparation of organic compost using waste tea powder, *National Conference on Biodiversity: Status and Challenges in Conservation - 'FAVEO' 2013*.
- [8] Wasewar K. L., 2010, Adsorption of Metals onto Tea Factory Waste: A Review, *IJRRAS* 3 (3), June 2010.
- [9] Zuorro A., Lavecchia R., Medici F., Piga L., 2013, Chemical Spent Tea Leaves as a Potential Low-cost Adsorbent for the Removal of Azo Dyes from Waste Water, *Chemical Engineering. transactions*, 32, 19-24.
- [10] Wasewar K., Atif M., Prasad B., Mishra M.I., 2008, Adsorption of Zinc using Tea Factory Waste: Kinetics, Equilibrium and Thermodynamics, *Clean* 2008, 36 (3), 320–329.
- [11] Malkoc E., Nuhoglu Y., 2005, Investigations of nickel (II) removal from aqueous solutions using tea factory waste, *Journal of Hazardous Materials B* 127 (2005) 120–128.
- [12] Wasewar K.L., Atif M., Prasad B., Mishra M.I., 2009, Batch adsorption of zinc on tea factory waste, *Desalination* 244 (2009) 66–71.
- [13] Nuhoglu Y., Malkoc E., 2007, Potential of tea factory waste for chromium(VI) removal from aqueous solutions: Thermodynamic and kinetic studies, *Separation and Purification Technology* 54 (2007) 291–298.
- [14] Amarasinghe B.M.W.P.K., Williams R.A., 2007, Tea waste as a low cost Adsorbent for the removal of Cu and Pb from wastewater, *Chemical Engineering Journal* 132 (2007) 299–309.
- [15] Cay S., Uyanik A., Ozasik A., 2004, Single and binary component adsorption of copper(II) and cadmium (II) from aqueous solution using tea-industry waste, *Separation and Purification Technology* 38 (2004) 273–280.

### BIOGRAPY

I was born in Kars in 1987, I completed my primary and secondary education in Kars, my high school education in Adana. He graduated from Firat University, Faculty of Engineering Metallurgy and Materials Engineering Department and graduated from Anatolian University Foreign Trade Program and Economics Department. I am a PhD student at Firat University Engineering Faculty Metallurgy and Materials Engineering Department where I work as a research assistant.



# The Effect of High Frequency Cold Plasma Obtained in Various Parameters, on the Electrochemical Activity of Co-Cr-B Based Catalysts

Tülin AVCI HANSU<sup>1</sup>, Fevzi HANSU<sup>2</sup>, Ömer ŞAHİN<sup>3</sup>

## Abstract

In this study, the catalytic activity of Co-Cr-B based catalysts reduced from  $\text{CoCl}_2 \cdot 6\text{H}_2\text{O}$  is investigated under Alternating Current cold plasma obtained in various applying frequency parameters. Co-Cr-B catalyst reduces by the known procedure, was put into a special reactor and then exposed to the cold plasma obtained in various applying frequency conditions. Each sample of Co-Cr-B catalysts was treated by AC plasma obtained in various applying frequencies separately. In the presence of a plasma-treated catalyst, the hydrolysis reactions complete within shorter time intervals than in the presence of untreated catalysts. In the period of 20 minutes, the best chosen cold plasma-treated Co-Cr-B catalyst produces 785 ml Hydrogen gas whereas the untreated catalyst produced 600 ml in the same hydrolysis reaction conditions. The experimental results show that the frequency of applying voltage of plasma is very effective on the catalytic activity of catalysts.

**Keywords:** Cobalt-Chrome-Boride Catalyst, AC Cold Plasma, Hydrogen generation, Sodium borohydride

<sup>2</sup>Corresponding author Tel: +90 (544) 343 41 88 Fax: +90 (484) 212 11 11  
E-mail: f\_hansu@siirt.edu.tr

## 1. INTRODUCTION

Catalysts play an important role for a chemical reaction utilized in the industry. In fact, a catalyst can be defined as a key of a chemical reaction. It accelerates a chemical reaction depending on the activity level of which. In this case, enhancing of catalysts' activity has become very attractive for scientists recently. A catalyst activity can be increased by various methods. The famous one of them is cold plasma method. Plasma mechanism can be basically defined as a charge bomber in order to make the surface of catalyst full of holes. In that case, the total surface area of a bombarded catalyst by plasma highly increases. This effect directly increases catalytic activity.

From experimental studies, it was seen that surface modification, which is very effective for a catalyst activity, can be highly effected by cold plasma discharges. Cold plasma method is widely used in the area of plasma chemical vapor deposition, pollution control, excitation of  $\text{CO}_2$  lasers and excimer lamps [1]. Recently, cold plasmas have been applied to many chemical reactions, too. In addition, many of chemical reactions produced in cold plasma medium, were found to be much activated.

Catalysts play such a good roll in hydrogen generation from  $\text{NaBH}_4$  solution because the rate of hydrogen generation from self-hydrolysis of  $\text{NaBH}_4$  is not satisfactory at room temperature. The efficiency of hydrogen production can be significantly increased by using such an effective catalyst during the hydrolysis reaction. Schlesinger et al. (1953) showed that the hydrogen generation from alkaline  $\text{NaBH}_4$  solution could be accelerated by cobalt chlorides and nickel chlorides [2].

Hydrogen is a famous fuel and an attractive alternative power source, recently [3]. In energy industry, PEM fuel cells use pure hydrogen and pure hydrogen can be easily obtained from self-hydrolysis of borohydrides. Among the chemical compounds, sodium borohydride (NaBH<sub>4</sub>) is known a good source of pure hydrogen utilized in fuel cells at room temperature [4-6].



Plasma is an ionized gas that can basically be generated by electrical discharges. In recent years, cold plasma techniques have been widely used in producing effective catalysts [7-15]. The best advantage of Alternating Current (AC) cold plasmas is low temperature that will result in less energy consumption, minimum electrode erosion and surface modification. Cold plasmas are so-called non-equilibrium plasmas. This types of plasmas usually can be simply occurred between two electrodes called high voltage electrode and low voltage electrode.

The aim of this study is to determine the effect of cold plasma methods on the catalytic properties of Co-Cr-B catalysts utilized in hydrogen generating by the way of NaBH<sub>4</sub> hydrolysis. In fact, cold plasma methods produced in various conditions are found to be very effective at increasing catalytic activity of Co-Cr-B catalysts.

## 2. EXPERIMENTAL

As a first step, Co-Cr-B catalyst was synthesized by the known chemical reduction method. To do this, a certain amount of CoCl<sub>2</sub>.6H<sub>2</sub>O (0.004 moles) and Cr (NO<sub>3</sub>)<sub>3</sub>.9H<sub>2</sub>O (0.0002 moles) salts were taken into an aqueous solution containing 50 ml de-ionized water while being stirred. At the same time, another aqueous solution containing 50 ml de-ionized water and a certain amount of NaBH<sub>4</sub> (0.053 moles), which was used as a reducing agent, was added drop by drop to the first solution. Before starting the experiment, it is accepted that all the reagents used in this experimental study are of analytical grade and at certain concentrations (NaBH<sub>4</sub> concentration 3.2–25 % and NaOH concentration 1.5–10 %) [16]. All chemical synthesis of catalysts was done at 6 °C temperature.

Figure 1 shows the schematic diagram of the experimental setup used for plasma treatment of Co-Cr-B catalysts in solid state. The plasma treatment processes of the catalysts were performed in a vacuumed plasma reactor system in order to isolate from oxidation. The plasma reactor system was made of a glass tube with a 4 cm inner diameter, 12 cm in length and 150 ml in volume. The reactor has two applied voltage electrodes placed in the center of the reactor as bottom and top in position. The top electrode is called high voltage electrode, and is circular in shape with 50 mm in diameter. The other one is called low voltage electrode, which was placed the bottom of the reactor with 80 mm in diameter and directly connected to earth. The gap between up and down electrode is 5 mm in length. Furthermore, the reactor has a gas inlet-outlet hole. The plasma was generated by a High-Voltage Alternating Current Transformer that could apply various voltages (from 0 kV to 33 kV) with the frequency changing from 50 to 500 Hz interval. By using this reactor and plasma system, the Co-Cr-B catalysts were separately treated by AC cold plasma types with various applied voltages and frequencies depending on time.

All the processes were done in the following ways:

Firstly, a certain amount of Co-B catalyst powder (more than 0.05 gr.) were put on the low voltage electrode then AC cold plasma obtained in a certain voltage and frequency, was applied to the surface of the catalyst with a certain time and all the experimental study are done into the vacuumed plasma reactor.

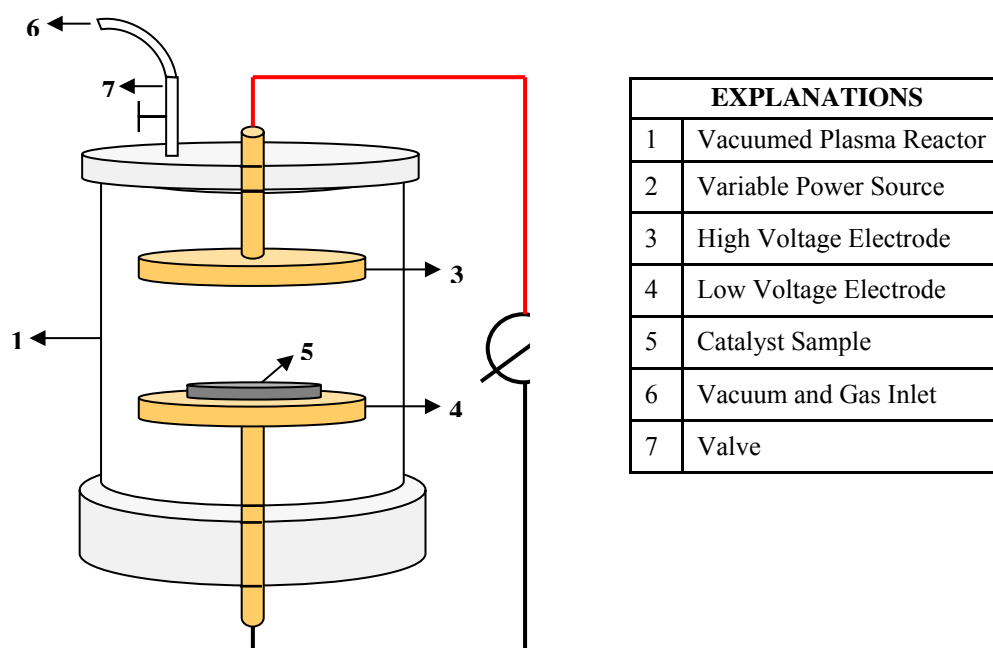


Figure 1: Schematic diagram of the experimental setup

The plasma occurred between upper and lower electrodes by applying varied voltages such as 3 kV, 5 kV and 7.5 kV and 50 Hz, 150 Hz, 350 Hz and 500 Hz frequencies separately in vacuum medium, at approximately 5 min time intervals. Finally, the plasma treated catalysts obtained by the ways mentioned above were added to the hydrolysis reactions of  $\text{NaBH}_4$  according to known procedure, separately. In the known procedure, a certain amount of  $\text{NaBH}_4$  (0.008 moles) and  $\text{NaOH}$  (0.0038 moles) were taken into a solution containing 15 ml de-ionized water, and then a certain amount of plasma treated Co-B catalyst (0.05 gr.) was added to the prepared solution to generate hydrogen gas. The generated gas volume was measured during the hydrolysis of  $\text{NaBH}_4$  simultaneously [17]. The measured volume of released gas was afterwards converted into a yield of generated hydrogen and compared to known results. The hydrolysis of  $\text{NaBH}_4$  aqueous solution was carried out at 30 °C.

### 3. RESULTS AND DISCUSSION

The effect of AC cold plasmas on the activity of Co-Cr-B catalysts utilized in generating hydrogen gas from the hydrolysis of  $\text{NaBH}_4$  was investigated at various applied voltages and frequencies. The applied voltage values have to be limited depending on certain dimensions of the reactor used in this study. In that case, the maximum applied voltage for plasma was limited to 7.5 kV and similarly, the maximum frequency rate was limited to 500 Hz because of maximal rates of power supply. Therefore, to produce the AC cold plasmas in the reactor given in Fig 1, the applied voltages could not be increased to more than 7.5 kV and similarly, the applied voltage frequency could not be increased to more than 500 Hz because of the limited dimensions of the reactor. Otherwise, if the applied voltages or frequencies increase to more than the upper limits of the reactor dimensions, there could be an arc between the closest points of the electrodes and this results non-homogeny electrical field. In that case, the effect of plasma on the catalytic activity would be sharply decreased. Even so, arc may burn or destroy the catalyst.

Hydrogen generation volumes obtained from the hydrolysis of  $\text{NaBH}_4$  in the presence of Co-Cr-B catalysts processed in various applied voltages of AC cold plasma mediums and non-plasma mediums depending on time are shown in Fig. 2. According to Fig. 2, the catalysts treated at various applied voltages of AC plasma showed different behaviors, and it can be said that the higher the applied voltages, the more activity could be obtained from the catalyst. In Fig 2, it is seen that the catalysts treated by AC plasma for 7.5 kV applied voltages made hydrolysis processes faster than untreated catalysts.

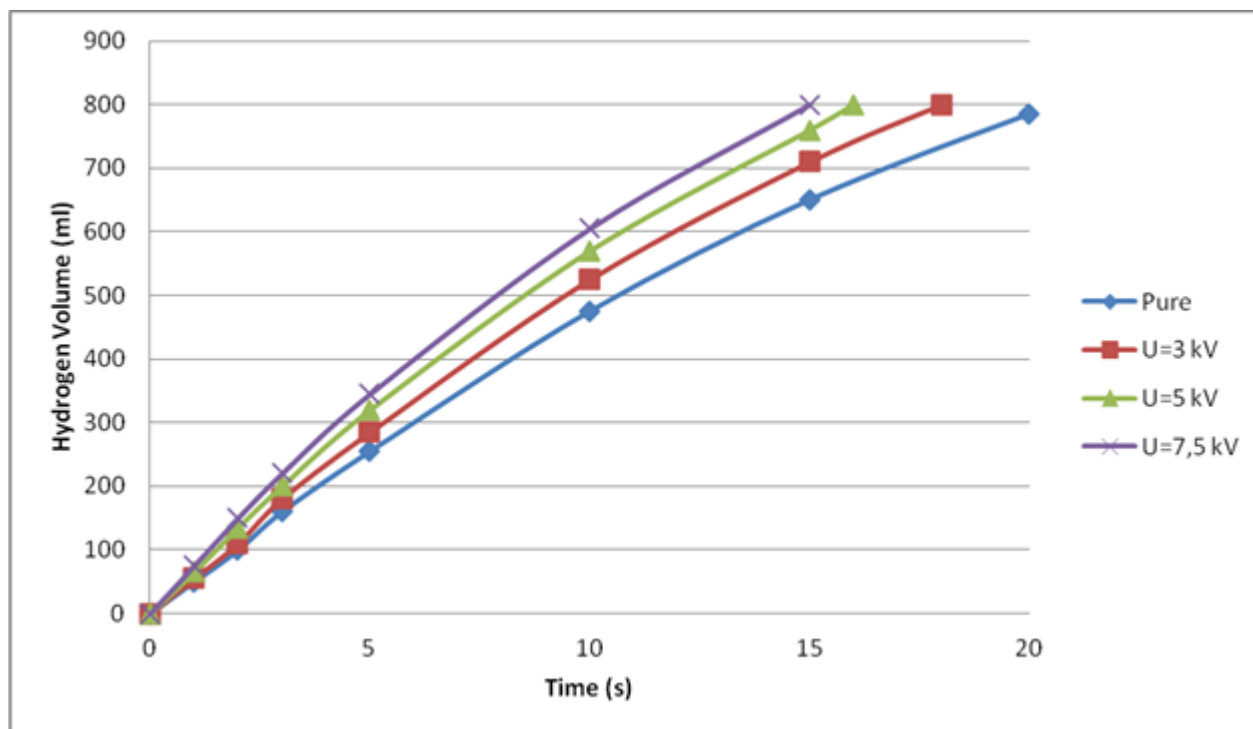


Fig. 2: Time-dependent Hydrogen volumes obtained in the presence of Co-Cr-B catalysts treated by cold plasma in various applying voltages.

Similarly, in the presence of Co-Cr-B catalysts treated with AC cold plasma obtained in various frequencies, the changes of hydrogen generation volumes depending on various applying voltage frequencies of AC cold plasma and time are given in Figure 3. It is seen from the Fig. 3; the catalysts treated by AC cold plasma with 500 Hz frequency became much more active than untreated catalysts. As it is known that, one of the main effects of cold plasmas on catalysts is surface modification. By using AC cold plasma methods, the catalysts' surfaces are considerably modified. Sahin et al. showed that hydrogen production is related to the catalysts' surface area and the greater the surface area of catalysts, the higher hydrogen generation volume [15]. In a study given in [18], From SEM morphology of the plasma treated catalysts, it can be seen that the surface area of catalysts treated by AC cold plasma was considerably corrugated compared to the untreated catalyst surface area and this clearly results surface enhancement for a catalyst. Therefore, it can be inferred that if the surface area is wider, the contact between the catalyst and the  $\text{NaBH}_4$  solution will increase so that hydrogen generation volume will increase, too. To sum up, the more surface width, the higher chemical activity for a catalyst.

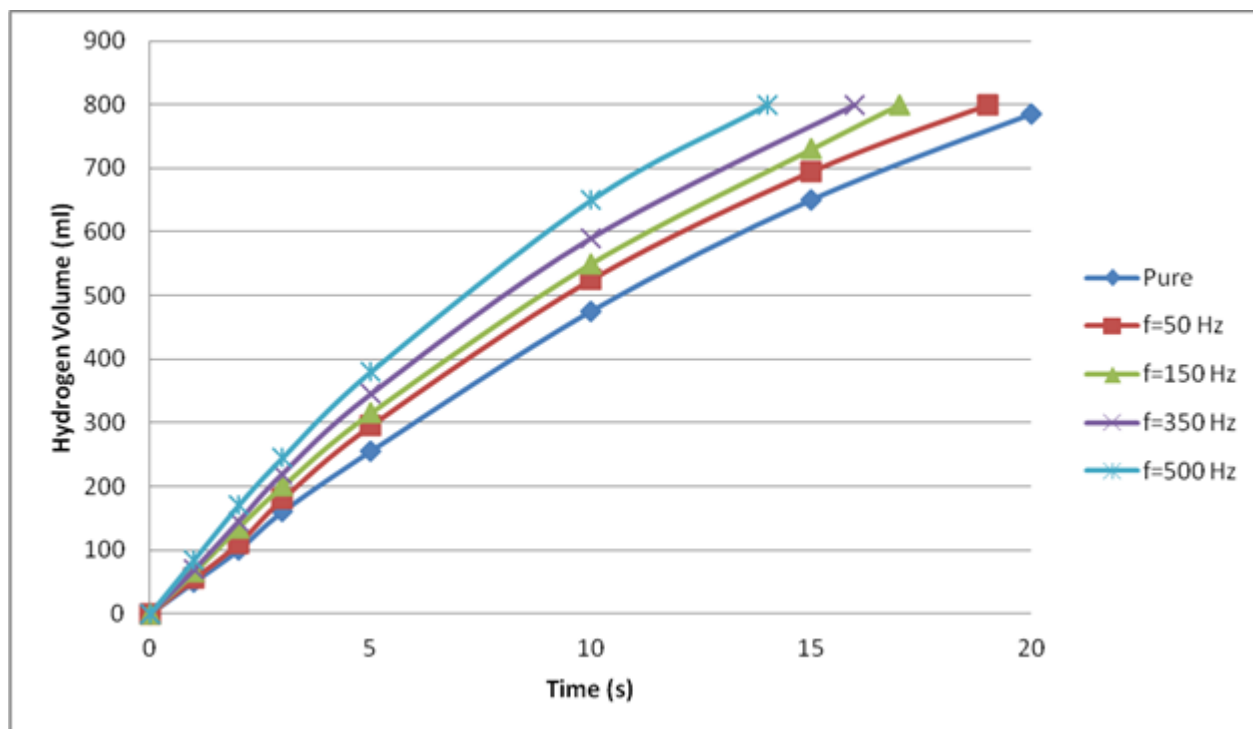


Fig. 3: Time-dependent Hydrogen volumes obtained in the presence of Co-Cr-B catalysts treated in various applying voltage frequencies of plasma.

There is a common misconception that plasma synthesized catalysts are expensive because of power consumption. If the main characteristics of plasma treated catalysts are taken into account, including a simple production system, short preparation period, miniaturization of equipment, low energy consumption and so on, it is safe to predict plasma treated catalysts will soon prove their advantages. Note that the cost of catalysts is a small part of the total cost of the production system. The power consumption values of AC cold plasma methods were studied in [18].

#### 4. CONCLUSIONS

In this study, the effect of AC cold plasmas on Co-Cr-B catalysts utilized in hydrolysis of  $\text{NaBH}_4$  to generate hydrogen gas was investigated in various applying voltages and frequencies conditions. Therefore, the effect of this plasma method with various applied voltages and frequencies on activity of Co-Cr-B catalysts was clarified and related optimal parameters were obtained. In experiments it was concluded that besides the chemical activity of a catalyst, the cold plasma method used in this study are also known as being quite effective at surface modification. The results show that AC cold plasmas are very effective in surface modification that has an important role in enhancing catalytic activity of Co-Cr-B catalysts. From the results it can be inferred that applying electrical parameters such as voltage and frequency can be very effective at increasing chemical activity of a catalyst. For this study it was also concluded that high frequency AC applying voltage plasma treated catalysts became much more active than untreated catalysts.

#### REFERENCES

- [1] Ulrich Kogelschatz. *Plasma Chemistry and Plasma Processing*, Vol. 23, No. 1, March 2003
- [2] Schlesinger HI, Brown HC, Finholt AE, Gilbreath JR, Hoekstra HR, Hyde EK. 1953. *J Am Chem Soc.* 75:215–219.
- [3] Wei Y, Huamin Z, Dongyan X, Li M, Baolian Y. (2007) *Hydrogen J. Power Sources* 64: 544.
- [4] Kitzling M.B and Jaras S.G. 1996. *Appl. Catal. A.* 147: 1-21.
- [5] Biniwale, RB, Mizuno A, Ichikawa M. 2004. *Appl. Catal. A: Gen.* 276: 169.
- [6] Liu, C., Zou, J., Yu K., Cheng, D., Han, Y., Zhan, J. et al. 2006. *Pure Appl Chem.* 78: 1227–1238.
- [7] Li, Z.H, Tian, S.X, Wang H.T., Tian, T.B. 2004. *J Mol Catal A: Chem.* 211:149–153.
- [8] Liu, C., Vissokov, G.P, Jang, B. 2002. *Catal. Today.*72: 173–184.
- [9] Wei C, Tao Z, Yongxiang Y, Xumei T. J. (2009) *Natural Gas Chemist* 18: 35-38.
- [10] Tong, D.G., Luo, Y.Y., Chu, W., Hu, J.Y., Wu, P. 2010. *Plasma Chem Plasma Process.* 30: 663–677.
- [11] O. SAHİN, F. HANSU et al. *J. Energy Sources, Part A: Recovery, Utilization, and Environmental Effects.* UESO–2010–0817. R2. (08-Jan–2011).
- [12] O. SAHİN, O. BAYTAR, F. HANSU et al. *J. Energy Sources, Part A: Recovery, Utilization, and Environmental Effects.* UESO–2010–0800. R1. (12-Jan–2011).
- [13] Chun YN, Yang YC, Yoshikawa K. 2009. *Catalys Today.* 148: 283.
- [14] H. Z. Alisoy, C. Yeroglu, M. Koseoglu, F. Hansu. (2005) *J. Phys. D: Appl. Phys.*, vol. 38, pp. 4272–4277.
- [15] Ömer Şahin, Cafer Saka, Orhan Baytar, Fevzi Hansu. *Journal of Power Source*, 240, 15 2013, 729-735.
- [16] R Fernandes, N Patel, A Miotello. *Applied Catalysis B: Environmental* (2009).
- [17] Sahin O, Dolas H, Kaya M, Izgi MS, Demir H. (2009) *Int. J. Energy Res.* 34: 557.

- [18] **Hansu F** (2014). The Effect of Dielectric Barrier Discharge Cold Plasmas on the Electrochemical Activity of Co-Cr-B Based Catalysts. *Journal of The Energy Institute*, Doi: [10.1016/j.joei.2014.09.004](https://doi.org/10.1016/j.joei.2014.09.004).

## **BIOGRAPHY**

Tülin AVCI HANSU was graduated from Harran University, department of Chemistry in 2011. She works especially in catalyst production area. She has been working as Research Assistant at Siirt University, Department of Chemical Engineering



# A KINETIC STUDY FOR OLIVE OIL RESIDUE PYROLYSIS: MODEL FREE APPROACHES

*O. Cepeliogullar<sup>1</sup>, H. Haykiri-Acma, S. Yaman*

## *Abstract*

---

*In this study, olive oil residue was selected as biomass feedstock to study thermal and kinetic behaviors at high temperature region. Pyrolysis experiments were carried out from room temperature to 900°C at 5, 10, 20 and 50°C/min heating rates in the presence of nitrogen. The obtained thermal data was used to calculate the kinetic parameters using Coats-Redfern, Friedman, Flynn-Wall-Ozawa (FWO) and Kissinger-Akahira-Sunose (KAS) methods. Experimental and modelling studies showed that thermal behaviors of olive oil residue can be divided into three main regions which are i) moisture removal, ii) main decomposition of the structure (hemicellulose and cellulose degradation together with the start of the lignin degradation) iii) lignin decomposition. The activation energies for this process were determined very close as 158.9, 155.2 and 153.4 kJ/mol for each kinetic model in the given order.*

---

## 1. INTRODUCTION

From the current perspective, it is important to underline that alternative and renewable resources, for instance biomass, have been attracted serious attention considering the negative effects of fossil sources on the environment and the unevenly distribution or depletion of these sources. Therefore, this situation direct countries to diversify their energy sources towards more sustainable and alternative feedstocks. Thermochemical processes such as pyrolysis provides economically viable routes for the conversion of biomass into transportation biofuels and valuable chemicals. However, the structure of solid biomass is extremely complex and its thermal degradation products are even more heterogeneous. Therefore, a detailed thermal and kinetic analyses should be carried out to investigate the pyrolytic behaviors of the selected feedstock at high temperature region.

Thermogravimetric analysis (TGA) has been widely used to study the apparent kinetics of biomass pyrolysis that attributes to the high-precision in weight loss recording, perfectly suitable for low heating rates condition. Based on the TGA, the pyrolysis kinetic parameters and mechanisms can be estimated using two main procedures: model-free and model based approaches. The model-free procedure can estimate the kinetic parameters (i.e. apparent activation energy and pre-exponential factor) accurately without knowing the pyrolytic mechanism (model) by combining the isoconversional methods, master-plots methods and energy compensation effects [Bach and Chen (2017); Hue et al. (2016)].

In this study, olive oil residue (OOR) was selected as biomass resource to evaluate the thermal and kinetic behaviors during pyrolysis process. Having long coasts along the Aegean and Mediterranean seas, Turkey is rich in olive trees. Annually, about 1 million tonnes of olive is used in olive-oil production and approximately 450,000 tonnes of olive-oil residues are produced. Therefore, utilization of this oil rich residue could be a promising solution for the energy and chemical production [Uzun et al.(2007)]. At the first step of the study, pyrolysis experiments were carried out from room temperature to 900°C at 5, 10, 20, and 50°C/min heating rate in the presence of nitrogen. The obtained thermal data was then used to calculate the activation energy of the prolysis process. To do that three different kinetic models which are Friedman, FWO and KAS were applied to thermal data. In the light of experimental and modelling studies, it can be concluded that olive oil residue is a very promising feedstock to evaluate as biomass source in pyrolysis process.

## 2. MATERIALS AND METHODS

### 2.1 Materials

In this study, olive oil residue (OOR), provided from Marmarabirlik Inc. located in Bursa, was selected as feedstock. After drying step at room conditions, feedstock was grinded, sieved to the particle size less than 250 $\mu$ m. Following this preparation step, characterization of the feedstock was carried out in terms of proximate, ultimate and component analyses. More explanation about the procedures of these analyses can be found in our previous study [Cepeliogullar et al.(2016)]. From the results, it is possible to say that the moisture content of OOR was appropriate for thermal processes and found as 4.0%. The volatile and the ash contents were ~83% and ~2.5%. Considering the component analysis, the holocellulose, lignin and extractives amounts were determined as 54.7, 19.9 and 22.7%. The ultimate analysis showed that OOR had 57.9% of C and 33.8% of O content. The calorific value was 20.3 MJ/kg.

### 2.2 Thermal decomposition experiments

Thermal decomposition experiments were performed in TA Instruments SDTQ600 model thermal analyzer from room temperature to 900°C with sample amount ~10-15 mg, at four different heating rates which were 5, 10, 20 and 50°C/min in the presence of nitrogen gas with a flow rate of 100ml/min. This nitrogen flow ensured an inert atmosphere on the sample during the run, while the small amount of sample and the slow heating rate ensured that the heat transfer limitations can be ignored. The data obtained from thermal decomposition experiments were used for both kinetic analysis.

### 2.3 Kinetic studies

Solid state kinetics can be studied with thermal methods by measuring the sample property as it is heated or held at a constant temperature. In this study, reaction kinetics was applied to thermal data obtained under non-isothermal conditions with a constant heating rate. The pyrolysis reaction of the solid material may be given as below:



Under isothermal conditions the rate equation for solid fuel decomposition can be expressed as;

$$\frac{d\alpha}{dt} = kf(\alpha) \quad (2)$$

where  $k$  is the rate constant of the reaction,  $f(\alpha)$  is the function of  $\alpha$ , and  $\alpha$  is the conversion or weight loss rate that can be calculated with the following equation,

$$\alpha = \frac{W_o - W_t}{W_o - W_f} \quad (3)$$

In Eq.3,  $W_o$  is the initial weight of the sample (mg),  $W_t$  is the weight of the sample at a given time (mg) and  $W_f$  is the final mass of the sample (mg). The temperature dependent reaction constant  $k$  can be described with the Arrhenius law as given,

$$k = A \exp\left(\frac{-E}{RT}\right) \quad (4)$$

where  $A$  is known as the pre-exponential or frequency factor ( $\text{min}^{-1}$ ),  $E$  is the activation energy (kJ/mol),  $R$  is the universal gas constant ( $8.3145 \text{ Jmol}^{-1}\text{K}^{-1}$ ) and  $T$  is the absolute temperature (K). Substituting Eq.4, into Eq.2 gives the following equation,

$$\frac{d\alpha}{dt} = A \exp\left(\frac{-E}{RT}\right) f(\alpha) \quad (5)$$

To solve this equation, different  $f(\alpha)$  can be proposed.

$$f(\alpha) = (1 - \alpha)^n \quad (6)$$

In the non-isothermal thermal experiments, heating rate is also function of time as expressed in the following form,

$$\frac{d\alpha}{dT} = \frac{d\alpha}{dt} \cdot \frac{dt}{dT} \quad (7)$$

For non-isothermal measurements, linear heating rate,  $\beta$  (K/min) may be defined as,

$$\beta = \frac{dT}{dt} \quad (8)$$

Finally, inserting linear heating rate (Eq.8) into Eq.5 gives,

$$\frac{d\alpha}{dT} = \frac{A}{\beta} \exp\left(\frac{-E}{RT}\right) f(\alpha) \quad \text{or} \quad \frac{d\alpha}{dt} = \beta \left(\frac{d\alpha}{dT}\right) = A \exp\left(\frac{-E}{RT}\right) f(\alpha) \quad (9)$$

This equation is known as “the general equation of TGA curve”. Integration and recombination of Eq.9 gives,

$$g(\alpha) = \int_0^\alpha \frac{d\alpha}{f(\alpha)} = \frac{A}{\beta} \int_0^T \exp\left(\frac{-E}{RT}\right) dT \quad (10)$$

where  $g(\alpha)$  is known as the integrated reaction model, so called “integral function” or “temperature integral”. From this point on, different approaches can be applied to solve this equation. The detailed explanation about these approaches can be found elsewhere [Cepeliogullar et al. (2016)]. Here, model free kinetic approaches were applied to determine the activation energy of the pyrolysis process. The selected models which are Friedman, FWO and KAS models were summarized in Table 1.

Table 1. Summary of model free kinetic methods

|                 | General forms and assumptions   | Plotting method  |
|-----------------|---|--|
| Friedman Method | $\ln\left(\frac{d\alpha}{dt}\right) = \ln\left[\beta\left(\frac{d\alpha}{dT}\right)\right] = \ln[Af(\alpha)] - \frac{E}{RT}$<br>Assumes $f(\alpha)$ remains constant.<br>Degradation is independent of temperature and depends only on the rate of mass loss.   | $\ln\left(\frac{d\alpha}{dt}\right)$ vs $(1/T)$<br>Slope = $-E/R$                                    |
| FWO Method      | By an empirical formula proposed by Doyle:<br>$\log p(x) \cong -2.315 - 0.4567x$ , for $20 \leq x \leq 60$<br>Taking natural logarithm and rearranging by using Doyle's approximation gives,<br>$\log \beta = \log\left(A \frac{E}{Rg(\alpha)}\right) - 2.315 - 0.4567 \frac{E}{RT}$<br>Assumes apparent activation energy remains constant during the degradation<br>(From $t=0$ to $t_\alpha$ where $t_\alpha$ is the time at conversion is $\alpha$ ). | For different heating rates at fixed conversion<br>$(\log \beta)$ vs $(1/T)$<br>Slope = $-0.4567E/R$ |
| KAS Method      | This method also employs another derived approximation by Doyle:<br>$\log p(x) \cong \frac{\exp^{-x}}{x^2}$ , for $20 \leq x \leq 50$<br>Rearranging by using Doyle's approximation gives,<br>$\ln\left(\frac{\beta}{T_m^2}\right) = -\frac{E}{R} \left(\frac{1}{T_m}\right) - \ln\left[\left(\frac{E}{AR}\right) \int_0^\alpha \frac{d\alpha}{f(\alpha)}\right]$ , $T_m$ : temp. @max reaction rate<br>Assumes $\alpha$ has a fixed value.               | $\ln\left(\frac{\beta}{T_m^2}\right)$ vs $(1/T_m)$<br>Slope = $E$                                    |

### 3. RESULTS AND DISCUSSION

#### 3.1 Thermal behaviors of olive oil residue

TG (Thermogravimetry) and DTG (Derivative Thermogravimetry) curves of OOR decomposition were given in Fig.1. The pyrolytic behaviors can be explained in three stages which are *i*) moisture removal, *ii*) main decomposition of the structure (hemicellulose and cellulose degradation together with the start of the lignin degradation) *iii*) lignin decomposition as well as combustion of fixed carbon, and decomposition of tars. At the beginning of the process, OOR lost almost ~5% of its initial weight. The maximum peak temperatures were 53, 58, 69 and 84°C while the recorded weight loss rates were 0.36, 0.58, 1.40 and 3.70%/min, in the increasing heating rate order. From that point to ~180-200°C, almost no significant weight losses were observed. When the temperature reached 200°C, the main breakdown in the structure started. As can be seen from DTG curves (Fig.1), the maximum peaks were recorded between 200-500°C. In this temperature interval (STAGE 2), fundamental constituents of biomass, cellulose and hemicellulose began to decompose. The hemicellulose is constituted by sugar monomers, such as xylan and its derivatives, and the pyrolysis temperature range mainly cover 220-315°C. On the other hand, the stability of cellulose is stronger than hemicelluloses due to its crystal structure that starts to decompose around ~320-350°C. In general, it is possible to detect decompositions of these polymers blocks from the peaks in DTG due to sharp or slight divisions in the peaks. In our case, it is possible to observe some slight divisions in the main decomposition peak (see Fig.1, STAGE 2). The left division in the main peak can be attributed to hemicellulose decomposition while the right division in the peak is the indicator of the cellulosic decompositions. During thermal breakdown of hemicellulose, OOR lost ~38% of its initial weight. The maximum peak temperatures that represented the cellulose decomposition were

recorded at 310, 321, 337 and 353°C. Above 400°C, the small changes in the weight were the indicator of the lignin decomposition. Lignin decomposition peak covers wider range overlapping by the other two peaks; hemicellulose and cellulose (200-800°C) slowly over a very broad range of temperatures. At the final stage of the pyrolysis (STAGE 3), the reactions were caused by the combustion of fixed carbon, decomposition of tars and other concerns between the temperature ranges of 500-800°C. It is known that the remaining residue after thermal treatment has brought about the char and the ash. The yields of residues were recorded as 22.7, 22.3, 20.4 and 21.7%.

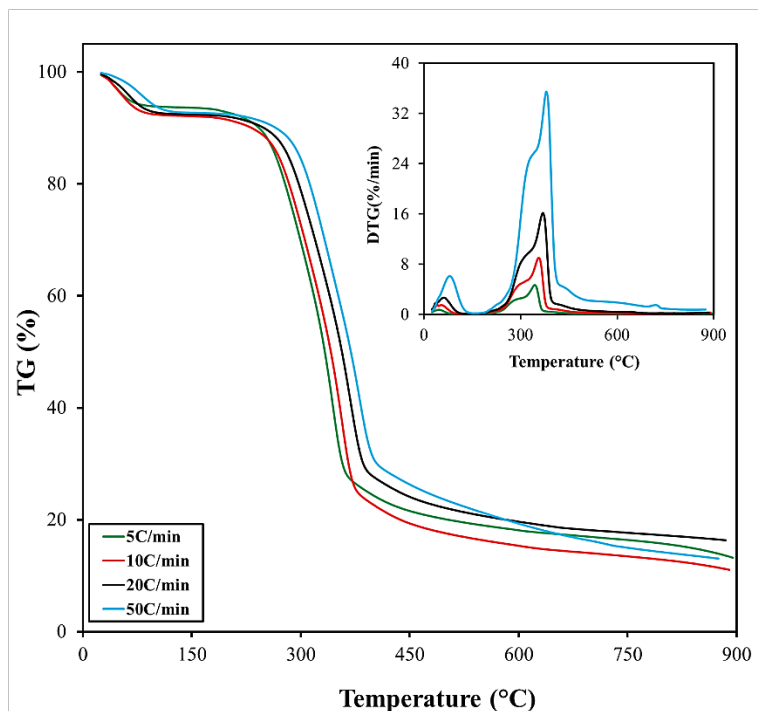
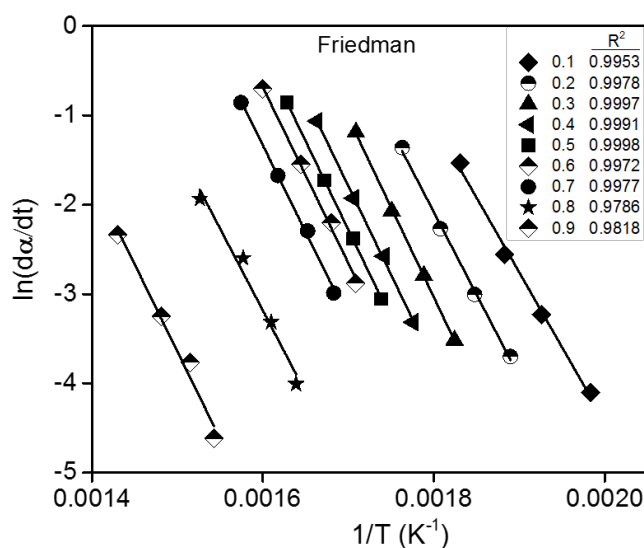


Figure 1. TG and DTG curves of OOR decomposition

### 3.2 Kinetic behaviors of olive oil residue

In the present paper, Friedman, FWO and KAS kinetic models were applied to obtained thermal data to calculate the activation energies. The models were applied to main decomposition region between 200-500°C. The fitted equations of linear lines as well as  $R^2$  values for each kinetic model can be seen in Fig.2 while calculated activation energies were given in Table 2. It can be seen that each line had good correlation with the selected models. In the literature, the parallelism of these lines is attributed to the similar kinetic behavior probably the same reaction mechanism is achieved [Alvarenga et al.(2012)]. It is clear that for all three kinetic models, the obtained  $R^2$  values within this temperature range were really high ( $>0.97$ ) which indicates the good accuracy in the determination of the activation energies.



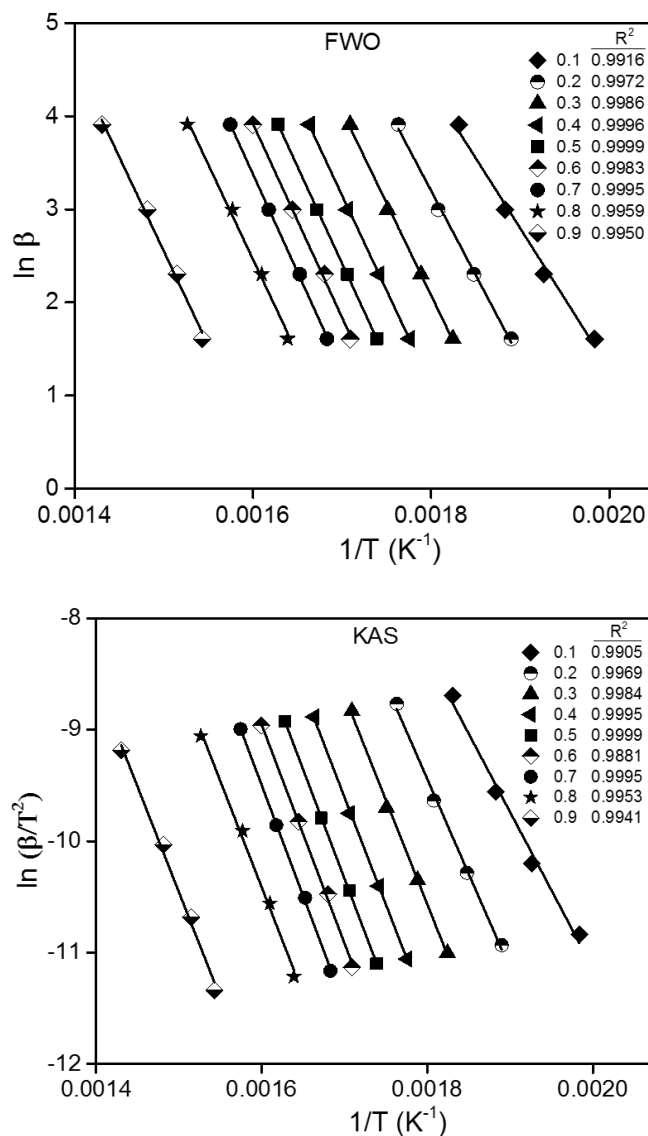


Figure 2. Linear plots of kinetic models calculated from experimental TG data

The activation energy increased as the reaction progress increased until  $\alpha=0.5$  and stayed almost constant between 0.5-0.7. For Friedman model, it is noticeable from Fig.2 that thermal decomposition of OOR included two different regions between  $0.1 < \alpha < 0.7$  and  $0.7 < \alpha < 0.9$ . This first region including  $\alpha=0.7$  (until  $\sim 320-350^\circ\text{C}$ ) can be attributed to the thermal decomposition of hemicellulose in the structure. The activation energy for this range was found as  $\sim 165$  kJ/mol. Decomposition of hemicellulose generally followed by the degradation of the cellulose at higher temperatures due to its more stable structure. So that, it is possible to say that the second region starting from  $\sim 320-340^\circ\text{C}$  between  $0.7 > \alpha > 0.9$  represents the cellulose decomposition. As can be seen from Fig.2, the reaction mechanisms at the final stage of the pyrolysis varied and this situation created a second increment in the activation energy requirement. The apparent activation energies at  $\alpha=0.9$  were found to be  $\sim 162$  kJ/mol. The average activation energy for this temperature range was determined as 158.9 kJ/mol. For the other two kinetic models, FWO and KAS, the apparent activation energy showed an increase between  $\alpha=0.1-0.7$ . The calculated activation energies were found between 119.5-166.4 and 117.1-164.8 kJ/mol, respectively. For FWO, at the final progress, the activation energies did not change that much and calculated  $\sim 160$  kJ/mol for both  $\alpha=0.8$  and  $0.9$ . Considering the results from KAS model, it was observed that similar trend occurred and the activation energies slightly increased at the beginning of the process and then began to decrease since  $\alpha=0.7$ . The average activation energy was 153.4 kJ/mol for this model.

Table 2. Comparison of activation energies calculated from different kinetic models

|                | Friedman     | FWO          | KAS          |
|----------------|--------------|--------------|--------------|
| $\alpha$       | $E$ (kJ/mol) | $E$ (kJ/mol) | $E$ (kJ/mol) |
| 0.1            | 139.2        | 119.5        | 117.0        |
| 0.2            | 153.5        | 143.2        | 141.5        |
| 0.3            | 167.1        | 156.7        | 155.5        |
| 0.4            | 165.1        | 161.5        | 159.8        |
| 0.5            | 165.0        | 164.4        | 163.0        |
| 0.6            | 163.7        | 164.5        | 163.1        |
| 0.7            | 161.3        | 166.4        | 164.8        |
| 0.8            | 152.5        | 160.6        | 158.5        |
| 0.9            | 162.3        | 160.2        | 157.3        |
| <i>Average</i> | <i>158.9</i> | <i>155.2</i> | <i>153.4</i> |

#### 4. CONCLUSION

In the present study, OOR was evaluated as biomass source and investigations into thermal and kinetic behaviors were carried out. To calculate the activation energy of the pyrolysis process, three different kinetic models which are Friedman, FWO and KAS were applied to thermal data. Experimental and modelling studies showed that thermal behaviors of olive oil residue can be divided into three main regions which are *i*) moisture removal, *ii*) main decomposition of the structure (hemicellulose and cellulose degradation together with the start of the lignin degradation) *iii*) lignin decomposition. The activation energies for this process were determined very close as 158.9, 155.2 and 153.4 kJ/mol for each kinetic model in the given order. In the end, it can be concluded that OOR can be an alternative feedstock for the thermochemical processes such as pyrolysis.

#### REFERENCES

- [1] Alvarenga L.M., Xavier, T.P., Barrozo, M.A.S., Bancelosa, M.S., Lira, T.S. (2012). Analysis of reaction kinetics of carton packaging pyrolysis, *Procedia Eng.*, vol. 42, 113-122.
- [2] Bach Q.V., Chen W.H. (2017). A comprehensive study on pyrolysis kinetics of microalgal biomass, *Energy Convers. Manage.* vol.131, 109-116
- [3] Cepeliogullar O., Haykiri-Acma H., Yaman S. (2016). Kinetic modelling of RDF pyrolysis: Model-fitting and model-free approaches, *Waste Manage.* vol. 48, 275-284
- [4] Hu M., Chen Z., Wang S., Guo D., Ma C., Zhou Y., Chen J., Laghari M., Fazal S., Xiao B., Zhang B., Ma S. (2016). Thermogravimetric kinetics of lignocellulosic biomass slow pyrolysis using distributed activation energy model, Fraser-Suzuki deconvolution, and iso-conversional method, *Energy Convers. Manage.* vol. 118, 1-11
- [5] Uzun B.B., Pütün A.E., Pütün E. (2007). Composition of products obtained via fast pyrolysis of olive-oil residue: Effect of pyrolysis temperature, *J. Anal. Appl. Pyrolysis* vol. 79, 147-153.

# ICACCHE

International Conference on Applications  
in Chemistry and Chemical Engineering



ISBN 978-605-67917-0-3

[www.icacche.com](http://www.icacche.com)